Radargrammetric Image Data Evaluation

DIBAG Report 30

Institute for Image Processing and Computer Graphics
JOANNEUM RESEARCH, Wastiangasse 6, A-8010 Graz, Austria

JOANNEUM RESEARCH

Radargrammetric Image Data Evaluation

Final Report

EUROPEAN SPACE AGENCY

CONTRACT REPORT

The work described in this report has been performed under
ESA contract No. 6.621/85/F/FL (SC)
Responsibility for the contents resides in the authors or
organisation that prepared it.

DIBAG Report 30

Graz, im December 1987

Institute for Image Processing and Computer Graphics
JOANNEUM RESEARCH, Wastiangasse 6, A-8010 Graz, Austria

ESA STUDY CONTRACT REPORT

No ESA Study Contract Report will be accepted unless this sheet is inserted at the beginning of each volume of the Report

ESA CONTRACT NO	SUBJECT	NAME OF CONTRACTOR
6.621/85/FL/FL(SC)	**Radargrammetric Image Data Evaluation**	**Institute for Image Processing and Computer Graphics**
* ESA CR( ) No	* STAR CODE / No. of Volumes This is Volume No 1	CONTRACTOR'S REFERENCE

ABSTRACT

This volume is the final report on ESA Contract No. 6.621/85/F/FL(SC) entitled *Radargrammetric Image Data Evaluation.* In this study, the identification and assessment of computer software capabilities which are required for the *radargrammetric* utilization of synthetic aperture radar images is performed.

Geometric concepts for the processing of and the information extraction from radar images are reviewed and evaluated, dealing with single radar images, multi-parameter radar images, and combinations of radar images with collateral information and with other types of remote sensing data. Existing software tools are described and the specific needs of further developments are assessed. Three *radargrammetric software libraries* are suggested and *software specifications* are given for selected modules.

The use of radar *resection-in-space* and image *intensity pyramid* techniques is evaluated more closely using Seasat and airborne synthetic aperture radar data. A number of experimental results are given.

As a testbed for radargrammetric software tools in application-specific environments a *structural geologic mapping experiment* has been selected, using mainly Space-Shuttle-borne (SIR-B) radar data and Landsat TM data for comparison purposes. Radargrammetric processing is demonstrated in lineament mapping experiments and the usefulness of existing software is discussed.

Names of authors:

M.F. Buchroithner, G. Triebnig; G. Domik, W.G. Kropatsch, F.W. Leberl, G. Paar, J. Raggam, A. Riasa, D. Strobl.

** NAME OF ESA STUDY MANAGER	** ESA BUDGET HEADING	
DIV: DIRECTORATE		

* Sections to be completed by ESA

** Information to be provided by ESA Study Manager

Study Team

Project Management:	Manfred F. Buchroithner[1]
Study Management:	Gerhard Triebnig[1] Manfred F. Buchroithner[1]
Study Elaboration: (see page 9 for key of authorship)	Manfred F. Buchroithner[1] Gitta Domik[2] Walter G. Kropatsch[1] Franz W. Leberl[2] Gerhard Paar[1] Johannes Raggam[1] Asuncion Riaza[3] Dieter Strobl[1] Gerhard Triebnig[1]
Technical Management by ESA:	Stefano Bruzzi, ESA Headquarters D/EOM Jean-Pierre Guignard, ESA ESTEC/ORM

Participating Organisations:

1 Institut für Digitale Bildverarbeitung und Graphik,
Forschungsgesellschaft Joanneum Ges.m.b.H., Graz, Austria (Main Contractor)

2 Vexcel Corporation, Boulder, Colorado, USA (Sub-Contractor)

3 Instituto Geologico y Minero de España, Madrid, Spain (Sub-Contractor)

Contents

Introduction

This report details the work carried out by the Institute for Image Processing and Computer Graphics of the Forschungsgesellschaft Joanneum (Graz Research Center), Austria, under contract to the European Space Agency (ESA) concerning the identification and functional description of computer software tools for *radargrammetric* evaluation of radar remote sensing image data with emphasis on spaceborne synthetic aperture radar (SAR).

Overview of Contract Activities

The identification of processing capabilities for the evaluation of SAR image data naturally requires an indepth investigation of the role which radargrammetry plays, and what can be expected from it in present and in future applications of remote sensing data. On the other hand, it is of importance how one adequately designs the software tools to be provided to "the User", be it a prominent processing center or a single geoscientist.

At the outset, the contract had four declared objectives:

1. Review of the current understanding in the technology of extracting geometric information about objects from SAR images.

2. Description of computer software libraries to be utilized in radar image data evaluation, i.e. libraries for

   - basic radargrammetric image data exploitation;
   - multi-sensor image combination and analysis;
   - processing of radar image time-series.

3. Assessment of existing prototype software capabilities in geoscientific application studies. (For the contract a structural geological mapping experiment was selected.)

4. Identification of a development plan for the above software libraries.

In the theory-oriented investigations which have been part of the contract a cristallization of opinions about radargrammetry has been noted, which leads to the conclusion that radargrammetry must be considered not just to be a tool for various applications but also as an application field in its own right. A thorough review of the current state of radargrammetry carried out during this contract revealed that numerous products and new fundamental findings can be derived from radargrammetric evaluation of SAR imagery. Examples are the extraction of topographic information using SAR stereopsis, object recognition by synergetic analysis of multi-sensor imagery, or the determination of microwave response signatures of objects from the SAR image.

It has been tried to match the identification of particular requirements for computer software capabilities for SAR image utilization in radar-oriented application fields with this extended view of the role of radargrammetry. However, to carry out this intention would have been a very extensive task. Therefore, this contract has mainly addressed the georeferencing of SAR data, because the accurate geometric modelling of the SAR imaging process is the basic problem in the correction of geometric distortions in SAR images, and also because geometric distortions hinder most cartographic applications. The software modules to be contained in the above-mentioned software libraries are so far mainly related to the geometrical processing of SAR image data. The identification of modules for multi-sensor and time-series processing had to be postponed to some later investigations. To give a concrete development plan for the software libraries was not possible because of the preliminary specification status of many of the software modules.

The basic structure of the contract has therefore been as follows:

- A *review phase* has dealt with radargrammetric issues surrounding the individual SAR image and with the characteristics of its quality, as well as with processing and information extraction techniques. It has also covered overlapping images, as they are used for better image analysis, for the creation of secondary image products, and for the derivation of three-dimensional topographic information such as digital elevation models.

  Geocoded data sets consisting of combinations of SAR and geobased non-radar data have been addressed, as well as the possibilities to evaluate synergistic data sets consisting of SAR and other remote sensing data.

- Suggestions have been compiled for the specification of capable *software libraries* to be utilized in the multitude of tasks relevant for radar image data evaluation. A description of modules for basic radargrammetric data exploitation is contained in this report, comprising programmes for SAR image setup (determination of analytic imaging model), three-dimensional reconstruction, geometric analysis and precision rectification, radiometric manipulations, secondary image generation and representation, and various capabilities for the analysis of SAR image content.

- Computer-based tools have been studied in detail and have been utilized in a *structural geological mapping* experiment using SIR-B data sets acquired over the Cantabrian Mountains in Spain. Two main conclusions can be drawn from these investigations. First, the geological user has been much more satisfied by sets of data which have undergone some type of radargrammetric processing, in particular geocoding, than by using just the provided original radar data. Second, the results of this study activity have been a valuable aid for the identification of further processing requirements for semi-automated lineament analysis from SAR imagery and of typical user interface requirements a software development concept has to take into account.

- A number of achievements in *selected development activities* have been made in
  - a detailed study of the problem of identifying ground control information and the homologue features in SAR imagery;
  - the development of software for semi-automated tie-point identification in SAR images;

- an assessment of a procedure for radar resection-in-space, which is required for analyzing and refining the mapping parameters contained in radar projection equations;
- a preliminary investigation of the usefulness of image pyramids applied to SAR imagery. Lee, Frost and Gauss filters have been used and studied for SAR data volume and speckle reduction using intensity pyramids.

During this contract progress has been made in the assessment of radargrammetric concepts and currently available software tools. However, the bulk of the work lies still ahead. The functional requirements for software to evaluate the objects visible in SAR images, to utilize multi-sensor data, multi-parameter SAR data and image time series have not yet been identified comprehensively.

The algorithmic details and implementation aspects for numerous modules of radargrammetric software will have to be a matter of further investigations. The kernel software existing at the Institute for Image Processing and Computer Graphics in Graz required as the essential element of any kind of radargrammetric processing has positively proven its capability. However, the stage of developing concepts for operational implementation of these modules has so far only been reached with geocoding software. Many other modules, existing in test implementations or even just as ideas recommend themselves to be developed further and to be transferred into an operational environment as well.

The Scope of Radargrammetric Work

Radargrammetric work may be separated into two classical domains:

- coordinate processing;
- grey value processing or digital image processing.

The latter category is rapidly gaining importance. In fact, all major current and planned radar imaging systems produce digital data. As argued in Part I of this report, the frontiers of current radargrammetric work are in

- the development of an improved understanding of the geometric modelling of the SAR imaging process, and the interrelation with classical "pointing" to a target in a SAR image, and with image matching;
- the development of capabilities to create so-called "secondary" radar image products to include "geocoded" images, for improved applicability and interpretability of radar images;
- the improved ability to deal with multiple radar image coverages in order to take advantage of the so-called "incidence angle signature" of objects;
- combining measurements of geometric disparity (stereo parallax differences) and of thematic disparity (in the form of shadow differences, edge migration, specular point migration etc.) for image matching and terrain shape reconstruction;
- the creation of tools to deal efficiently with synergistic data sets consisting of synthetic aperture radar images and non-remote sensing data such as maps and digital elevation models.

- the creation of tools to deal efficiently with the geometric processing of image time series in order to exploit temporal changes using SAR images.

In the advance of processing sophistication it becomes less meaningful to maintain a strict separation of coordinate-based and grey-value-based operations. In fact, from a geometric point of view radargrammetry may preferably be grouped according to data sets instead of processing concepts. Data may be:

(a) single images;

(b) pairs of overlapping images, potentially leading to stereopsis;

(c) radar images with collateral non-image data;

(d) blocks of connected images covering a large area,;

(e) successive image coverage of one area forming a multi-temporal data set;

(f) multi-sensor image data sets.

The concept of "radargrammetry" has found applications with mainly two types of data sets, namely (a) and (b). It is clear, however, that the other types also need to be addressed since in a strict sense

> *radargrammetry is the technology of extracting geometric information about objects from radar images.*

Relevant geometric information may consist of positions or dimensions of objects and their changes. A broad interpretation of radargrammetry, in analogy to photogrammetry, includes the processing for geometric calibration of radar images, the creation of derived image products with a defined geometry, and the most important task of interpreting the contents of an image in general not application-specific terms.

Structure of Report

The content of the report follows the work structure of the contract (see page 6).

The remainder of this introductory chapter contains a short summary of the SAR principle and of SAR processor technology for airborne and spaceborne image data.

Part I contains a comprehensive treatment of radargrammetric concepts which document the current status of radargrammetric research and achievements. Chapter 1 describes the geometric model which is fundamental to radargrammetric processing. Chapter 2 gives an introduction to what can be expected from the information contained in SAR images in terms of geometric and radiometric quality. In Chapter 3 an overview is given of the radargrammetry-relevant processing of *single* SAR images, above all georeferencing, exploitation of grey value information and certain object recognition tasks. In Chapters 4 and 5 radargrammetric concepts which might be useful for the processing of *multiple* SAR images (multi-parameter SAR) and for combined evaluations of SAR images and non-radar data, such as collateral data (maps, digital elevation models etc.) and other remote sensing data are considered.

In Chapters 1 through 5 the preliminary functional requirements for computerized processing tools are derived, which are summarized and structured in Chapter 6. Three

radar software libraries are suggested in Chapter 6; the processing modules proposed for inclusion in these libraries are described in detail. Chapter 7 concludes Part I with recommendations where to focus future radargrammetric research and how to proceed best in the development of capable processing tools.

While Part I should be understood as an *overview* of the current status of radargrammetry-related fields leading to general conclusions and to recommendations of areas for future research, Part II reports on findings from *practical* investigations and experiments carried out during the contract. Part II contains a somewhat caleidoscopic collection of topics:

First of all, the importance of radar resection-in-space has been found worth considering more closely. The results of an assessment of an existing resection-in-space procedure are given in Chapter 8, together with a presentation of a new method, which has been developed during the contract for identification of ground control points in SAR images.

Image pyramid techniques are of increasing importance in digital image evaluation. Chapter 9 therefore summarizes the developments carried out to adapt this technology to radar-relevant requirements.

Chapter 10 reports on a geological study carried out as a part of the contract to assess the available radargrammetric prototype software in a concrete geoscientific application.

The Appendix is a supplement to Section 3.1 and contains a discussion of various algorithms for SAR image geocoding.

Relevant literature references are found in the Bibliography at the end of the report.

Key of Authorship

This report has been compiled from draft work package reports, which have been reviewed and improved, where necessary, by M. F. Buchroithner and G. Triebnig. The latter also supplemented the report with the introductory chapters, Section 2.3 and Chapter 7. The author of Chapter 1, which presents the basics of radargrammetry, of Section 8.1, and of the Appendix is J. Raggam with contributions having been made by G. Triebnig. D. Strobl compiled and reviewed Chapter 6, and contributed Sections 8.2 and 8.3, which are related to tie-point identification in SAR images. G. Paar and W. Kropatsch are the authors of Chapter 9 on Image Pyramids. M. F. Buchroithner is the author of Chapter 10 on the geological application study. Software developments for the application study are described by D. Strobl.

During the review phase of the contract the consultative services of Vexcel Corporation, Boulder, Colorado, represented a highly valuable support. The author of Sections 2.1, 2.2, 2.4, 2.5, 3.2, and of Chapters 4 and 5 is F. Leberl. Essential inputs were also received from G. Domik in the description of software libraries, Chapter 6.

For the geological application experiment A. Riaza of the Instituto Geologico y Minero de España, Madrid, kindly served as "the User". Most of the necessary field work in Spain has been performed by her institution.

In addition, the authors are greatful to S. Bruzzi and J. P. Guignard of ESA who made many valuable suggestions and recommendations during the contract and after their review of the draft version of the report.

The Principle of SAR

Synthetic Aperture Radar (SAR) is the name commonly given to moving platform based coherent imaging radar. The moving platform can be an aircraft, space shuttle or satellite.

The principle of SAR is well documented—see for example the books by Harger [42] and by Hovanessian [51]. Further background information will be found in the papers of Brown and Porcello [7], Raney [88],and Tomiyasu [96]. Briefly, a SAR is a pulsed radar which transmits encoded (e.g. linear FM) pulses and which performs *two-dimensional filtering* of the receiver signals for pulse compression or image generation, respectively. The aim of the following sections is to give a brief introduction to the technology of SAR. The terms explained in the following will be referred to in the subsequent parts of this report.

Cross-Track Measurement

If the vehicle carrying the radar moves relative to the targets being imaged, the return signal from each target will have the characteristics of the transmitted signal except that it will be shifted in frequency due to the Doppler effect. A SAR achieves high cross-track (range) resolution by applying pulse compression to the returned signal. This is performed on each pulse by correlating the pulse against a replica of the transmitted pulse. The compressed signals are then range-gated or processed in some equivalent way. Resolution elements associated with a particular slant range distance from sensor to target contain echo information from targets at this distance, which are distributed across the whole antenna footprint width.

Along-Track Measurement

A SAR achieves high along-track (azimuth) resolution by effectively synthesizing an aperture much larger than the physical antenna. The relative movement of sensor to target within the synthetic aperture causes a change in the coherent phase return from each target. Proper processing of this phase information with a matched filter [12] can yield an azimuth resolution much finer than that obtained by the physical antenna beamwidth.

Accurate estimates of the expected *phase history* of targets are required for the design of the matched filter and consequently are essential prerequisites for generating high-quality images. Matched filter parameters are determined by either using ancillary data, such as the ephemeris and attitude of the platform which carries the sensor, or utilizing the coherent radar echo data alone.

This determination of the phase history represents one of the major problems in the design and mechanization of a SAR data processing system. Today a number of satisfactory operational solutions exist, however, many examples can be noted where processing systems have been driven across their design limits causing severe degradation of image quality and usefulness.

SAR Processing

The signal processor in a SAR system must store the incoming coherent returns for each range resolution element across the footprint width, preserving amplitude and phase of the returns at the highest Doppler frequency of interest. After a synthetic aperture length

of data has been stored, the processor must perform the azimuth filtering operation mentioned previously.

An optional possibility is offered by SAR processors to reduce the appearance of *speckle* in the image. Speckle is an effect that results from the coherent nature of the SAR imaging process—see Section 2.4. In the SAR processing the synthetic aperture can be divided into a number of sub-apertures. The images generated for each sub-aperture can be added incoherently in order to average the speckle effect. However, the azimuth resolution is decreased with an increasing number of "looks".

Two general classes of SAR processors are currently in operation, i.e. optical and electronic processors. The focused optical processor remains the best processor for wide-swath high-resolution applications where immediate access to the imagery is not required. Electronic processors, both digital and analog, provide a greater range of operating modes and the possibility of immediate access to the mapped imagery.

Several operational *digital* SAR processors operating at non-real-time rates have been developed. These processors do provide some advantages over optical and analog processors such as: completely reproducible processing, large inherent dynamic range, more flexibility in signal processing capability, etc.

Digital range-compression and azimuth-correlation produce a digital image in *slant range representation* with fixed along-track (azimuth) pixel spacing of

$$\sigma_a = \dot{s}/2\,\Delta F_a$$

and cross-track (range) pixel spacing of

$$\sigma_r = c/2\,\Delta F_r,$$

where c and $\dot{s}$ are the velocities of light and of the radar platform, ΔF_a is the Doppler (sub-aperture) bandwidth, and ΔF_r is the frequency modulation bandwidth of the transmitted radar pulse (see Barber [4, equation (15)],—for further details on pixel spacings in digital SAR images, see page 30 of the report).

SAR Modes

There are at least three modes in which a SAR may operate. These are the normal mode, the squint mode and the spotlight mode. In the normal mode the radar looks out sideways to the track and perpendicular to it. In the squint mode the radar is focused either forwards or backwards to the normal mode. In the spotlight mode the radar squint angle is varied continuously as the radar passes a target so that the target is constantly illuminated, and hence the synthetic-aperture length is no longer limited by the real aperture footprint width.

Airborne SAR

When a SAR is flown mounted on an aeroplane, the requirement of highly accurate information about the recorded phase history, which is equivalent to a very accurate distance measurement, needs a consideration of flight path stability. A reasonable criterion for the straightness of the flight path within a synthetic aperture length is a maximum tolerance of flight path deviation $\pm\lambda/8$ (λ beeing the radar wavelength), or one must correct for larger deviations from such a straight line motion to avoid detrimental phase errors.

Considering the fact that, for example, $\lambda = 3.2$ cm at X-Band and that the synthetic length of an airborne SAR can be 100 meters and longer, it is not possible to control the aircraft path so closely. Furthermore, irregular platform movement is dependent on weather conditions.

Airborne SAR platforms are commonly equipped with accurate inertial navigation systems where the output from the navigation system is fed back to the radar. In this way the transmitter's pulse repetition frequency is kept proportional to the speed of the platform relative to the ground, thereby trying to maintain equal spacing between consecutive radar pulses. The accuracy of this process must be in the order of the maximum uncompensated acceleration ($\leq \lambda/T^2$, T is the time to fly the synthetic aperture length). The process is further complicated by the fact that the accelerometer has to compensate for varying gravity effects. This exlains why it has been noticed that navigation systems were not able to give the feedback to the radar, which is necessary to produce high quality image.

A number of *correction methods* have been developed that can correct phase history errors introduced by an irregularly moving SAR platform:

Estimates of the phase errors are derived form applying *automatic focusing* techniques to the recorded data (Herland [46]). If this is done for successive points in time, the velocity history of the platform can be estimated and azimuth correlation is done with a time-varying filter. Thereby the image data is geometrically corrected in the along-track direction.

Autofocusing techniques can also be applied as long as the sum of across-track deviations over the lenght of the synthetic aperture is well below one range resolution interval (range bin). In case of severe cross-track irregularities, the target histories will be distributed over several range bins. The resulting range migration cannot be removed by autofocusing. This error usually remains uncorrected for airborne SARs and may in the severest case lead to strong defocusing of the SAR as well as to corruption of image information over broad azimuthal strips.

Spaceborne SAR

In the case of a spaceborne SAR the platform is moving very regularly. Therefore, no correction by acceleration measurements like in airborne SARs is performed during data acquisition. However, the situation is complicated by the fact that the shuttle or satellite carries the SAR sensor along a generally elliptic (i.e. non-linear) orbit. If the radar data are required to be processed into images soon after the satellite pass, nominal (and possibly inaccurate) orbital elements will have to be used in SAR processing. The same is true for the attitude parameters of the platform.

Moreover, it has to be considered that the targets to be imaged are themselves moving with the earth's tangential velocity and that the geometry depends on latitude and longitude due to the earth's oblateness and on the shape of the chosen orbit.

Because of these reasons, processing of spaceborne SAR data has to include range migration correction. The relative movement of sensor to target is deterministic if the nominal orbit and attitude can be assumed to be correct. A phase reference function can therefore be determined for any instance in time, which then can be utilized for SAR processing.

Seasat and SIR-B SAR Data have been evaluated in a number of experiments (e.g. Jin [52], Lin et al.[76]) with the result that the use of phase reference functions derived from nominal orbit and attitude information often leads to significant defocusing (blurring) of

the imagery and strong displacements of the image of a target both in azimuth and range from its true location.

Therefore, methods for the accurate estimation of the instantaneous Doppler frequency (the time-derivative of the phase history) have been developed, denoted as Doppler-Centroid Clutterlocking and Doppler Frequency Rate-Autofocusing [76], and used to extract Doppler parameters automatically from the coherent radar return. So far, no consensus on the performance of these techniques can be observed.

Accurate spacecraft ancillary data will be available for the up-coming European ERS-1 mission from an attitude control system on the platform, laser-tracking and the PRARE experiment. However, these data will only be introduced in non-real-time SAR processing where Doppler parameters can then be calculated from spacecraft ancillary data. In addition, the ERS-1 *Fast Delivery* Processor will include a Doppler centroid tracker.

Part I

Radargrammetric Concepts and Processing Tools

Chapter 1

The Basics of Radargrammetry

1.1 Geometric Modelling of SAR

1.1.1 Radargrammetric Model

Modelling of an *imaging geometry* first of all concerns a formulation for the geometric link between object and image. The classical and common model for SAR image geometry relates an object point, $\vec{p}$, to a SAR sensor position $\vec{s}$, using Doppler equation and slant range equation. In addition, a description of the surface of the earth (digital elevation model, ellipsoid, sphere or plane) as well as equations to relate radar image pixel coordinates to radar range measurement and imaging time are required for the definition of the so-called *radargrammetric model.*

Slant Range and Doppler Equations

On the assumption that both the position vector of a target on the earth's surface as well as the position vector of the spacecraft are continuous functions $\vec{p}(t)$ and $\vec{s}(t)$, respectively, the *phase history* of this target is given by

$$\phi(t) = \frac{4\pi}{\lambda} \cdot |\vec{p}(t) - \vec{s}(t)| \tag{1.1}$$

where λ is the wavelength of the radar. With the relative movement between spacecraft and target $\phi(t)$ changes. The instantaneous *Doppler frequency* is then given by

$$f(t) = \frac{1}{2\pi} \cdot \frac{d}{dt}\phi(t) = \frac{2}{\lambda} \cdot \frac{d}{dt} |\vec{p}(t) - \vec{s}(t)| \tag{1.2}$$

The target's motion $\vec{p}(t)$ as well as the spacecraft's motion $\vec{s}(t)$ may be modelled by simple polynomials:

$$\vec{p}(t) = \vec{p}(0) + \dot{\vec{p}}(0) \cdot t \tag{1.3}$$

$$\vec{s}(t) = \vec{s}(0) + \dot{\vec{s}}(0) \cdot t + \ddot{\vec{s}}(0) \cdot t^2/2. \tag{1.4}$$

$\dot{\vec{p}}$ and $\dot{\vec{s}}$ are the target and platform velocities and $\ddot{\vec{s}}$ is the acceleration of the platform (see Figure 1.1). A substitution of equations 1.3 and 1.4 into 1.2, after neglection of quadratic and higher order terms, leads to an expression for the Doppler frequency as follows:

$$f(t) = f_{DC} + f_{DR} \cdot t, \tag{1.5}$$

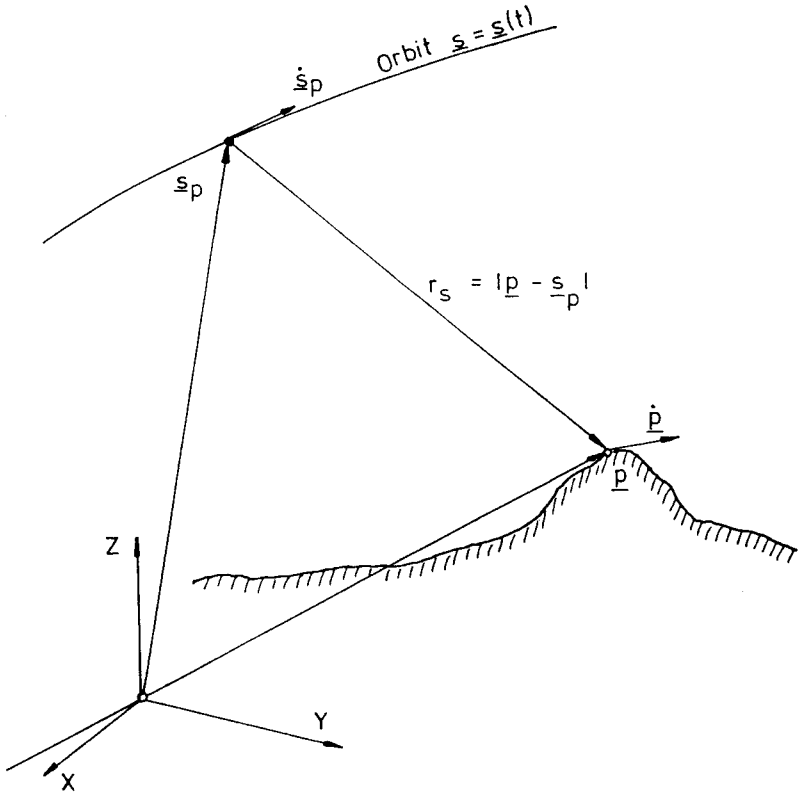

Figure 1.1: Vector entities for SAR sensor and target motion modelling.

where the *Doppler centroid frequency* is given by

$$f_{DC} = \frac{2}{\lambda} \cdot \frac{\left(\vec{p} - \dot{\vec{s}}\right)(\vec{p} - \vec{s})}{|\vec{p} - \vec{s}|}, \tag{1.6}$$

and the *Doppler frequency rate* is given by

$$f_{DR} = \frac{2}{\lambda r} \cdot \left[\left(\vec{p} - \dot{\vec{s}}\right)\left(\vec{p} - \dot{\vec{s}}\right) - \ddot{\vec{s}}(\vec{p} - \vec{s})\right]. \tag{1.7}$$

The *slant range* r from the sensor to the target is a SAR measurement given by

$$r = |\vec{p} - \vec{s}|. \tag{1.8}$$

This equation defines a sphere of radius r and its center at sensor position $\vec{s}$.

A value for f_{DC} may be determined from the phase history reference function used in SAR processing. The *Doppler equation* can be defined as

$$\frac{\lambda f_{DC}}{2} = \left(\vec{p} - \dot{\vec{s}}\right)(\vec{p} - \vec{s})/r \tag{1.9}$$

According to Figure 1.1 this equation describes the closing rate of sensor and target. If the effect of target velocity, $\vec{p}$, caused by rotation of the earth can be either neglected—as it can be done for airborne SAR—, or has already been compensated in SAR processing—this will be the usual situation in future spaceborne SARs—then equation 1.9 can be simplified and rewritten by incorporation of an angular parameter τ for the definition of the Doppler cone (see Figure 1.2):

$$-\frac{\lambda f_{DC}}{2} = \dot{\vec{s}} \cdot \frac{(\vec{p} - \vec{s})}{r} = \left|\dot{\vec{s}}\right| \cdot \sin\tau \tag{1.10}$$

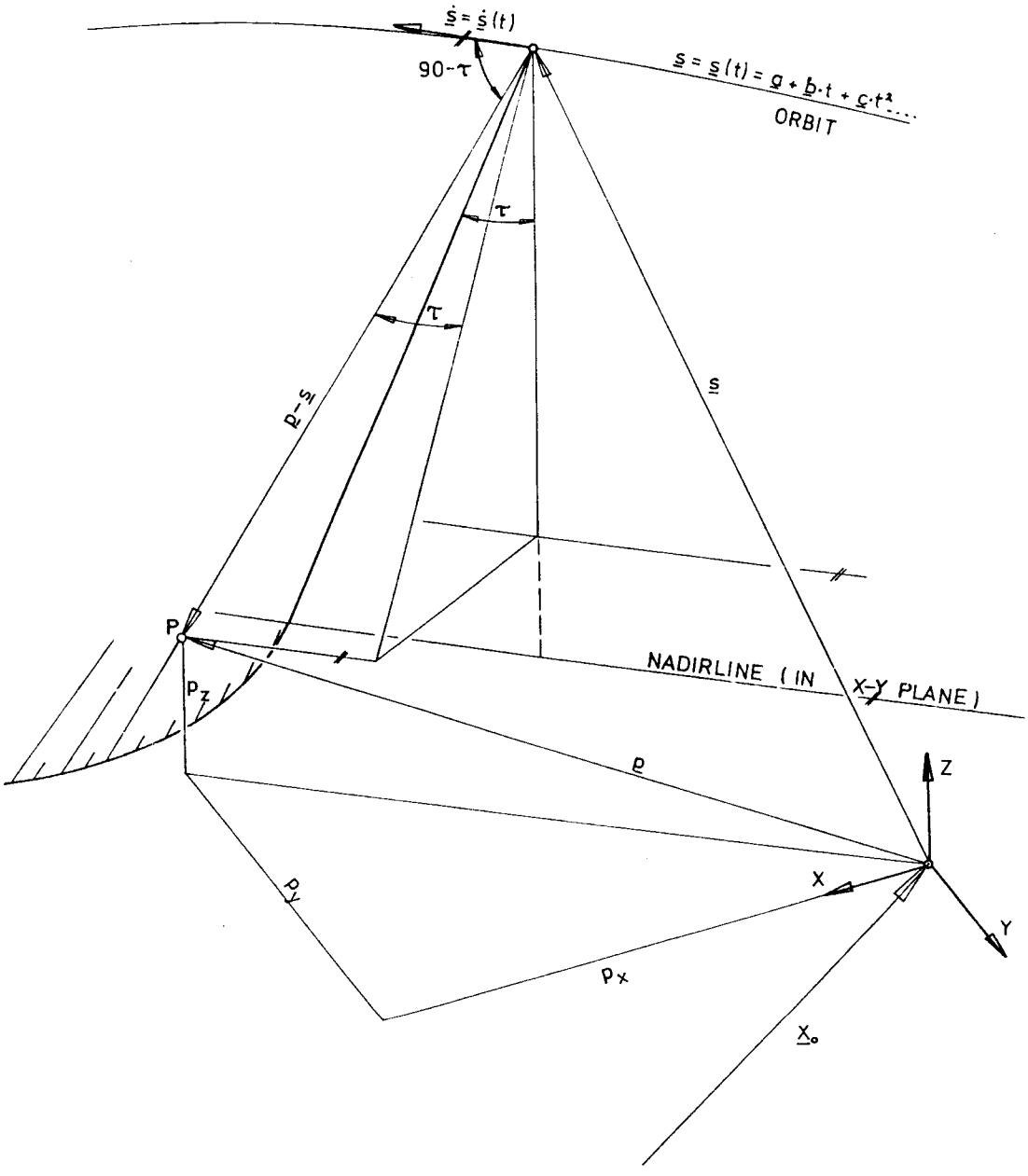

Figure 1.2: Slant range and Doppler cone.

The second equality in 1.10 geometrically describes a cone with cone angle τ, vertex at $\vec{s}$ and axis along the sensor velocity vector $\dot{\vec{s}}$.

This formulation for the Doppler equation is commonly used by photogrammetrists [34], [69]. It is equivalent to formulations used by people from the domain of SAR signal processing [14], given in the first equality of the equation. Consequently, the cone angle can be considered to be a geometric equivalent of the Doppler centroid frequency function if the modulus of the sensor velocity is approximately constant.

Inner Orientation

The SAR image presents r and t in the form of a two-dimensional display with a time (or azimuth) coordinate axis and a range coordinate axis, commonly as a rectangular cartesian system. For digital images, the azimuth and range pixel coordinates i, j have to be converted into radar range and time entities. The most common method is the use of linear conversion functions:

$$t = t_0 + m_i \cdot i \tag{1.11}$$

$$r = r_0 + m_j \cdot j \tag{1.12}$$

where t_0, r_0 are coordinate offsets and m_i, m_j correspond to the pixel spacings along- and cross-track, respectively.

Description of Earth's Surface Geometry

For the determination of the location of a radar image pixel on ground some representation for the earth's surface is required. Depending on the situation various reference surfaces can be used:

- digital elevation model (DEM);
- geoidal surface;
- ellipsoidal surface;
- spherical surface;
- plane.

While the use of geoid, ellipsoid or sphere is sufficient to consider the earth curvature within geometric radar image processing tasks, the use of a digital elevation model is essential for the compensation of topography-related distortions in SAR images.

1.1.2 Solution of Radargrammetric Model

The range equation 1.8, the Doppler equation 1.10, and the equations for the interior orientation 1.11, 1.12 represent a system of relations to determine object coordinates p_x, p_y, p_z of an imaged point on the earth's surface from image pixel coordinates i, j, or inversely. Under the assumptions made in the following, a solution of this system of equations, in principle, will be obtained by three steps:

A: i, j given; t_0, r_0, m_i, m_j assumed to be known:

$$i,\ j \longrightarrow \text{equations 1.11, 1.12} \Longrightarrow t,\ r$$

B: $\vec{s}(t)$, $\dot{\vec{s}}(t)$ assumed to be known, also r (or f_{DC}):

$$t,\ r \longrightarrow \text{equations 1.10, 1.8} \Longrightarrow \text{"projection circle"}$$

(The projection circle is the intersection line of Doppler-cone and range-sphere)

C: Earth's surface shape assumed to be known:

$$\text{projection circle} \cap \text{earth's surface} \Longrightarrow p_x, p_y, p_z$$

The inverse procedure to compute i, j from a given $\vec{p}$ is described in Section 1.2.2.

In practical situations, however, the assumptions about "known" entities need further discussion.

1.1.3 Image Pixel Spacing and Offsets

The numbers m_i, m_j for pixel spacings in the slant range SAR image are defined in SAR processing, just like the range- and time-offsets r_0, t_0. This means that these parameters are available and should be communicated from SAR data processing centers to those who do radargrammetric computations—unfortunately, this is very rarely done. Therefore, m_i, m_j, r_0 and t_0 often have to be determined from the comparison of slant range image with topographic maps. Methods for the determination of the interior orientation of SAR images have been described, e.g. in [79], [86].

1.1.4 Sensor Position $\vec{s}(t)$ and Velocity Vector $\dot{\vec{s}}(t)$

Since each SAR image pixel is created along an extended portion of the sensor flight path, there is no "unique" sensor position $\vec{s}$ from where a particular point has been imaged. SAR image correlation is based on the assumption of an unperturbated position $\vec{s}(t)$ of the real antenna when the sensor moves along the synthetic aperture. Should the real antenna motion be irregular in position, then a motion compensation system needs to be installed.

No study concerning the rigorous definition of a sensor position for SAR images has come to the attention of the authors yet. A *working assumption* is that the effective sensor position is the result of a low-pass filtered actual sensor path. The filter window is the length of the synthetic radar antenna. This may seem like a mute issue when dealing with spacecraft SAR, since the orbit will be very smooth. However, if SAR images are created in "real time", a nominal (and possibly inaccurate) orbit needs to be employed in

a real-time SAR processor. If refined orbit data become available one may have to recreate the SAR image or be content with geometric image errors due to "preliminary $\vec{s}(t)$".

The consideration for $\vec{s}$ applies also to the sensor velocity vector $\dot{\vec{s}}$. The actual SAR image point is created over an extended travel distance of the antenna. Therefore, the apparent velocity $\dot{\vec{s}}$ has to be considered again a low-pass filtered result of the actual velocity vector, with a filter window of the length of the synthetic antenna.

If neither preliminary nor refined ephemeris data are available, they must be reconstructed from comparing the SAR image with map control points, under the assumption that each azimuth line in the image corresponds to a single sensor position on the flight path. The reconstruction of the flight path is done by *resection-in-space*, which is described in Section 1.2.3.

1.1.5 Sensor Attitude

Equations 1.8 and 1.10 do not contain any sensor attitude parameters. The synthetic antenna is oriented along the velocity vector, $\dot{\vec{s}}$, and is therefore unrelated to *pitch, roll* or *yaw angles* of the platform carrying the sensor. Velocity vector $\dot{\vec{s}}$ defines a pitch and yaw angle for the *synthetic* antenna. Roll is of relevance only with respect to localisation and antenna elevation.

The only effects of real antenna pitch and yaw consist of the lack of coincidence of the real radar beam and the so-called Doppler surface. Therefore, provisions have to be made that the real radar beam always illuminates the terrain in the direction of the synthetic radar "beam" (Doppler cone). This is of course well understood in satellite SARs where the earth's rotation can lead to a synthetic antenna beam looking forward (positive cone angle τ), so that the real beam also needs to look forward, or in spotlight mode SARs (variable cone angle τ).

In SAR processing a Doppler centroid frequency and a Doppler frequency rate are determined from an assumed sensor motion. If multi-look processing is applied, the several single-look images created from sub-aperture segments of the Doppler signal history should be geometrically identical and follow certain rules of image brightness distribution. If this is not the case, there exist a focusing problem and an error in the Doppler centroid frequency used, both resulting from errors in the assumed $\dot{\vec{s}}$ and attitude. Clutter-lock and autofocus refine these two parameters. These techniques for example are described, in Lin et al. [76].

If clutter-locking and autofocusing techniques are applied in the SAR processing, the altered Doppler centroid frequency and frequency rate should be communicated to the users. This is a prerequesite if one wants to establish the link between image pixels and precise ephemeris data without using complicated reconstruction techniques.

1.2 Elementary Radargrammetric Coordinate Processing

The mathematical relations which are used in radargrammetry for the geometric description of SAR imaging are given in the foregoing section. In the geometric evaluation of SAR images one or more of the following processing elements will commonly be required:

- Projection of an image point (r, t) onto the earth's surface (to object point(s) $\vec{p}_{(i)}$);
- Projection of a ground point $\vec{p}$ into the SAR image (to image point (r, t));
- Computation of the SAR sensor flight path $\vec{s}(t)$ and velocity $\dot{\vec{s}}(t)$ from ground control points.

The third item becomes necessary if no SAR ephemeris data are available. The input information required in elementary radargrammetric coordinate processing can be listed:

- SAR image in digital or analog form, in slant- or ground-range representation;
- sensor position $\vec{s}(t)$, velocity $\dot{\vec{s}}(t)$ (both can be reconstructed if not available), and attitude data;
- scale factors m_i, m_j (or pixel size if the image is digital); image offsets r_0, t_0 in range and time (all of them can be reconstructed if not available);
- geo-based data:
  - the related digital elevation model (DEM), used for image-to-map processing;
  - three-dimensional linear or areal terrain feature maps, used for map-to-image processing;
  - ground control points or ground control chips, used as input to parameter reconstructions.

This section gives an overview of the numerical methods used for the above elementary elements of radargrammetric coordinate processing. On the other hand, requirements for additional data to be input into the processing are considered.

1.2.1 Projection of SAR Image Points onto Earth's Surface

The problem can be described as intersecting the range sphere and the Doppler cone, given by equations 1.8 and 1.10, respectively, with the earth's surface to solve for the three unknown positional target coordinates $\vec{p} = (p_x, p_y, p_z)$. This can be done by following the scheme of Section 1.1.2.

An easy solution for the problem exists if the earth's surface is represented by a sphere or by a plane (see the paper by Leberl [69]). If an ellipsoidal reference surface is assumed for the earth as done in Curlander's paper [14], the range and Doppler equations are solved together with the equation for the earth's ellipsoid

$$\frac{p_x^2 + p_y^2}{R_e^2} + \frac{p_z^2}{R_f^2} = 1 \tag{1.13}$$

where R_e is the mean equatorial radius, $R_f = (1 - 1/f)R_e$, and f is the earth flattening factor.

In case that the earth's surface is represented by a DEM it becomes a rather complicated and time-consuming procedure to determine $\vec{p}$. Basically, the radar projection circle (the intersection line of range sphere and Doppler cone) must be intersected with the DEM using a numerical search algorithm, because the DEM is not given analytically.

1.2.2 Projection of a Ground Point into the SAR Image

If a ground position $\vec{p}$ is known but its slant range r_p and time of imaging t_p are unknown, one first has to find the sensor position, $\vec{s}(t_p)$, from where the ground point was imaged, which then leads to r_p and t_p. Again, one "unique" sensor position $\vec{s}(t_p)$ is assumed to be connected with one azimuth line of the image.

Under the assumption that the sensor path $\vec{s}(t)$ is known in the form of a continuous function of time, one has to search for $\vec{s}(t_p)$ along $\vec{s}(t)$ until the tangent, $\dot{\vec{s}}(t_p)$ (the velocity vector of the sensor), together with the sensor to target vector $(\vec{p}-\vec{s})$ satisfies the Doppler equation 1.10.

In case the function $\vec{s}(t)$ can be assumed to be linear (or piecewise linear), extending from a point $\vec{s}_i$ into the direction $\dot{\vec{s}}_i$, and assuming, for the sake of simplicity, a zero-Doppler imaging mode ($\tau = 0$), a solution can be obtained by simple interpolation

$$\vec{s}_p = \vec{s}_i + \dot{\vec{s}}_i \cdot \left[\dot{\vec{s}}_i (\vec{s}_i - \vec{p})\right] / \dot{s}_i^2. \tag{1.14}$$

In the general case , one has to deal with a higher order function $\vec{s}(t)$ and an exact value for the parameter t leading to the required sensor position $\vec{s}(t_p)$ must be found iteratively. Raggam [86] utilizes the SAR Doppler equation or squint angle equation, respectively, in a formulation slightly different from equation 1.10 because it allows a more convenient description of the algorithm given beneath. To calculate $\vec{s}(t_p)$, the Doppler equation in the form

$$F(t) = \dot{\vec{s}}(t)\,(\vec{p} - \vec{s}(t)) - \sin\tau \cdot |\dot{\vec{s}}(t)| \cdot |\vec{p} - \vec{s}(t)| = 0 \tag{1.15}$$

is solved iteratively in the following algorithm (see Fig. 1.3).

$t = t_0$

REPEAT

$$\begin{aligned}
\vec{s} &= \vec{s}(t);\ \dot{\vec{s}} = \dot{\vec{s}}(t);\ \ddot{\vec{s}} = \ddot{\vec{s}}(t); \\
&\text{solve for } t: \\
F(t) &= \dot{\vec{s}}(\vec{p} - \vec{s}) - \sin\tau \cdot |\dot{\vec{s}}| \cdot |\vec{p} - \vec{s}| \\
\dot{F}(t) &= \ddot{\vec{s}}(\vec{p} - \vec{s}) - \dot{\vec{s}}^2 + \\
&\quad \sin\tau \cdot \left(\dot{\vec{s}}(\vec{p} - \vec{s})\right) \cdot |\dot{\vec{s}}|/|\vec{p} - \vec{s}| - \\
&\quad \sin\tau \cdot (\dot{\vec{s}}\ddot{\vec{s}}) \cdot |\vec{p} - \vec{s}|/|\dot{\vec{s}}| \\
t &= t - F(t)/\dot{F}(t)
\end{aligned}$$

UNTIL $F(t)/\dot{F}(t) < \Delta t$

$r = |\vec{p} - \vec{s}|$

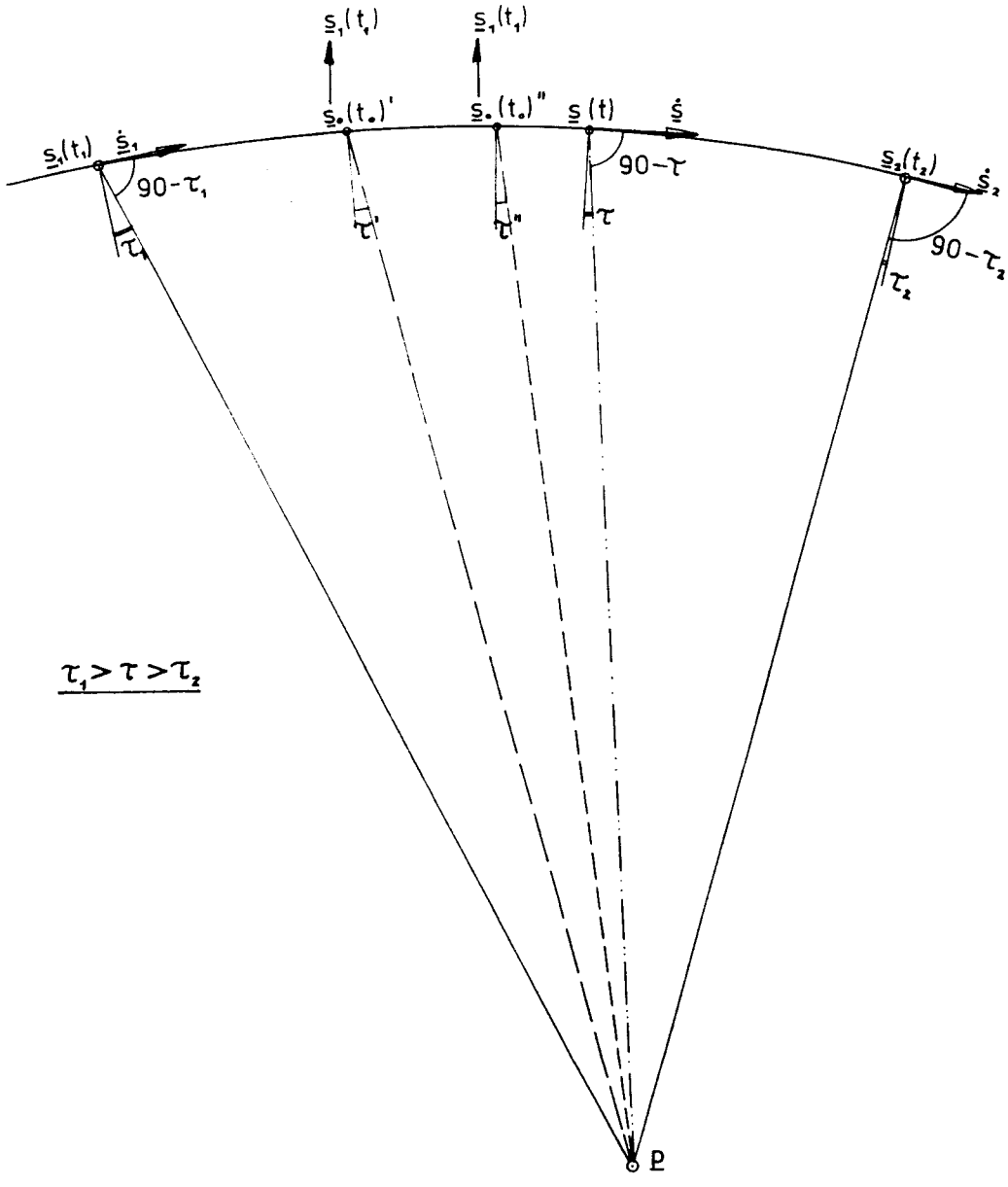

Figure 1.3: Iterative object to image transformation of point $\vec{p}$.

The iteration starts with an initial value t_0 for the time when target $\vec{p}$ was imaged. By each iteration step an improvement for this parameter is obtained, and the iteration stops when the increment for imaging time t becomes smaller than a certain small Δt.

1.2.3 Resection-in-Space

The above image-to-object and object-to-image projection algorithms were based on the assumption that the parameters m_i, m_j, r_0 and t_0 of the radargrammetric model were known at least with an accuracy that allows a consistent computation of the projections. In addition, the sensor flight path $\vec{s}(t)$ and velocity $\dot{\vec{s}}(t)$ were assumed to be given accurately. In many cases, however, the required parameter values are not available or accurate enough and must be refined or completely reconstructed.

An important radargrammetric algorithm is the so-called *resection-in-space*. It uses known ground control points with their world coordinates p_x, p_y, p_z, measured image points with their time and slant range coordinates t, r and, if possible, data on the sensor path $\vec{s}(t)$ and velocity $\dot{\vec{s}}(t)$, tying them together with imaging constants such as scales and offsets, in order to:

- detect, describe and remove inconsistencies in the projection relations;
- compute a consistent sensor path $\vec{s}(t)$ and velocity $\dot{\vec{s}}(t)$;
- reconstruct consistent imaging constants;

A resection-in-space method for the recovery of the geometric image acquisition parameters by a *radar bundle adjustment* is suggested by Raggam et. al. [87]:

In the bundle adjustment the position of the sensor is modelled by

$$\vec{s} = \vec{a}_0 + \vec{a}_1 \cdot t + \vec{a}_2 \cdot t^2 + \ldots, \tag{1.16}$$

the orientation of the synthetic aperture (not to be confused with antenna pointing direction) being defined by the first derivative of these polynomials, i.e. by the sensor velocity vector.

The "observations" (called so analog to the photogrammetric term) for the adjustment are:

- a number of sensor position measurements (s_x, s_y, s_z), each providing a system of three equations from vector equation 1.16;
- image coordinate measurements i, j of identified ground control points, each providing a system of two equations from equations 1.8 and 1.10.

Poorly and well-known observations are assigned with variable weights.

These observations lead to a system of non-linear observation equations which is usually linearized, and numerically solved to determine the refined SAR image acquisition parameters. The final result is a consistent radargrammetric model, for which a three-dimensional object point can be related directly to radar image coordinates, using equations 1.8, and 1.10. Here "consistency" means that targets in the slant range SAR image can be mapped accurately to their corresponding location on the earth, or vice versa, by using refined or reconstructed model parameters. The values of these parameters are not necessarily identical with the values of the physical entities which they actually describe, but they satisfy the radargrammetric projection model.

SAR resections-in-space are currently highly exotic techniques with very few references in literature. There is a lack of good understanding how various parameters interrelate in more complex SAR resection-in-space. The kinematic SAR imaging process could suggest that the mathematical model be developed to contain a very large number of unknown parameters. This invariably leads to an unstable system of equations. Therefore a trade-off exists between:

- the complexity of the mathematical models as expressed in the number of parameters to be considered in radargrammetric computations;
- the requirements for external control data such as ground control points;
- the statistical assumptions or constraints imposed on the parameters (how accurate are the input data describing the SAR configuration);
- the stability of the numerical solutions (trade-off between accuracy, number of unknowns and number of observed control points).

These trade-offs have been investigated during the contract. A resection-in-space procedure available at DIBAG is assessed in Chapter 8.

As accuracy requirements increase with increasing ground resolution and with increased processing sophistication for multi-sensor and multi-temporal remote sensing analysis, radargrammetric models must be refined as well to meet the new requirements: therefore non-linearities in the imaging process need to be modelled, too.

1.2.4 Requirements for Input Data

Ephemeris and Attitude Data Requirements

Due to the principle of SAR a specific image point cannot be considered to be the product of the radar illumination from a single, specific sensor position of the real flight path. One might rather think of having a synthetic flight path defined by the sequence of centre positions of the synthetic antennas, where one specific image point or image line, respectively, has been imaged.

Thus, precision-processing of radar images would require that sensor position, velocity and attitude are calculated for the *centres* of the synthetic antenna to define the synthetic flight path. Still, one has to consider two problem fields when wishing to compute ephemeris and attitude data (the first one is only applicable to spaceborne SAR):

- If real orbit and attitude parameters are available within certain accuracy limits (as it is announced for ERS-1), proper mathematical and statistical models still need to be defined to transform the accurate real flight path data to the *synthetic* flight path and sensor velocity vectors, which are the subject of the radar projection equations.
- No consideration of the parameters of the real flight path or of the SAR processing step is required if ground control point measurements were used in a reconstruction process. Although this determination of synthetic flight path and imaging parameters would lead to a consistent system of radar projection equations, it does not allow the comparison with the actual parameters used in SAR processing.

Another critical problem concerns the compensation of the *azimuth-skew*, which sometimes can be detected in SAR images and which results from the difference between the

actual Doppler response and the Doppler centroid frequency used for processing the SAR image. This calls for a consideration of the role of the angular parameter τ in the radargrammetric projection equations, which defines the opening of the Doppler-cone. Due to the fact that the Doppler frequency is a function of the position of the target within the swath, it is obvious, that one uses a range-dependent function for τ as has been suggested by various authors. A linear function is used e.g. by Curlander [15]. Meier and Nüesch [79] use a second order range polynomial, where these functions can be derived from a set of ground control points. DFVLR[1] is planning to dump Doppler information during the processing of ERS-1 SAR images to be able to derive proper functions for τ directly from this information.

Digital Terrain Elevation Data

These data are collected from digitized source maps or from stereo-evaluation of optically or digitally correlated stereo-image pairs with either perspective or any other type of projection geometry. The combination of the digital data together with a procedure to reconstruct and provide height information for any ground coordinate set (not only those contained in the data file) is hereafter denoted as a *digital elevation model* (DEM). In radar-related processing *raster* DEMs are commonly utilized, which can be considered to be digital images with grey values describing terrain height.

It is extremely difficult to quantify the accuracy of a DEM, as the final representation varies with the generation method adopted. Geomorphologic fidelity or accuracy of the stored elevation data may not be the only criteria with which to assess a DEM for SAR image processing purposes. Errors may be kept at an acceptably small level with high height accuracy in the DEM nodes and small grid spacings.

An essential point concerns the way how elevation values are determined through intersection of the radar projection circle with the terrain surface. In a recent paper by Rauste [89] it was shown that in cases where the terrain slope approaches the radar layover limit (where the incidence angle of the radar wave at the terrain surface equals the radar look angle), the error in computing the object position from the SAR image theoretically may become infinite already for DEM height errors in the order of one meter. Therefore, it is important how the software component of the DEM, i.e. the height reconstruction algorithm, is adapted to the intersection problem. Related accuracy and DEM generation considerations have recently been addressed by Raggam et al. [87].

[1] Schreier, private communication

Chapter 2

SAR Image Properties

Much has been written about the principle of SAR and of SAR data processing. A short summary is also given in the introductory chapter of this report. The image user, however, who must interpret SAR images, would anticipate to have a coherent treatment of what he should expect in terms of the interpretability of images in his respective application. Interpretability is connected with various image properties and to understand the latter very often an explanation of the SAR data acquisition process and the image generation chain becomes necessary. The material presented in this chapter is an attempt to analyze image properties by merely avoiding the reference to SAR processor theory. This approach has been chosen to—hopefully—be of practical help for the image user.

On the other hand, for an effective monitoring of the quality of SAR image products, the specification of how to measure digital image quality and to develop quality-control procedures is a responsibility of data distributors. A sound quality-monitoring concept has not yet been developed for SAR images because here quality-control is more problematical than for optical sensors. Reference [36] lists some of the problems involved in attempting objective measurement of image quality for SAR images. Since many of these topics are under active investigation the current Chapter will demonstrate that the study of possibilities for SAR quality-control is a problem that is certainly not completely solved.

2.1 Interpretability

Some efforts have been reported in literature to evaluate how well certain objects can be detected, recognized and identified in SAR-images. Apart from classified military research, there has been an abundance of thematic mapping work on the subject. This relates to geometric resolution in particular when man-made details need to be mapped. Dowman and Morris [27], and Konecny et al. [56] are examples of authors who evaluated the identifiability of specific map-relevant objects in SAR-images. In general the conclusions are unfavorable, expectations from photographic resolutions do not translate into SAR resolution. Some factors for the discrepancies between photographic and SAR resolution cells are normally enumerated:

- mirror reflections of SAR echoes;
- strong returns versus so-called "no-shows";
- speckle;

- extreme mono-chromaticity of SAR.

It remains open to what extent each of these factors is of relevance. Therefore, one has to solve the problem of understanding the geometric resolution of SAR images and analyze its effect on interpretability. Another spectrum of problems is related to geometric and radiometric distortions be they introduced by the SAR sensor or the processing, or be they inherent to the imaging principle (like the cross-track terrain-induced distortions).

2.2 Geometric Resolution

Geometric resolution and its effect on geometric measurements are well understood in mapping photography and other passive sensing systems; this does not apply to active sensing, in particular to SAR. Relating one to the other is, however, of value because of the incomparably larger knowledge base for passive imaging.

2.2.1 Definitions

Obviously, SAR geometric resolution is expressed by two numbers: *azimuth* and *range resolutions* σ_a and σ_r. In addition, one typically specifies a number of "looks" associated with the azimuth resolution. Although look summation is one way to improve the radiometric resolution, it can be done only at the expense of decreasing the spation resolution.

If, as it is valid for *digital* SAR images, σ_a and σ_r are defined by the equations given on page 11, they denote azimuth and range pixel spacing. However, there is a difficulty. For certain reasons, which are explained in Barber [4, page1047], it is necessary to increase the image sampling rate in SAR processing and thus decrease the pixel size. *Pixel diameter* therefore must not be confused with SAR resolution, e.g. a SAR image generated from 14 m slant range resolution may be presented with 12.5 m pixels. In other situations it may be desirable to average pixels to sizes larger the resolution. In particular, pixel size confuses the issues that are based on SAR resolution if pixels are defined in ground range.

If pixel size is much smaller than azimuth and range resolution, it is obviously irrelevant for geometric analysis. If it is much larger, then range and azimuth resolution values become irrelevant and are replaced by pixel diameter. There is a transition area, where it can affect the usefulness of range and azimuth resolution numbers.

2.2.2 Experiments

A particular experiment in preparation of the Shuttle Imaging Radar and Magellan efforts was performed by D. N. Held in 1981: digital SAR images were created from one source signal history at various resolutions, varying both range resolution and azimuth number of looks. This resulted in data of variable speckle—see Section 2.4—and of variable resolution. The conclusion was that for the geometric purpose the highest geometric resolution is best.

Other experiments, for example with *analog* SIR-A images[1], have been attempted with corner reflectors, placing them at varying distances from one another and observing how close they can be until their images are no longer detectable as separate objects. These experiments have confirmed that two points are separated in the image if they are a distance a apart as follows:

$$a \geq \sigma_a/2 \text{ or } a \geq \sigma_r/2 \tag{2.1}$$

[1] W. Johnson, personal communication (1986)

2.2.3 Current Understanding

Although *resolution* is a frequent topic of study it has not been addressed in a radargrammetric context. The current level of understanding considers azimuth and range resolution numbers σ_a, σ_r, as if they were pixel diameter values in passive digital imaging; e.g. a SIR-B range resolution number of $\sigma_r = 14$ m is the equivalent of a Landsat TM pixel diameter number of 30 m (This means that SIR-B has approximately twice as good a resolution as Landsat TM). One can argue then that SAR range and azimuth resolution relates to classical photogrammetric resolution concepts.

Resolution is expressed in passive imaging either by the diameter of the Airy disk, by line pairs per milimeter at image scale, by line pairs per kilometer on the ground, by pixel diameters or by instantaneous field-of-view or angle-of-view; in the case of SAR there is an opportunity to define resolution separately in range and in azimuth. However, when interpreting SAR images one has to deal with pixel diameters which are, in general, different from SAR resolution (see above), or with analog SAR imagery where the concept of resolution is even more unclear:

One could argue that SAR resolution in *analog* SAR imagery relates to the classical line-pair resolution as follows:

- 1 line-pair is resolved by $2\sqrt{2}$ SAR image resolution cells,

where $2\sqrt{2}$ is called "Kell-factor" in analogy to television-type resolution. On this assumption one could translate now the existing body of understanding from photography into SAR. This has not been done, and most certainly has not been verified in any experimental manner.

As part of the Magellan Mission of NASA, a need exists to relate the existing passive imaging resolutions as obtained for various planets to the expected SAR resolution to be obtained of the surface of planet Venus. A common translation is to relate

- 1 line-pair to 2 SAR image resolution cells[2].

This is different from the Kell-factor-based relationship.

Another important concept is the error of the observed slant range, ε_r. It is currently unclear how this error relates to the slant range resolution σ_r. If the slant range resolution is the diameter of the half-value of the point spread function in range direction (compare Barber [4, equation (6)]), then a standard error of slant range ε_r should be:

$$\varepsilon_r = \sigma_r / 2 \tag{2.2}$$

No experiment has come to the attention of the authors to determine statistically the distribution of errors of slant range, nor is a theoretical study accessible at this time.

If range resolution σ_r were the diameter of a uniformly distributed range error, then the statistical standard deviation would be

$$\varepsilon'_r = \frac{\sigma_r}{2\sqrt{3}} \tag{2.3}$$

Current literature does not address this question; wherever an assumption is made it is $\varepsilon_r = \sigma_r$ which may be misleading.

[2] M. Kobrick, private communication (1986)

2.2.4 Pointing Accuracies

It is relevant to every photogrammetric/radargrammetric effort to understand how a specific object on the ground manifests itself on an image and how well one can point to an imaged target.

In photography, pointing accuracies have been the subject of extensive efforts in the late '60s and early '70s. One understands well that pointing errors may vary between 2 μm and 10 μm at image scale, depending on the type of objects. This of course does not translate easily to SAR. First of all, image *scale* is non-existent in digital data. But even the more recent results obtained for pointing accuracies in digital photography cannot be translated to SAR.

One needs to find the pointing accuracies to targets in digital SAR data (This should not be confused with radar antenna pointing accuracies. "Pointing" as it is used here refers to measurements of image points). In early work on real aperture radar over open water in which reflectors were placed, Leberl [68] reported an accuracy of 0.02 of the apparent target diameter in the image. The shape of the target's image conformed to the theoretically expected Gaussian point spread function.

Experiments are needed to explore how various objects manifest themselves in SAR images as a function of geometric resolution parameters, how well one can point to the object's image and what the statistical errors for time and range measurements would be.

2.2.5 Presentation Scale for SAR Images

The concept of *image scale* is deeply engrained in all practitioners of geoscience fields. It is therefore meaningful to relate this concept to SAR data.

This, however, requires that the concept of geometric resolution be made transparent. In the event that a geometric resolution can be described by a single length a in meters on the ground, it appears meaningful for analog data to rely on the Kell-factor to relate this to line-pairs per millimeter on film used to present the image to an observer. A number of n line-pairs per millimeter of presentation film permit one to hold $2\sqrt{2} \cdot n$ resolution cells in one millimeter. This leads to the image scale factor M of:

$$M = a \cdot n \cdot 2\sqrt{2} \cdot 1000 \tag{2.4}$$

where 1000 is used to convert the meters of a into millimeters.

Of course one can make a case for other presentation scales to be defined for digital data as is occasionally proposed by authors of so-called image maps. Colvocoresses, [10,11] argues that 3 pixels should be presented per millimeter for use with the unaided eye. The scale factor then is:

$$M = 3000 \cdot a \tag{2.5}$$

2.3 Geometric Distortions

A first question to ask about a SAR image is how it relates to map geomery. This leads to a description of the geometric differences, essentially employing deformation polynomials (Derenyi [19,18]) or other specific entities such as image skew, scale distortions in the major coordinate directions, non-linearity of the coordinate axes. A recent effort by Quegan [84] for SAR CV-580 data employed a regression line through co-linear ground control points

in both near and far range, thereby deriving a description of scale errors and non-linearity of coordinate axes. Topographic relief was not considered.

Since the purpose of the evaluation generally is only a crude statement about the image as a map substitute, the algorithmic complexity of such formulations is modest. As the SAR imaging geometry is not actually modelled, the range of possible techniques to merely "describe" major defects of the image is very large; every author is free to formulate his own tool to perform the analysis.

2.3.1 Slant Range Representation of SAR Image

The principle of side-looking SAR to measure the signal round-trip time for the determination of slant ranges to objects causes several types of geometric distortions. In a *slant range representation* of a SAR image the range to the objects on ground is used as the cross-track coordinate axis. As a matter of fact, these images are nonlinear in ground range. Ground range nonlinearities result from sampling the return echo data at constant time intervals. Since the radar look angle ($\angle$ between sensor-to-nadir line and sensor-to-object line) varies across the swath, the ground range distance represented by each sample Δr is not uniform. The effect is that features in the near range appear compressed with respect to far range.

For satellite-borne SAR the curvature of the earth is enhancing this distortion. For an assumed smooth spherical earth surface a slant range increment Δr is transformed into the ground range increment Δr_g by the approximation (compare [15])

$$\Delta r_g = \Delta r / \sin\varphi. \tag{2.6}$$

The incidence angle φ of the radar at the target can be related to the look angle θ by

$$\varphi = \arcsin\left[\frac{(h + R_e)\sin\theta}{R_e}\right] \tag{2.7}$$

where R_e is the radius of the earth, h is the spacecraft height, and the look angle is given by

$$\theta = \arccos\left[\frac{r^2 + (h + R_e)^2 - R_e^2}{2r(h + R_e)}\right]. \tag{2.8}$$

2.3.2 Terrain Effects

In addition to the ground range nonlinearities described above, severe distortions may occur if pronounced terrain relief is present in the imaged scene. The amount of distortions depends on the particular side-looking geometry and the undulation of the terrain surface. In many applications the terrain-induced distortions degrade the usefulness of SAR images or even prevent information extraction.

Foreshortening

This is the most predominant effect in SAR images of mountainous areas. Especially for small look angles, the differences in the cross-track slant ranges of two points situated on foreslopes of mountains are smaller than they would be in flat areas. This effect is illustrated in Figure 2.1. It results in an additional cross-track compression of the radiometric information reflected from foreslope areas and displayed in the SAR image.

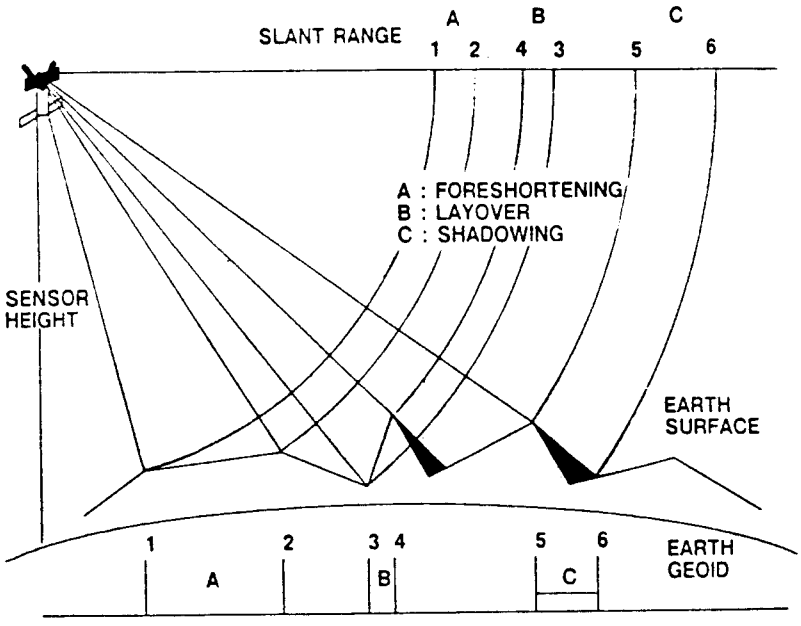

Figure 2.1: Sketch of foreshortening, layover and shadowing

Layover

If, due to the steepness of the slope, valley points of mountains have a larger slant range than the mountain top, the foreslope is "reversed" in the radar image (see Figure 2.1). Thus, the radiometric information in the image is the result of an ambiguous superposition of the response of many objects.

Afterlenghtening and Shadowing

The opposite effect to forshortening occurs at mountain backslopes. In the radar image the distance between two points is lenghtened (see Figure 2.1) or appears stretched in the image compared to true ground range distances.

For steep backslopes, the top of a mountain shadows parts of the scene and no radiometric information is collected there. Imagery from airborne sensors operating at shallow look angles is severely degraded in its usefulness by shadowing. Fortunately, the look angle of the orbital SAR sensor Seasat was very steep and even in very mountainous regions such as the Central Alps, only very few slopes were affected by shadowing.

2.3.3 Azimuth Distortions and Location Error

A correct phase reference function used in SAR processing is the prerequisite for the generation of images which are undistorted in azimuth direction. However, in many situations the phase reference is not known accurately enough, which results in azimuth distortions and in location errors of the image frame. The systematic error of uncompensated earth curvature and rotation results in an azimuth skew of the image (due to erroneous Doppler centroid frequency) and to a location error (due to erroneous Doppler frequency rate). For example, Lin et al. [76] have studied and quantified these errors for Seasat imagery.

2.4 Speckle

2.4.1 Definition

Speckle is an effect in SAR images that results from the fact that coherent radar pulses are reflected from the ground and constructive or destructive *interference* of echoes from the various parts of a distributed object within a resolution cell occurs. Differences in distance of only a fraction of the radar wave-length can lead to a stronger or a weaker return, depending on the exact shape of the object and its effect on the interference patterns. The power received at the antenna and the reconstructed SAR image density values are perturbated by interference effects. Although speckle is scene-dependent it must be considered as a random effect.

Speckle from homogenous scattering surfaces on the earth can be utilized for determining the response characteristics of a SAR sensor (e.g. Tilley [95]), i.e. speckle contains useful information. However, in the context of radargrammetry speckle causes numerous problems for SAR image analysis.

Many attempts are reported in literature to reduce the speckle effect. It has been established by various research workers that speckle reduction always is at the expense of geometric resolution, employing some sort of low-pass filter. A generally accepted technique is that of Lee [74]. A definition of the Lee-filter and results from applying it to airborne SAR images are given in Chapter 9.

2.4.2 Significance for Radargrammetry

Speckle is of great significance to radargrammetric measurements since one's ability of object identification is reduced. Automated feature extraction for object recognition is hampered; slope reconstruction from image brightness values is not feasible due to speckle; radar stereoscopy limits are set by speckle effects.

Speckle is part of the SAR process and cannot be avoided. Speckle reduction is of relevance to radargrammetry as it is of relevance to other processing and analysis tasks.

The effect of speckle on image point measurements deserves better understanding. Also the effect on radar stereopsis should be quantified. The degree and type of speckle should be quantified as it relates to wavelength, look angles and other system parameters. Then the effect on image applications could be predicted.

2.5 Specular Returns and "No-Shows"

Specular radar reflections also reduce the usefulness of radar images because they lead to either saturated returns blurring the image, or they lead to so-called "no-shows" if a surface reflects the electromagnetic pulses away from the antenna.

In mapping one is concerned particularly with cultural features, i.e. things that man makes on the earth's surface: bridges, roads, buildings, dams, etc. These objects have a tendency either to cause bright, specular returns, or they do not show at all, depending on their orientation relative to the radar looking direction. Man-made features can therefore only be identified in an incomplete manner when the geometric resolution suggests otherwise.

Much like speckle, specular returns are SAR peculiarities one needs to work with. They cannot be avoided. In fact, specular returns are more frequent as the geometric resolution increases, since the occurrence of radar-smooth (mirror-like) surface segments increases.

Specular radar returns can be useful in the analysis of man-made objects in very high resolution SAR. Specific objects may have specific signatures depending on the look direction and incidence angles. However, this is of little significance for geo-science applications.

Chapter 3

Processing of Single SAR Images

3.1 Geometric Processing

3.1.1 Introduction and Terminology

In Section 2.3 the geometric distortions which degrade the usefulness of SAR images are discussed, the worst among them being the cross-track terrain-induced displacements. For a comparison of the information contained in SAR images and topographic maps, or for comparison of images acquired by different sensors at different times and with different imaging parameters and the like, it is desirable to generate imagery with a common internal geometry and defined cartographic location. If different information sources can be overlaid, either cartographic referencing or, possibly, synergetic utilization of the data can be performed.

As a consequence of the complicated image formation process, the geometric rectification of SAR images is a sophisticated problem. In the following a number of possibilities for geometric transformation of SAR image data is discussed. An overview of the algorithms used by different institutions is given in the Appendix. Also the algorithms available at DIBAG are summarized there and some results obtained from tests which have been carried out during the contract are presented.

Before proceeding in the explanation of algorithms, the terms used must be made clear:

"Registration" or "relative rectification": One information source, be it a map or one of the remote sensing images to match, is declared to be the reference copy. All the other sources are modified in their image geometry to fit the geometry of the reference copy. Following this philosophy, matching algorithms are called *registration* algorithms, *merging* algorithms, or algorithms for *relative rectification.*

"Georeferencing": If one of the information sources is a topographic map, a special type of registration is considered, which will here be denoted as *georeferencing*[1], i.e. either the map will be registered to the SAR image, or the SAR image will be registered to the map—see Figure 3.1. The latter case will be denoted as

"Geocoding" or "absolute rectification": A *geocoded* SAR image is defined as having its image lines aligned with and registered to a topographic map grid. It possesses

[1] Curlander uses this term in a much different sense, i.e. he defines a "georeferenced image" to have its image frame aligned with the ground-track of the spacecraft and to have geometric properties not well-defined. This definition is not considered adequate by the authors.

the geometric properties of the specified cartographic projection. The geocoded product is sometimes also called *ortho-image* because it has been converted into an ortho-projection.

3.1.2 Georeferencing

Georeferencing algorithms (see Figure 3.1) are either relating image information to the geometry of a map projection, or, vice versa, three-dimensional map information to the geometry of a radar image projection.

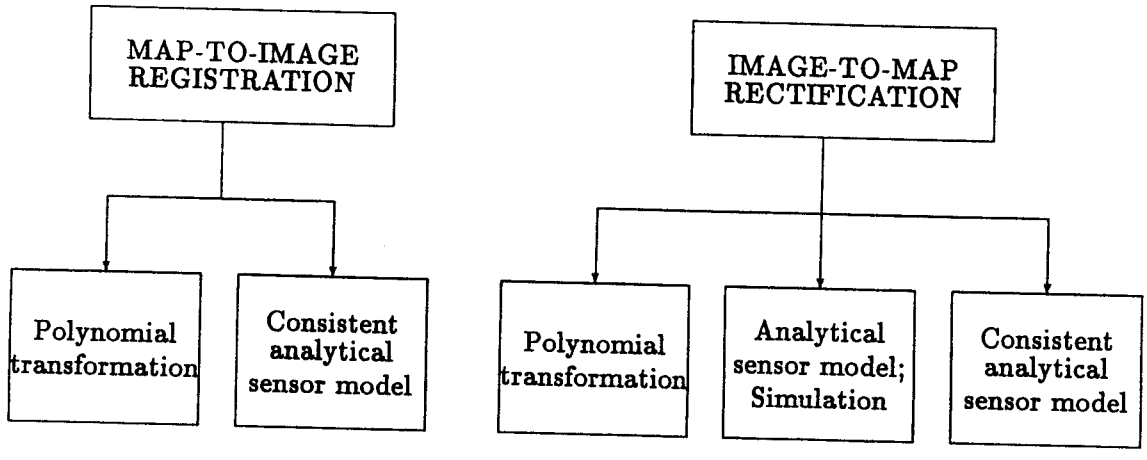

Figure 3.1: Overview of SAR Georeferencing Algorithms

The usual approach of *application-oriented users* is to rectify or merge images by using ground control points or homologue points and warping functions (usually polynomial functions of first or second order). More general algorithms, which make use of orbit parameters, flight positions, Doppler parameters and radargrammetric transformations, are not widely distributed. Integration of height models into digital rectification has only been approached within recent years:

Various geocoding algorithms have been suggested in papers by Curlander [15], Domik [25,23], Guidon et al. [38], Hoogeboom et al. [50], Kratky [57], Meier and Nüesch [79], and Raggam et al. [87]. An algorithm for map-to-image transformation is reported by Lukes and Raggam [77]. These algorithms are reviewed in the Appendix.

3.2 Single Image Grey Value Processing

3.2.1 Calibration

The radargrammetric significance of grey value or radiometric concepts may not seem directly apparent. However, as will be shown later, geometric processing relates intimately to radiometry, in particular when SAR data need to be "calibrated". This implies that one can relate a specific image resolution cell to the object area that caused the specific image density number (DN) of that resolution cell. It is thus immediately evident that geometric target positioning is an important tool for radiometric SAR calibration.

Calibration requires that

- the geometric x, y, z location on the ground is precisely registered to an image t, r position;
- the surface properties around the x, y, z location are well-known;
- the image density number DN actually is proportional to the received power at the antenna and not manipulated by image processing methods.

Surface properties include, apart from the terrain slope, the statistical power spectrum to describe surface roughness to reflected energy, as described by Ulaby et al. [98, equation (12.110)].

Surface roughness measurements can be made by photogrammetry. One current approach is by helicopter stereo-photography from altitudes of 15 to 25 m with a pair of Hasselblad cameras at a base length of 6 m and focal length of 100 mm. Achieved accuracies are about 2 mm.

3.2.2 Radar Clinometry

Radiometry is the basis for proposals to reconstruct the geometric object shape in a process called "radar clinometry" (Wildey, [100]). This is a single-image analysis technique best described by "shape-from-shading".

The technique exploits the fact that the received power P_a at the radar antenna is a function of the incidence angles. Therefore, one can argue that received power is a measure of incidence angle or terrain slope. This would only be true if the effects of other parameters were negligible, such as effects of dielectric constant of the material, surface roughness, moisture, specular reflection, shadow, layover etc. Another relevant perturbation factor is speckle. Therefore, proposals on radar clinometry do not produce the expected meaningful results.

3.2.3 SAR Image Simulation

SAR image simulation can support numerous analysis and mission planning tasks. There is a variety of systems currently available for image simulation, with an emphasis on faithfully predicting SAR DN-values as a result of radar-relevant surface properties, or with an emphasis on faithfully predicting image t, r positions when sensor path $\vec{s}(t)$ and velocity $\dot{\vec{s}}(t)$ are given. The concepts described in Section 1.2 are geometric concepts. Radiometric concepts are based on a variety of principles where the most complex elements relate to the simulation of speckle and geometric resolution. SAR image simulation is a widely studied topic, however concentrating on successfully predicting backscatter and noise instead of image geometry. Extensive work has been previously reported by Domik [22], Kaupp et al. [53,54], Holtzman et al. [48], and Smith et al. [94].

3.3 Object Recognition

The automated interpretation of objects and extraction of geometric properties can support a multitude of remote sensing applications, and can serve as a tool in speeding up various routine processing tasks. The first may be obvious in the context of long-time monitoring of environmental phenomena, or in the context of multi-dimensional data sets

too complex for human analysis; the second statement refers to tasks such as registering time-sequential images or image-map combinations. However, these techniques support the extraction of geometric information, and they are an essential tool in a number of tasks involving combinations of multiple image or images and non-images. Therefore, they are a thoroughly integral and important tool of radargrammetry.

In a single SAR image, object recognition can be based on only a limited selection of so-called "features":

- image tone;
- image texture;
- image shape.

Current terminology differentiates between *objects* in the real world, and *features* that are elements of a feature vector used to classify the image contents. Specific objects can be analyzed in the signal history data if phase, amplitude and frequency information is of relevance. This is the case with moving land targets, with ocean phenomena such as surface wave patterns and with polarization-relevant phenomena. Phase and frequency features will not be discussed here. Instead, we will only deal with SAR imagery.

3.3.1 Techniques Using Texture and Tone

Automated object recognition is generally done in two steps: first a number of features are extracted from the image and entered into a feature vector. Vectors are then classified. The major technique of SAR feature definition relates to texture and image brightness. Various texture measures have been investigated, however with limited results. Recent work has been done by Hevenor [47] with co-occurrence matrices, obtaining good results with four land use classes. Churchill et al. [8] conclude that texture is only useful if very distinct; otherwise it is corrupted by speckle to an extent that it becomes fully correlated with tone and carries no independent information.

SAR image tone is the sum of dielectric properties, roughness and slope. Since dielectric properties are volatile when moisture changes, and roughness dominates if slope is absent, tone is essentially indicative of surface roughness.

3.3.2 Field Classification

Workers in the field have proposed to form image regions by aggregating connected pixels of uniform properties, and then to classify the pixel aggregate (image segmentation prior to classification; or *field classification*: Binnenkade et al. [5]; Churchill et al. [8]). Segmentation in itself is , of course, also affected by speckle. Derin et al. [20] specifically address the speckle in a segmentation technique based on Markov random fields.

Wooding (1985) proposes to rely not on segmentation by statistical means, but to use existing maps or collateral data instead. Once the SAR image is segmented, proper features can be extracted and classification can follow.

The combined use of a single SAR image and collateral information will be further discussed in Chapter 5.

3.3.3 Edge Detection, Line and Contour Following

Object shape is determined by a contour. Although it is a major concept in the analysis of passively sensed imagery, there is no open literature report on line following in SAR images. This may be related to anticipated noise-type effects due to speckle. Also edge images from SAR suffer such limitations.

3.3.4 Suggested Focus of Radargrammetry-Relevant Object Recognition

It will be evident in the later chapters that automated SAR image analysis techniques are of great relevance to radargrammetry. Beyond this, object recognition is important for many forms of automated image interpretation involving more than a single image. There is a radargrammetric interest in fully understanding automated object recognition.

It is evident that single SAR images present a more difficult data source than common photographic imagery for automating the analysis process. This relates to speckle and the many effects contributing to the image grey value. Therefore the current concept of *image pyramids* promises particular value in image analysis where speckle effects are a major problem for texture measures, line definition and edge detection. Speckle removal is possible if the resolution is degraded: this is what an image pyramid achieves. Full resolution data are employed when a preliminary description of the SAR image contents exists. Chapter 9 will address the importance of pyramids on SAR images more closely.

For future research it appears essential that a comprehensive data set of differing wavelengths, resolutions, imaging parameters and land uses should be compiled and subjected to a structured set of analysis experiments to develop an improved understanding of the limitations of automated SAR interpretation and extraction of relevant geometric data.

Chapter 4

Processing of Multiple SAR Images

4.1 Introduction

The usefulness of SAR data over land has been traditionally limited because of the "competition" from other sensors. This is particularly evident with high-altitude aerial photography at scales 1 : 80,000 to 1 : 140,000, and with satellite scanning at pixel diameters of 10 m to 30 m, leading to scale equivalents of about 1 : 500,000 and up.

Recent work on radar imaging has led to significant new concepts such as

- multi-frequency SAR;
- multi-polarization SAR;
- multi-incidence angle SAR.

The Shuttle Imaging Radar SIR-C experiment is expected to create extensive data sets to evaluate the usefulness of these concepts. Meanwhile, aircraft SAR and SIR-B data are being used to further explore, in a preliminary manner, the prospects of additional dimensionalities of SAR data.

In spite of these advances, SAR has two distinct advantages that are absolutely unique and of particular value to the geo-science community:

- active illumination that penetrates any atmosphere, even with rain, fog or snow;
- sensitivity to surface roughness and dielectric properties of the material.

The other characteristics, such as incidence angle variation, polarization and choice of frequency variation, have not been a driving force to use SAR rather than other sensors. Therefore, it is unclear how various sensors compare if one requires the modelling of surface properties. The sensitivity of the various sensors to them and proper data analysis techniques are not well understood in a trade-off among individual sensors.

A question of considerable concern is therefore whether a combination of SAR with more traditional sensors would create an added value to geo-science work. One refers to this as *multi-sensor* data sets. However, the answer to the question is not clear. A number of workers have investigated synergistic data sets that consist of SAR and other, usually

passively imaged data. Indications exist that such data combinations are very useful. However, the prohibitively extensive effort that goes into the creation of such data sets keeps workers concentrating on image registration.

It is conjectured that workers in the field currently lack the proper tools to actually combine SAR and other data, and therefore are unable to evaluate the usefulness of multi-sensor data sets in an optimistic manner. This evaluation is dependent on the specific application fields, on many potential types of data, and on various possible ways of data utilization. Common to these is a need to create sets of data that belong together.

This leads one to suggest the creation of tools to produce *synergistic* multi-sensor image data sets.

Among the major advantages of SAR over all other sensors with comparable or higher geometric resolution, the *all weather capability* is by far dominant. Modern satellite remote sensing, on the other hand, is meaningful and competitive with airborne systems if repetitive coverages are desired. One could state that for any one-time coverage of even large areas, an aircraft-based approach is more economical, be it with photograpy, radar or scanning. At typical rates of US \$3.00 per km^2 for data acquisition and preprocessing, even a large territory such as Brazil with its 9 mio km^2 would be covered for \$27 mio. Given economies of scale, the entire land surface of the earth may well be covered with aircraft SAR for less than \$100 million, except for problems of national sovereignity.

However, once the high expenses for a satellite, sensor, receiving and data distribution systems are made, multiple coverages can be obtained for little added variable cost. Given this evident fact, it is only weather and sun-light that need to be cooperative if visible light sensing is to be used. Europe, for one, of course poses problems in this domain. SAR is unaffected.

SAR is therefore exceedingly well suited for monitoring tasks that require predictable imaging periods. Commonly discussed applications concern ocean ice phenomena, ocean ship traffic monitoring and monitoring in the event of natural disasters. Such phenomena require the joint use of several multi-temporal images. The major processing problem lies in the registration of the images or the data extracted from them.

The previously discussed new dimensionality of SAR data with varying incidence angles, frequencies and polarizations may also pose processing requirements that essentially consist of precision registration, unless the multiple data set was acquired in a single orbit. The latter is expected regarding frequency and polarization, not however, if incidence angles are to be varied.

One therefore could differentiate between two types of multiple SAR data sets:

- multiple parameter SAR data for improved analysis of static or near-static phenomena;
- time sequential SAR data for monitoring of changing phenomena.

Multi-temporal remote sensing data of large areas quickly become unreasonably and unnecessarily voluminous since they will present considerable redundancy. This is not an unavoidable situation if proper processing techniques are available.

This leads one to suggest that concepts and tools should be developed to master repetitive SAR coverages of given areas.

4.2 Multi-Parameter SAR

4.2.1 General

Recent research provides indications that specific thematic geo-science applications can benefit from multiple SAR-images of differing parameters such as:

- wavelength;
- look-angle off-nadir or incidence angles;
- polarization;
- flight direction.

The question of look angles, frequency and polarization have been investigated in geology (e.g. Bloom [6]), in vegetation mapping using scatterometer investigations in Kansas and Ann Arbor (e.g. Ulaby et al. [97]), and with snow and ice (Waite et al. 1970). Essentially, polarization and frequency variation do not require geometric image processing since data are inherently registered through simultaneous acquisition.

Application of look-angle multiplicity requires that different SAR images be registered to one another; again, these images are dissimilar since illumination changes; however, they are all still SAR.

Churchill et al. [8] and Quegan et al. [85] have reported on multiple SAR image data sets for agriculture, forestry and land use. Binnenkade et al. [5] discuss an agricultural data set of several similar images. The conclusions are qualitative. The significance of incidence angles has been investigated by several authors, such as by Waite et al. (1982), and by Kaupp et al. [53]. Elachi [28] introduced the concept of *incidence angle signature* and referred to work with SIR-B data, a major source of multiple incidence angle SAR images (Cimino et al. [9]). These publications show that the incidence angle signature may be a significant parameter to classify certain geo-scientific objects. Therefore, sub-pixel matching of SAR images with different illumination and incidence angles is required.

4.2.2 Methods of Matching

In the event of flat terrain, any geometric differences between two SAR images should be removable as systematic effects. *Geocoding* of the individual images should lead to a high accuracy of the matching of separate images.

In the event of mountainous terrain, one encounters the same difficulty as in radar stereoscopy and in efforts of matching dissimilar images. Edges may have immigrated from one to another image because of

- shadow differences;
- specular point migration;
- layover differences;
- variation in azimuth angles.

Therefore, limits exist for the quality of image correlation techniques. To overcome them the image matching method would have to be complemented by grey value corrections, also called *radiometric rectification*, to undo the edge migration due to relief and illumination differences. This concept has not yet been studied. An additional supporting concept is the use of image pyramids to obtain preliminary matches that in turn lead to the support of refined matching methods.

If, in addition, one image is from an ascending, the other from a descending satellite orbit, one may encounter large incidence angle differences and considerable differences in the two images. This is expected to lead to low correlation coefficients and noisy correlation peaks. The extent of these limitations is not understood and needs to be explored.

An additional matching concept could be along the lines of the *object-oriented* method outlined in Section 3.3.

4.3 SAR Stereopsis

4.3.1 Concepts and Background

The previous discussion addressed individual SAR images and was based on a considerable body of literature and reported experiences. Processing of pairs of SAR images for stereopsis, or reconstruction of the 3-dimensional terrain shape, is much less frequently discussed. The fact that a valid and stress-free stereoscopic impression is obtained when an observer views two SAR images has been known since LaPrade [64] reported first experiences.

A certain interest in the possibility to create topographic maps from stereo-radar images peaked during the early 1970's; achievable accuracies were, however, too poor to pursue the possibility further (about 5 times range resolution). At that time, a number of publications produced the fundamental mathematical formulations (Rosenfield [92]; Gracie et al. [34]; Leberl [68,65]). Even equipment was built (Graham [35]; Yoritomo [102]). The work and research suffered from a lack of appropriate data; overlapping radar images hardly existed. However, it was well understood that there is a basic imaging configuration that leads to meaningful images: the so-called same-side radar stereo case. Other arrangements were judged not to be usable (opposite-side, cross-wise). Stereo-geometries were poor due to minute stereo intersection angles (5 to 10 degrees). Essentially, they were only used to support visual geomorphological image interpretation in the later radar reconnaissance mapping projects of the tropical belt.

The situation changed with the advent of satellite radar. The following new elements applied:

- look angles off-nadir became a near-constant across the swath;
- look-angle disparities could be made much larger than from aircraft (30 degrees or more);
- platform stability is much higher in the satellite than in an aircraft;
- SAR images now were digital and subject to computer manipulation;
- stereo-measuring machines now were *analytical* or computer-driven and processing of stereo-SAR was feasible without hardware developments.

These facts, the realization of the usefulness of stereopsis for thematic analysis, and the need to consider slope effects on radiometric SAR properties, led to a renewed interest in stereo-radar.

Currently, available SIR-B radar image pairs are the subject of several thorough stereo radargrammetric analyses. First results indicate that raw SAR images at a look-angle disparity of 25 degrees provide a thematically appealing stereoscopic impression. Measurement accuracies, however, are less than error propagation led one to hope for. The reason for this is still subject of speculations and needs to be further investigated. Speculations suggest that

- look-angle disparities in two images lead to thematic disparities of image contents that make it more difficult to fuse the stereo model as disparities increase;
- speckle reduces one's radar stereo-acuity;
- specular point migration may reduce stereo-viewability or even lead to false matches.

It appears that major obstacles to exploiting the expected accuracy potential of stereo radar are caused by thematic disparities which in turn are the result of topographic relief. These disparities are thus not simply perturbations or noise, but carry information about the shape of the terrain surface. This may suggest that the classical stereo-technique of passive images that is solely based on geometric disparities (*parallaxes*), should be combined with *shape-from-shading* concepts when dealing with active sensor data.

4.3.2 Geometric and Thematic Disparities in Overlapping Radar Images

Visual stereo fusion is the result of an image match or a "registration". Geometric disparities along the eye axis are perceived as "height". Geometric disparities perpendicular to the eye axis are perceived as a degradation of the stereo-effect. Thematic disparities due to differences of illumination are also perceived as a degradation of the stereo effect. Speckle and geometric resolution limit the so-called *acuity* of defining a terrain surface. SAR stereoscopy is an *odd* phenomenon. Photographic stereoscopy is a direct analogy to natural binocular viewing of the environment. The eye performs like a central perspective device and presenting it with a photograph instead of a natural scene is geometrically entirely equivalent.

Presenting the eyes with a SAR image pair is not an analogy to presenting it with a natural scene: the two SAR images have different contents due to differences in illumination which in turn lead to differences of

- image brightness,
- specular returns,
- shadows,
- speckle.

Conceptually, the two SAR images have geometric differences only along the range directions. If these directions coincide then the only geometric disparities that should exist between the SAR images can be perceived by an observer as a stereo parallax. This would

be the same as when one perceives a stereo model of a central perspective photograph after the so-called *relative orientation* of the photographs. It is also similar to perceiving a stereo model formed by a pair of photographic "strip" images or of scanner images.

The range directions of two SAR images coincide if the two SAR flights are parallel. One can demonstrate that also non-parallel flight lines can produce viewable stereo SAR image pairs, as in SIR-A (Kobrik et al. [55]); this is the result of the fact that the eye can sustain a limited amount of so-called "y-parallax", or geometric disparity of the two images perpendicular to the eye base.

4.3.3 Stereoscopic "Acuity"

No experiments have been reported on the stereo acuity of an observer as a function of the various influencing factors. Simulation-based predictions were performed by Domik [22] and Kaupp et al. [53], but results may be of limited value due to the nature of the simulations and the judgemental nature of the subjective evaluations.

An evaluation of visual SAR image matching performance is only feasible via the measurement of terrain coordinates. This combines all effects on acuity as well as factors unrelated to acuity such as geometry and geometric deformation. A detailed study of matching performance as a function of individual influencing factors can be based, however, on computer image matching: image *similiarity* can be quantified, and acuity can be expressed by correlation factors.

The mere inspection of a number of SAR image pairs quickly shows that one must anticipate the ability of stereoscopic fusion of SAR images to depend on:

- look angles off-nadir;
- look angle disparities between the two images;
- terrain type or extent of topographic relief;
- absence of geometric image defects such as along track scale variations;
- the extent of speckle.

4.3.4 Vertical Exaggeration

One regularly finds that the *quality* of a stereoscopic model is discussed with the help of vertical exaggeration. This uses the ratio between the width of a pyramid over its height, and relates this actual ratio to the subjectively perceived one. An exaggeration factor 1 describes a stereoscopic arrangement where dimensions are perceived as they are in nature. An exaggeration factor 3 shows height scale three times larger than the horizontal scale.

Vertical exaggeration is a purely geometric concept. It does not deal with vertical resolution nor with the quality of the subjective stereofusion. It does, however, relate to the size of the stereo-parallax that a particular height difference creates: a larger parallax produces a larger vertical exaggeration. It is thus directly proportional to the so-called "base-to-height" ratio of photographic stereo pairs.

Vertical exaggeration in SAR image pairs does not need to be smaller than in conventional photographic stereopsis, where it commonly reaches a value of 3. In radar data, it may be somewhere between 1 and 5. In fact, it can be easily shown that vertical exaggeration normally is larger than in photography when small look angles off-nadir are used.

4.3.5 Quality of SAR Image Matching

It was stated before that it is not possible to judge the quality of stereoscopic SAR image matching simply from an evaluation of the accuracy of terrain height observations. Instead it is meaningful to address this question by machine correlation of overlapping SAR image segments. Thus far, SAR image correlation work has only been published by Ramapryan et al. (1985) in the context of SIR-B using the massively parallel processor (MPP). The match quality was not investigated.

The essential question is the effect of thematic differences of image contents on the quality of the match. In terms of image matching algorithms, two SAR- stereo mates are "dissimilar", with the dissimilarity increasing as the two illumination directions subtend larger intersection angles.

4.3.6 Speckle

The SAR image speckle is unknown to photography. Therefore the current body of know-how on stereoscopic vision does not include conclusions on the effect of speckle. It is not identical to graininess of photographic images; this graininess is more related to geometric resolution than to speckle.

The lack of analogy is reason for the fact that speckle is not understood in its effect on SAR-stereopsis.

4.3.7 Opposite-Side SAR Stereopsis

Illumination, and therefore imaging, of a given terrain by two imaging passes with coinciding range coordinate axes can be with illumination from two sides. This helps to achieve maximum geometric disparities (size of parallaxes or vertical exaggeration), and to minimize also thematic redundancy: in one image certain back slopes may not be imaged if they were in a shadow, but they would not be in a shadow and show up as front slope on the other image. However, lack of redundancy destroys the stereo-effect. Opposite-side SAR image pairs of accentuated terrain generally cannot be viewed in stereo.

Recent experimental work indicates that through some image processing manipulations, the two opposite-side SAR images can be made to look more similar and can become stereo-viewable (Fullerton, Leberl and Marque [32]). Insufficient results are available to evaluate the usefulness and quality of the stereo-model.

4.3.8 Accuracy and Digital Elevation Models

The currently available SAR stereo accuracy values are typically the result of single, unique image pairs. A coherent evaluation of accuracies as a function of various parameters was impossible due to the lack of available data. The only parameter studies for accuracy evaluation addressed theoretical error propagation.

The major limitation of error propagation modelling is the fact that it is purely geometrical and neglects the thematic quality of the stereo image match.

Past studies reported coordinate accuracies in SAR-stereo models ranging from 1 to 15 times the range resolution. Examples include the work of Gracie et al.[34], achieving a height error of 13 m with a radar system resolving 17 m (AN-APQ 102). Goodyear [33] reported errors of 93 m with its GEMS radar, resolving 12 m. The same radar was used by Derenyi [19] and led to errors between 33 m and 177 m. DBA-systems [17] obtained 17 m to 20 m errors with a resolution of 3 m.

It was only the SIR-B experiment that actually created sequences of SAR-images that permit one to form several SAR stereopairs of one area, but with different illumination angles (33 to 56 degrees) and look angle disparities (5 to about 23 degrees). The only results thus far obtained are by Leberl et al.[70] and report height errors of 55 to 100 m from a SIR-B range resolution of 14 m. A major discovery of this experiment consisted of the observation that accuracies did not necessarily improve with increasing intersection angles. Additional SIR-B stereo-imagery exists, including also one opposite-side pair. This will still need to be analyzed.

The above accuracy results lead one to conclude that as illumination angles differ more, the quality of the stereo-fusion deteriorates and thereby sets off any gains achieved by a better stereo-geometry.

The question regarding an appropriate spacing for a digital elevation model (DEM) obtained from SAR can be answered if the height accuracy is taken as the input. In photogrammetric DEMs the point spacing is recommended to be about 10 to 20 times the accuracy of individual height points. With height errors e.g. of about 5 times the range resolution, the DEM interval d would be

$$d \leq 50 \cdot \sigma_r \tag{4.1}$$

where σ_r again is range resolution.

4.3.9 Ortho-Images from a Radar Stereo-Pair

It can be concluded from Sections 3.1.2 that three-dimensional information about the surface of the terrain has to be employed in the geocoding procedure if one wishes to obtain accurate results for mountaineous scenes as well. In case of the algorithms described for single radar image rectification, this information source consists of a digital elevation model, probably in a proper modification.

However, the three-dimensional information also could be derived utilizing the three-dimensional impression obtained from overlapping radar imagery and *radar stereo evaluation*. A number of software developments and experiments have been carried out at DIBAG in radar stereo-evaluation with analogue radar images:

The software package SMART (Stereo MApping with Radar Techniques) has been developed for mapping with stereo radar images on an analytical plotter (DSR-1, Kern). It includes the possibility of recovering the geometric image acquisition parameters by a radar resection-in-space, that is based on radar projection.

For geocoding, radar stereo-images could be used in one of the following ways:

- A DEM is already available for the imaged area. In this case geocoding can be done in the common way for each of the two images seperately. In case that the geometric image acquisition parameters are improved by means of a radar bundle adjustment, the homologue information given by the two images can be used for this procedure.

- A DEM can be derived from the radar stereo pair, e.g. utilizing the software system SMART. Rectification of the image pair can be done subsequently in the same way as described in the above first item. A demonstration study concerning this procedure has been presented in Domik et al. [25].

- Rectification of one or also of both stereo partners could be done based only on the homologue information of the two images and without utilizing a digital elevation

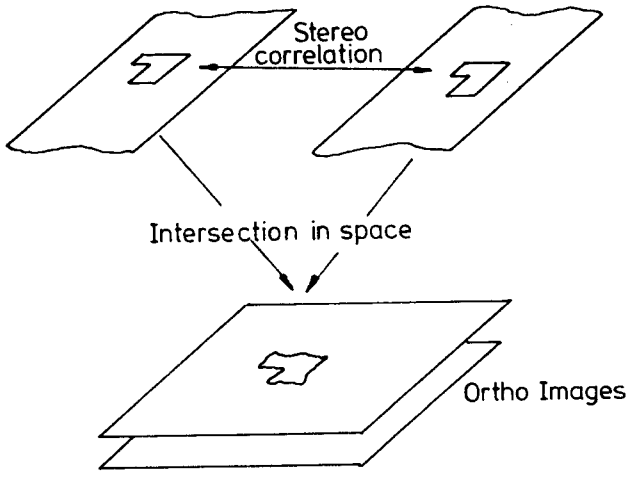

Figure 4.1: Geocoding using radar stereo-images.

model. After the restitution of the image acquisition parameters for both images the rectification procedure might consist of processing steps as follows:

- identification of homologue image points
  - * manually or
  - * automated with digital stereo correlation
- intersection of the two projection circles defined by the homologue points. This leads to the object point coordinates of these points and thus to their location in the geocoded image.
- resampling of a grey value for one or both of the stereo-partners

The philosophy of this procedure is illustrated in Figure 4.1.

4.4 SAR Image Time-Series

Long-time monitoring of rapidly changing phenomena such as sea-ice motion, ship traffic, and natural disasters, may be similar to reading newspapers: only the changes and the most recent one are of interest. Old ones are only kept for historical interest. One deals with a problem of *image sequence processing.*

A specific processing strategy is required to efficiently monitor such ephemeral phenomena.

Multi-date images have a different application in the event of a significant time-signature of an object to be studied. As has often been emphasized in agricultural and vegetation work, seasonal changes in the object are of relevance to the analysis and can support the automated crop classification. However, such complex tasks as crop harvest forecasting requires data far in excess of a set of multi-temporal SAR images.

Therefore it is suggested to concentrate on the development of technology for, and experience with, the processing of multi-temporal SAR images for monitoring of ephemeral phenomena. This potential application is favored by repeatability of SAR coverages from satellites, and by the day-night and weather-independence of SAR imaging.

4.4.1 Methods

Multi-temporal or multi-date SAR image processing has not been the subject of published work. References to "image time series" were made by Leberl et al. [71], Hall and Rothrock [41], Kobrick et al. [55] and in various other sea-ice motion and monitoring work. Processing has been rather straightforward geocoding of individual images and manual interpretation of changes. An operational application of a spaceborne SAR to ice monitoring cannot be meaningfully based on manual work since it would be far too tedious.

Therefore new concepts must be developed for the future.

Similar to the *object-oriented* matching of dissimilar images it is proposed to segment and analyze an initial source SAR image. As a result one obtains a data base describing the then current status of the changing phenomenon and the unchanged environment. The data base can be organized in a manner of digital map data.

Multi-temporal image analysis is then the comparison of an image with a non-image data set, representing the description of the phenomenon. The *map data base* is a very relevant spatial/symbolic description of the scene containing radar-specific elements. A new image is matched to the existing data along the lines of *map-guided image analysis* (Leberl and Kropatsch [72]). The data base is updated. It is likely that the process will not be entirely automated but be monitored by an operator. This concept is new and therefore not implemented. As a result, no literature and no experiences exist.

The usefulness of satellite SAR for monitoring phenomena needs to be clearly understood and work in this area should be initiated. There is an issue of technology acceptance and of recognizing opportunities to improve the flow of information regarding changing phenomena.

Geocoding of individual images and subsequent manual change mapping is too tedious for expected operational systems. Automated change mapping is required. This implies the most difficult image analysis operations to be applied to dissimilar images.

Object-based approaches to SAR image sequence analysis may provide a means to control an otherwise unmanageable data stream from satellite SAR sensors.

4.5 Mosaicking

4.5.1 Concept

More than two overlapping images that cover a larger area are denoted as a radar *image block*.

Image blocks are typical of operational applications: single images are typical of small study areas. Processing an image block may result in an image mosaick. Automating this process is of value if many images and high data rates are involved.

If the individual images are transformed into a world coordinate system using predicted or observed ephemeris data one refers to "dead reckoning". One needs to anticipate that the result is erroneous so that the use of ground control may be advisable.

Questions on image blocks therefore concern the tieing together of the images to subpixel accuracy to eliminate discrepancies, and to fit the result to a ground coordinate system. This fit could be achieved by treating each image independently; however, this could mean that unnecessarily many control points be available to achieve a required accuracy. Also it would not ensure that overlapping SAR images fit together seamlessly.

One can explain a control point based SAR image block problem by referring to a simultaneous computation of many resections-in-space that need to satisfy the constraint

that each image must fit its overlapping neighbors.

Radar blocks employ ephemeris data, match or tie-points and ground control points. Tie-points enforce that overlapping images, after transformation, fit together; ground control transforms the combination of images into the world coordinate system of the objects and serve to remove the effects of erroneous ephemeris data.

Image mosaicks are of importance over sea ice, in large, previously poorly mapped areas, and for systematic archiving of images. The result of an image block computation is a set of computed, dense auxiliary points that can further serve to treat each image or stereo pair as if it were of an area with many ground control points. A key element to automating the mosaicking task is the definition of tie-points in an autonomous manner. This requires a solution to the problem of image matching when images are dissimilar.

4.5.2 Current Status

Only a few publications exist on radar image block computations (*block adjustment*): examples are by DBA Systems [17], Leberl [66,67], and Dowideit [26]. However, any operational application to large areas should be concerned with the concept. Operational applications have not dealt with geometric rigour and precision. Block computations were replaced by simple manual image mosaicking.

The four publications address the computational techniques when 3 or more SAR images form what can be called a minimum-size "block". Dowideit [26] modelled the flight path by Fourier series of trigonometric functions, DBA- Systems [17] by polynomials. Leberl [66], [67] developed an operational system for large, unlimited numbers of SAR strips and applied it to blocks of 24 and 120 strips in W. Virginia and Colombia. Flight paths are modelled by joint polynomials (splines).

Satellite radar images have not been the topic of block computations since no large areas have been covered by several overlapping images that found an application. However, satellite data streams have begun to be subjected to automated mosaicking (Curlander [16]). The need of pixel and sub-pixel accuracy will require that satellite images be subjected to precision computations involving both ephemeris data and ground control points. However, the image deformations in satellite data are very small when compared with aircraft data and data quantities are larger than from aircraft. Therefore, methods would emphasize automation of the task rather than sophistication of the radargrammetric approach.

Chapter 5

Combination of SAR and Non-SAR Data

5.1 Concepts

The usefulness of a single sensor data set may be increased by adding it to, or to it, data that already exist from other sources. Such sources can be:

- maps;
- graphical data in a data base;
- digital terrain models;
- non-graphical thematic data about a region;
- analysis results from other types of imagery.

This obvious concept has no tradition in photogrammetry. New photographs generally are used to create a new map or new data to replace the old ones, or to update them so that old data become redundant.

The above is not relevant with SAR. Radar images are sufficiently different from photography that the image contents are not redundant with available maps, and available maps may not need to be old or inaccurate to not show the details contained in SAR-images.

It is therefore proposed to consider the utility of new remote sensing products, namely a combination of available maps and new SAR-images.

The current review cannot discuss such new products since there is no work that has been reported. What can be reviewed are techniques of matching radar images with maps and digital elevation models so that from it new products can come into existence.

5.2 Non-Remote-Sensing Data

5.2.1 Matching Images and Maps

An obvious method to match an image with a non-image such as a map or DEM employs methods which have been denoted as *georeferencing* methods. These methods include map-to-image and image-to-map matching and is described in Section 3.1.2.

5.2.2 Matching Images and Non-Spatial Data

Should data be related to political districts or be otherwise non-spatial, then a spatial presentation must first be created, e.g. by a thematic representation of values per political district.

This iconic product can then be registered to the SAR image using techniques for maps.

The above applies equally to data from geophysical or geochemical measurements: via a transformation to an iconic form the matching task is one involving two dissimilar images.

5.2.3 Secondary SAR Image Products

To facilitate subsequent uses of SAR images, and combinations of these with other data, one can produce secondary image products from the primary inputs.

Table 5.2.3 (from Domik et al. [24]) is a listing of various image products. No studies exist to attach any value to some of the proposed products. However, some of them have analogies in photogrammetry. This can lead to the expectation that SAR-ortho-images, geocoded images, and stereo-ortho-images may be the accepted form of presenting a SAR image. The DEM is implicitly displayed in this case since it served to perform the geometric SAR image transformations.

5.3 Multi-Sensor Combination

5.3.1 General

Multi-sensor processing can be based on the concept of geocoded images. In this concept each raw image is separately converted to an geocoded, in the expectation that the component images of a multiple set register by pixel.

Existing literature contains numerous references to efforts where SAR is compared to, or combined with, other images. Early reports were by Murphy [81], Anuta et al. [2], [3], Murai and Maeda [80], Evans [29], and many others, all relating Landsat-MSS data to Seasat-SAR. Mader and McCandless [78] registered Seasat-SAR and Landsat-RBV images. Authors generally report that registration with conjugate tie points is difficult because the same details are not identifiable in two image types.

Combination of data from different sensors were created by Rebillard et al. [90], presenting a SIR-A and SEASAT image set; Rebillard and Evans (1983) co-registered Landsat-MSS, SIR-A and Seasat into a 9-dimensional data set for geological application. Classification accuracies improved from 60set.

Forestry data were extracted from a Landsat-MSS image combined with aircraft radar by Guindon et al. [40]; MSS-SIR-A combinations were by Wu (1985). Classification accuracies improved from 70the data. Crop classification with radar-MSS synergies were attempted by Eyton et al. [30], Li et al. [75], Nüesch [83] and others.

5.3.2 Manual Methods of Matching Multi-Sensor Images

Common methods of image matching are manual: the user attempts to find conjugate image features of the same object point in the various images.

Table 5.1: Types of secondary radar image products based on multiple radar images and digital elevation model (DEM).

Type of Product	Comment
1. Ortho-Image	Geometrically rectified black and white image to fit a map.
2. False color image from multiple ortho-images	Use three geometrically matched ortho-images.
3. Simulated radar image	Use of DEM to predict the geometry and radiometry of a radar image, based only on terrain slope and assumed backscatter of surface cover.
4. Radiometrically rectified image	Difference image between simulated and real radar images.
5. False color image from multiple radiometrically corrected images.	Use three radiometrically corrected images.
6. Stereo ortho-images from one single image	Create an image pair of which one is geometrically corrected, the other is the same radar image but has artificially introduced relief-displacement (so-called "stereo-mate").
7. Stereo ortho-images from two source images.	As in item 6, but the "stereo-mate" is produced from a second overlapping radar image.
8. Composite radar image and DEM	Radar image brightnesses are added to an artificially illuminated DEM to represent the relief in conjunction with the radar image.
9. Topographic radar image map	Composite of an ortho-image, contour lines and planimetric map detail (roads, settlements, names, legend, coordinate grid etc.).
10. Thematic radar image map	Composite of an ortho-image and planimetric detail from a thematic map.
11. Perspective view of DEM and image density numbers	Same as item 8., but presented as a perspective camera image, to further enhance topographic relief.

In order to create a useful multi-sensor image data set, matching should be with a sub-pixel accuracy. However, this would require that any geometric disparity be removed with the help of a very large number of tie points . This may prove to be an unrealistically difficult task when considering that objects look very different in a SAR and optical image.

In addition, the accuracy of individual point identification needs to be within sub-pixel levels. Again, also this is a non-trivial problem.

As reported by Mader and McCandless [78] and others, dissimilarities among images can make it entirely impossible to actually find sufficient homologue or conjugate features.

One procedure that has not been explicitly tested and evaluated would employ *features* instead of match points. In this case the dissimilar image segments would be shifted manually with respect to one another until an operator finds an optimum fit between the feature patterns that are shown on both images. In this event it is the visual (or automated) evaluation of context that leads to the match rather than the monoscopic identification of point-like features.

The different sensors present different sensing geometries and responses to illumination, either by the sun or the active sensing system. This is most notable when mountainous terrain is studied. The input images need to be pre- processed to achieve a degree of similarity. Preprocessing should consist of:

- geocoding each image;
- radiometric rectification.

One concept has recently been illustrated by Bloom [6] where a Landsat-TM image is presented with a SIR-B image in a stereoscopic mode. This is feasible if grey-values are dominated by relief effects. In the event of Landsat, this is by sun-illumination and shadows, in the event of SAR, it is the well-known sensitivity of terrain slopes to SAR illumination angles.

5.3.3 Automated Matching by Image Correlation

Image matching by correlation is difficult when the two images are dissimilar. At times grey-value based methods are not even applicable if two radar images alone need to be matched and flight or look directions are not parallel.

Image correlation is only applicable when component images show a high degree of similarity. After all, correlation is a mere method of "similarity detection". One may argue that grey values are of course variant from one sensor to another, but edges are not. If this is the case, then one can expect a good fit among two images by correlation of edge images (Yao et al. [101]).

The assumption of the invariant edges may create instability of the method in cases where they are variant. The extent to which a certain invariance can be correctly assumed would need to be examined. Guindon [37] reports on experiences with automated correlation of an airborne SAR and airborne optical image in the format of Landsat-TM. The accuracies amounted to two to three pixel diameters; pixel diameter was 7 m. without a careful evaluation of the types of images, illumination angles and other conditions, it is not meaningful to generalize from this singular experience.

5.3.4 Automated Matching Based on Objects

An alternative to automated correlation is the development of an interpretation of the contents of one image and to project this onto the terrain surface, possibly represented by a DEM. Then a *map-guided* search can be performed for the same objects in the other image. This method would be applicable in both directions: from image 1 to image 2 as well as vice versa.

It is proposed to call such a technique *object based matching* of dissimilar images to differentiate it from a pixel-based method.

Rosenfeld [91] have investigated the matching of dissimilar images after a dense set of image points was identified. The problem was to find the conjugate points in the two point patterns. The paper dealt with the problem of associating points in two point patterns; however, this may be secondary: the major problem may be to identify points with a high probability to also be present on another image.

Chapter 6

Software for Radar Remote Sensing

6.1 Introduction

Recently efforts of different institutions became apparent to make radar software and software products available to the user community in better quality, in higher quantities and in less time; e.g. at JPL with Curlander's "End-to-End System Considerations" (SIR-B Symposium in April, 1986), or at DFVLR with the system UPSTAIRS. Whereas these two systems include raw signal processing facilities, they also produce geocoded output images. Other sources of radar software derive from the recently finished program AgRISTARS, NASA sponsored programs and studies (e.g. the SIR program) and, last but not least, as results from ESA programs and studies at different European institutions. The forthcoming launch of ERS-1 makes the need for this software much more urgent; the high amount of data to be expected and to be processed asks for software in three levels:

1. Software to *correlate* the SAR signals into images (SAR processor software);
2. Centralized software to *exploit* radar images and create *secondary radar image products* (e.g. geocoded images, mosaicks) for end users; and
3. Software like under item 2 but for radar workstations for those who want to investigate on their own.

This chapter is dealing with items 2. and 3., i.e. with software that is relevant to exploit radar images, and radar images combined with information from other sources. Emphasis is put on radargrammetric image exploitation and related phenomena as this has been a major merit of DIBAG since its formation.

The overview of relevant software modules given below for radar image data exploitation attempts—from the current view—to be as complete and up-to-date as possible. Part of the suggested software modules already exist in a laboratory environment at DIBAG, are currently in a testing phase, are presently under development, or are existing as design ideas.

6.2 Radar Software Libraries

The following describes the software modules found necessary to exploit radar images in their single form, as stereo- or multiple images, or together with data from sources other

than radar.

In the first outlines of the software specification program which has been conceived to be part of the contract, it has been argued that the current effort should lead to three software libraries, namely:

RIDE , Software for **R**adargrammetric **I**mage **D**ata **E**xploitation;

MUSICA , Software for **MU**lti-**S**ensor **I**mage **C**ombination and **A**nalysis; and

PRITS , Software for **P**rocessing **R**adar **I**mage **T**ime **S**eries.

Currently, methods for single and stereo radar images are much farther developed than those for the use of multi-sensor data and radar time series. Thus no specific software modules could be suggested for MUSICA and PRITS during the contract. Instead it is suggested to perform more exploratory work to lead to a better definition of tools required for multi-sensor and time-series data.

So far, work with multi-sensor images and radar time series reflects mainly treatment series of single images. An efficient way to gather experience might be to use the software suggested under RIDE; general image processing software and utilities as described below; and software to exploit images from sensors different from radar (Landsat MSS and TM, SPOT etc.).

It is anticipated that innovative software tools for MUSICA and PRITS will need to be embedded into general purpose remote-sensing software much like UPSTAIRS, VICAR, LARSYS or similar. Studies carried out in this type of environment will classify the issues and thus further refine software specifications for MUSICA and PRITS.

6.3 The Software Library RIDE

6.3.1 Software Overview

Software for RIDE will need to contain capabilities for

(a) Single Image Setup and Data Extraction

(b) 3-D Reconstruction and Data Extraction

(c) Geometric Image Analysis

(d) Geometric Rectification (Geocoding)

(e) Radiometric Manipulations

(f) Alternative Image Representations

Table 6.3.1 provides an overview of basic radargrammetric software which essentially should be contained as modules in the library RIDE.

Image segmentation, feature extraction and image classification will be desired additional tools to be made available: for once, because the radargrammetric tools are used to obtain geometric fidelity or correct registration of images, but most applications want to exploit the image content; or, because geometric information should be extracted from the images. The decision on the organisation and algorithms of such modules will have to be generated from current literature with emphasis on previous ESA studies with such content.

Table 6.1: Overview of Software Modules for RIDE

SINGLE IMAGE SETUP AND DATA EXTRACTION	3-D RECONSTRUCTION AND DATA EXTRACTION
Input of Parameters	Parallax Removal
Ground Point Management	Bundle Adjustment of Stereo Pair
Inner Orientation	Automatic Correlation
Bundle Adjustment for Single Images	Extraction of Height and Planimetric Details from Stereo-Images
Shape-from-Shading	
Map-to-Image Correspondence	

GEOMETRIC ANALYIS	GEOM. RECTIFICATION (GEOCODING)
Image Simulation	Image Warping
Image Statistics	Rectification using DEM
Incidence Angle Map	Mosaicking
	Scaling/Rotating/Slant-Ground Range Conversion

RADIOMETRIC MANIPULATIONS	ALTERNATIVE IMAGE REPRESENTATIONS
Slope Effect Reduction	Stereo Ortho-Images
Filters	Perspective Views
Correction for Systematic SAR Effects	Topographic/Thematic Image Maps

6.3.2 Software Environment for RIDE

RIDE should be considered to be the radar-specific image processing software module within a complete image processing environment for remote sensing. A general image processing module, other sensor-specific modules, project-specific modules and a general utility package should stand aside the radargrammetric capability. A defined programming interface to data base, network driver, dialog manager and to a virtual display system would be a requirement for transportability of software; not to forget the requirements for a comfortable user shell.

DEM-Related Software

Somewhere in such a comprehensive system capabilities should be forseen for generation, manipulation, storage and retrieval of digital elevation models. Capabilities should be available for:

(a) Input: Digitize and scan maps; create square grid DEMs; transform DEMs between projections;

(b) Output: Quickplots for quality control; axonometric view plots; contour lines plots; output of raster files, e.g. via digital numbers or symbol overstriking;

(c) Vector-to-raster conversion; Contour-to-grid conversion;

(d) Manipulating DEMs: Create statistics, including heights; slopes; exposition. Illumination. Function to edit, rotate, mirror and resample. Display through color coding or grey value presentation of heights. Transform to correct for earth curvature. Smoothing;

(e) Geometric Transformation of DEMs between different map projections;

The software listed here is available at DIBAG in the program package GTM (Graz Terrain Model). A critical point in radar-related work is the quality control of DEMs. Algorithms for that are currently under active investigation at DIBAG. Software modules which will result from these investigations should be included into the discussed processing system.

6.4 Description and Discussion of Modules in RIDE

6.4.1 Single Image Setup and Data Extraction

Input of Parameters

Initial parameters for the analytical SAR sensor model have to be made available either by manual input or from SAR image header information readable from CCTs.

Required parameters are:

- information on flight path;
- information on sensor attitude;
- Doppler information;

- look direction;
- look angle;
- information, if slant or ground range image;
- parameters for slant to ground range conversion;
- offset and scaling parameters.

Besides, this module also should be able to handle different projections and user identifications, and input of supplementary information like file names, kind of user coordinates etc.

Ground Point Management

Input of ground control points (GCPs) should be available through several possibilities:

- digitize from map or image;
- input coordinates manually;
- receive coordinates from image processing system through manual identification;
- use automatic correlation to identify points;
- identify homolog points in left and right stereo-image.

It should be possible to mark points either as control data or as check points.

Transformation of points between different projections will usually have to take place, because all calculations will be performed in a three-dimensional cartesian coordinate system. Input might be from a rectangular cartesian coordinate system, geographical coordinates or any other map projection.

It might be an advantage to be able to display available GCPs at any given time over the image to check the quality and distribution density.

Inner Orientation

The inner orientation requires the establishment of a relationship between SAR pixel coordinates (i, j) and the physical radar measurements of time t and slant range r (or ground range r_g)—see equations 1.11 and 1.12.

A range reference line is used to identify the first image line with constant range (sweep delay). This line should also contain tick marks in time direction for the establishment of a relationship between azimuth pixel coordinate and imaging time. If they are not available from the sensor recordings, then the operator should define arbitrary time marks. They will be corrected later in a self-calibration process during the resection-in-space (cf. Section 1.2.3).

Bundle Adjustment for Single Images (Resection-in-Space)

The resection-in-space refines mainly parameters of the exterior orientation, such as a time polynomial for the flight path or the squint angle. It also refines the parameters of the inner orientation, like offset in range (sweep delay) or time direction and image scales. A resulting error analysis outputs the residuals at the GCP locations.

To satisfy the user's needs for accuracy it is important that either the orientation parameters are already of good quality, or that a sufficient number of GCPs was identified.

An outline of an algorithm is given in Section 1.2.3.

Shape-from-Shading

Radar clinometry, an analogy to photoclinometry, is a method to extract topographic information from the grey value information of a radar image. The subtasks to be resolved are:

(a) Radiometric calibration of the image: if grey values are used to extract the influence of the slope effect, it must be possible to trace these values back to theoretical equations.

(b) Segmentation of the image: the image is divided into areas of different backscatter properties.

(c) Assignment of theoretical backscatter functions to each of the segments.

(d) Calculation of topography in each segment.

(e) Matching of segment boundaries.

(f) Additional information extracted from shadows.

There has only been limited research in this area, and no actual experience of the value of such shape-from-shading exists yet for radar imagery.

Map-to-Image Correspondence

Project individual or groups of ground points into the radar image If ground point coordinates are given and the corresponding image coordinate should be defined, one has to find first the sensor location from where this point was imaged. The procedure requires a well known analytical sensor model and proper algorithms for the resection of ground points into the SAR image, like briefly discussed in Section 1.2.2. Then, single points or linear map features can be transfered to and displayed in the radar image.

The procedure thus is one necessary step in an "object based" match algorithm. A refinement by local pattern matching should follow after the projection and will upgrade the accuracy of the results.

Project individual or groups of image points onto the ground If only the image point coordinate is known and the corresponding ground point coordinates should be defined, one has to go through the steps of an inner orientation first. Assuming the sensor parameters are well known (e.g. through a resection-in-space) and a digital height model is available, the image point can be projected onto the height model, as explained in Section 1.2.1. This also can be performed for single points as well as for streams of points.

This image-to-map correspondence can be used to plot from single images (mono-plotting) to create maps or to update maps. Thus it is also a preliminary tool for change detection.

6.4.2 3-D Reconstruction and Data Extraction

Parallax Removal

When viewing a stereo-pair of images, the brain of the human operator translates the geometric difference of the two images along the eye axis (x-parallaxes) into a "height perception"; the geometric differences perpendicular to the eye axis (y-parallaxes) is perceived as nuisance. Consequently, one wants to remove the y-parallaxes and calculate the x-parallaxes.

Removing the y-parallaxes can be done manually in comparator measurements. For continuous removal of such y-parallaxes on can employ polynomial models.

Set up, viewing and measuring from, radar stereo pairs, has so far been on an analytical plotter Kern DSR-1 or DSR-11. The high costs of such devices and the availability of digital image data make it desirable to move the available software into a digital environment. The design of the stereo viewing device might be the biggest problem when actually performing the transfer from the analytical plotter to a digital computer.

Suggestions for stereo viewing of soft copy images are:

(a) View the images as an anaglyphic pair (one image in red and the stereo partner in green); this requires that the operator wears filtered glasses.

(b) Create two separate output images on two flat horizontal high resolution screens to view the images via stereoscope.

(c) Flicker the two images in rapid successive movements; this requires that the operator wears glasses synchronized to the image alternations.

(d) Polarized image projection and viewing systems.

Only option (a) is usually available under any general image processing environment. Other options need to be investigated. Thus the suggestion is to at least develop the tools to view and measure from, radar stereo-images, by means of anaglyphic viewing and alternative viewing and measuring devices for soft copies of stereo image-pairs should be investigated; their use will most probably enhance the three dimensional perception of the operator and thus increase measuring accuracies.

In viewing softcopy images one needs a measuring device in the form of a floating dot: this is obtained by a pair of cursors. One cursor will be defined for each of the images. During stereo-viewing, both cursors melt into one. The parallax between the images can then be defined by the coordinates of the two single cursors.

Bundle Adjustment of Stereo Pair

This module performs a bundle adjustment in an analogue way to the resection-in-space for single images. In this case a pair of equations is available for a point measured in both images. It is suggested that the bundle adjustment is first performed with the single images, provided that sufficient parameters and ground control is available, and then repeated with both images together.

Automatic Correlation

The definition of the parallax between two images can be done manually by moving the cursor over the images or it can be done automatically, by correlating the two images. The difference in geometry in the two images together with the sensitivity of radar to illumination direction and the speckle effect make this task very tough. Attempts to match radar images via automatic correlation has been mainly performed in flat areas. Even here problems occur due to the grey tone differences derived from different illumination direction, as could be shown with a sequence of SEASAT data and data from other radar sensors. Automatic correlation of radar images from topographically varied terrain is still under research. One expects that preprocessing of one of the images to match the second one in tone and geometry might be necessary, depending on how different the images are from the beginning. Then the matching techniques developed for flat regions might apply.

Extraction of Height and Planimetric Detail from Stereo Images

After the refinement of exterior orientation parameters within the resection-in-space the set-up of the radar stereo model can be performed at the analytical plotter and, consequently, 3-D coordinates can be measured in real time by the operator. It should be possible to measure at least contour lines, polygons and single points.

If coordinate extraction follows automatic correlation, the parallaxes and parallax differences have been defined automatically. Afterwards, height can be determined by solving simple equations.

6.4.3 Geometric Analysis

Simulation

The simulation of SAR images should be able to handle

- arbitrary flight parameters (sensor positions, velocity and attitude);
- arbitrary imaging parameters (squint, look direction, look angle);
- arbitrary file sizes (input/output).

Even though the emphasis is on the geometric fidelity of the simulation compared to the real image, speckle and resolution were found to have quite a strong influence on radargrammetric information extraction. Thus, speckle (at least with a proper statistics) and resolution should also be variables in the simulation. The possibility of using a ground cover and a backscatter data base would further enhance the possibilities of the simulation.

According to the specifications above, the input of the simulation has to consist of

- a DEM;
- flight/imaging parameters (see above);
- backscatter information;
- and (optionally) a ground cover and a backscatter data base.

Two different simulation algorithms were programmed and tested in terms of quality, power and CPU time uses. Their difference lies in the establishment of the relationship between the object space (DEM) and the image space (radar image):

SIMRISA starts by defining the image pixels and searches for a DEM address to each image location (image space algorithm). The coordinate values of an image pixel relate indirectly to sensor position and slant (ground) range. Thus, together with the necessary information on Doppler centroid, a circle is defined in the 3-D object space, which has to be intersected with the Earth's surface. Although, by knowing the look direction of the radar and the maximal height of the area to be imaged, the circle is reduced to a relatively small arc, the intersection of the arc with the DEM itself is a rather expensive and CPU consuming process. Flight and imaging parameters can be easily kept flexible with this algorithm.

SIMROSA is programmed as an object space algorithm, meaning that the object coordinates (the DEM cells) are the start values and the corresponding image coordinate positions the resulting values. The problem here is that there is no simple relationship between DEM coordinates and flight positions. The sensor position according to a specific DEM coordinate has to be determined within an iterative algorithm in case of non-linear flight path assumptions. The calculation of corresponding range and time image coordinates then is straightforward.

The assignment of grey values to an image coordinate is independent of the geometric modeling algorithm. After a relationship has been established between image coordinate, DEM cell and sensor position, the incidence angle is defined as the angle between the incident radar ray and the surface normal at this point. The radar grey value is calculated as a function of this angle. A possibility to differentiate between various radar reflectivity potential distributed over the area the DEM covers is given through the use of a "cultural file" (containing codes for the various textures or thematic contents) connected to a lookup table with the corresponding backscatter functions.

Image Statistics

When imaging with a side looking radar, the amount of useless image information can be defined by the amount of layover, foreshortening and shadow appearing in the image. Essential for this loss is the value of look angle: high look angles create low foreshortening and layover and high amounts of shadow. Information on this data quantity loss might be of interest when analyzing the image. Input for this statistics is the flight/imaging information and a DEM. After relating the flight path and the DEM similiar as during the simulation, the amount of these effects can be calculated by defining the incidence angle of the incoming radar ray i for each DEM cell. Layover is then defined wherever the incidence angle is negative; the amount of foreshortening in percentage is defined by

$$F_p = (1 - \sin i) \cdot 100. \tag{6.1}$$

Shadow is found by stepping through a presorted DEM array while the look angles are continuously increasing. If this premise is not true, shadow has occured.

Currently, in the DIBAG software the statistics are calculated during a simulation session. It is suggested to have a standalone procedure for this task to minimize the CPU time. Optionally, also the incidence angle values could be output at this stage and incidence angle maps could be generated of the area of interest.

Grey Values Curves

Once the radar grey values are registered to the DEM, auxiliary files from simulation or statistics can be utilized, e.g. the incidence angle file, and the cultural file. Two-dimensional plots (incidence angle axis vs. grey value axis) can show the relationship between the absolute (relative) grey value and the incidence angle. By including thematic information (cultural file), the slope effect vs. the texture/thematic dependent effect can be presented.

6.4.4 Geometric Rectification

Image Warping

Input to an image warping procedure usually is a set of homologue pairs of points whose coordinates are known in the distorted and undistorted image. These are used to compute correction polynomials to describe the trend of the image deformations. It is also possible to input the polynomials directly, if known. Residuals at control points serve then to compute refined corrections with some higher order interpolative method. Work is thus via "warping" or "rubber sheeting". Polynomials should be limited to a degree of 3 or less, so that they are both stable and overdetermined. Residuals are extracted at each anchor points, and serve to modify the original polynomials.

These correction polynomials are used for resampling based on a grid of anchor points; each set of object coordinates obtains image positions. Various methods may then be applied to determine grey values at those positions: interpolation followed by nearest neighborhood assignment, bilinear interpolation, and bicubic interpolation, are options within the currently implemented software. Control points will usually be defined by hand.

Analysis of residual errors should be available.

Rectification using a DEM

Image warping is not sufficient to rectify a radar image, if topographically varied terrain is involved. In that case the use of a height model is necessary.

Fundamentally, the problem is the same as with image simulation: a relationship has to be established between DEM cells and radar image coordinates through available flight/imaging parameters. This can be done in one of several ways: two possibilities are programmed under the names of GEOREC and GEOCOSA. GEOREC uses the available flight and imaging parameters to establish a close but not exact relationship between DEM and image. The final "fine tuning" is done via a warping function. GEOCOSA established the relationship between DEM and image within one step. Both algorithms are described in the Appendix.

Analysis of residual errors should be available.

Mosaicking

Mosaicking is a means to exploit large overlapping strips of radar imagery (radar blocks).

Depending on the need for accuracy, type of further use and geometric fidelity between two images, different algorithms will be usefull:

- Each of the image scenes can be rectified individually to a common DEM. Homologue (point) features are thus identified automatically in the overlapping area.

- Long data takes from satellite imagery are usually split up into separate image scenes while correlating the SAR signal data. If these scenes have to be mosaicked together again, it is usually sufficient to correctly align the image rows.

- If geometric rectification is not to be involved and the mosaicking is not a simple alignment of image rows, then homologue (point, lineal or areal) features have to be found in the overlapping area and put into relation. This process can be done automatically or manually:

  (a) Manually one can, for instance, identify homologue points on the image screen using joystick and cursor. Identification of linear and areal scenes prove to be more complicated, as there is usually no easy way to rotate and shift one image over the image screen. One solution could be to produce hard copies of image scenes of both images via printer or camera, in a sufficient pixel size, so that they can be overlaid (rotated and shifted) and their geometric relationship determined.

  (b) For automatic correlation a Marr-Hildreth algorithm is used, because it proved to be fairly independent of radar speckle influence.

  After identification of homologue features, one of the images will be registered to the other one by warping.

Mosaicking also involves a grey value histogram equalization between the mosaiced scenes. This can be a challenge if opposite side images or images from ascending/descending orbits are to be combined.

Scaling/Rotating/Slant-to-Ground Range Conversion

Scaling is also a warping process, but involves a very simple form of resampling, as does rotation. This option is the simplest form to register an image to a map. Menu items should include

- scale factor in x, y;
- scaling to specified scale;
- rotation to North;
- rotation for specified angle.

The conversion from slant to ground range is also a relatively simple task, involving a sampling process. This step might bring sufficient geometric fidelity, if no or not much topographic variation is present.

6.4.5 Radiometric Manipulation

Slope Effect

Radar image grey values reflect wavelength, incidence angle, polarisation, dielectric constant and surface roughness. In topographically varied areas the influence of the incidence angle surpasses the other parameters. Thus any attempt to segment and/or classify radar images by tone, will actually (unwantingly) classify the slopes in the image. To be able to

use the tone to understand the thematic image content, one has to reduce the effect of the incidence angle on the grey value of each single pixel. This can be done by comparing the grey values to their theoretical value derived as a function dependent only on the incidence angle. The relationship between radar grey value and corresponding incidence angle has to be established during the simulation/rectification process.

Filters

Besides other negative effects, the presence of speckle may reduce the stereo-viewability and the possibility to segment or classify a radar image. Thus a number of speckle reduction techniques have been developed. These techniques are discussed in Chapter 9 and should made available within the radar software library.

Correction for Systematic SAR Effects

Antenna Gain Correction To be able to define the antenna gain across the swath of an image, grey values from homogeneous scattering areas are plotted vs. their incidence angles and averaged. These averaged curves can then be used to correct the original data.

Grey Value Calibration After the SAR signal correlation process, the resulting grey values undergo enhancements like stretching, histogram equalisation etc. To recalculate the backscatter coefficient σ_o, one can set the grey values of one class (σ'_o) into relation to grey values of another class (σ''_o), if one σ_o value is known:

$$(\sigma'_o/\sigma''_o)^2 = \sigma'_o/\sigma''_o. \tag{6.2}$$

6.4.6 Alternative Image Representation

Stereo-Ortho-Images

The geometric fidelity of ortho-images can be of even better use when adding a third dimension to it by producing a stereo-ortho-mate. A DEM must be available for this process. The advantage of these to a normal stereo-pair is the correct geometry, which enables an interpreter to map information from an image without the usual distortions. Height information is needed when creating the stereo-mate. This process includes a shift of any image point position (pixel) according to the occuring height. The amount of shift s is calculated by

$$\tan(angle) \cdot height = s \tag{6.3}$$

where *height* is the elevation at the image point position, and *angle* defines the desired parallax.

The stereo-mate can be created from the original ortho-image or from a different ortho-image, if a second one is available. In photogrammetry, the superior solution is taking two different images to create a stereo-pair. This has the advantage that small scale features, which are not considered by the coarser height model, can be identified by the viewer. In radargrammetry, however, different images might mean sufficient changes in the illumination to decrease the stereo conception, and thus this solution could prove to be poorer than the use of a single ortho image.

Perspective Views

Perspective views of a topographically varied area enhances the perception of the terrain. Especially if the area is presented from different viewing angles, preferable from all sides, either as single identifiable images or in a film motion. The radar grey values are superimposed on the perspective view, either as single radar grey values or composed to a color-composite.

Topographic / Thematic Radar Image Map

The radar image can be presented in its ortho-image geometry and superimposed with graphic notations such as contour lines and planimetric detail (e.g. roads, towns, coordinate grid etc.) or thematic units. Color presentations will include RGB presentations of rectified radar images or IHS presentations of radar image grey values (in the intensity) and thematic information (as hue).

Chapter 7

Conclusion on Part I

7.1 Summary of Findings

In Part I of this report a wide range of topics relating to radargrammetry has been discussed. The intent was to give an overview of the current status of the field and to point to opportunities and needs for improvements to make SAR more useful to future applications. Each sub-topic addressed in Part I led to a discussion of required clarifications and future efforts which will be summarized now.

7.1.1 Error Budget of SAR Image Creation and Processing

The production of quality imagery from spaceborne SAR data requires extensive processing of raw echo data. This procedure is different from the one used for aircraft SAR imagery due to the large increase in sensor altitude. The image creation (correlation) procedure must compensate not only for undesirable spacecraft motion, but also for target motion resulting from earth curvature and rotation.

To simplify this procedure, approximations are often made that can result in both geometric and radiometric distortions in the image product. On the other hand, various efforts have recently been made to develop *auto-compensation* processes for the removal of the image-corrupting effects of undetected antenna motions. The limitations of Doppler "clutter locking" and "autofocusing" methods are still under extensive discussion just as the achievable quality characteristics of the resulting slant range/azimuth space SAR imagery.

Therefore, the radargrammetrist presently has to face a situation where no reliable information about the geometric errors can be included into the post-processing of SAR images. The urgent need exists that all SAR processor-induced errors should be calculated and compensated, if possible, but at least they should be communicated to those doing radargrammetric processing. This will be a prerequisite for estimating the *derived* SAR product quality, such as e.g. geocoding accuracy.

A need for sub-pixel accuracies of *georeferenced* SAR images will require that the most refined models be implemented in the SAR image processing chain, and that the awareness of the complexity of geometric processing issues be understood. *Error budgeting* of radargrammetric processes has been attempted in various studies but the present situation is far from being satisfactory:

- a lack of consensus on mathematical and statistical models for SAR platform behaviour, synthetic antenna position and attitude is noted;

- required accuracies of DEMs (elevation, slope, projection) and other collateral information essential to radargrammetric processing have not been fully identified;
- predicted accuracies for mapping from SAR do not match observed results;

These observations lead to recommendations for future investigations of the following critical aspects in elementary radargrammetric processing:

- interface must be created to standard radar acquisition and SAR processing parameter files;
- errors in statistical modelling (resection-in-space) of sensor position and attitude, and recharting of real antenna position to synthetic antenna should be analyzed;
- further development of error budgeting of radargrammetric processing elements should be envisaged;
- investigations into DEM induced errors should be performed;
- assessment of feasibility of end-to-end SAR processing (including geocoding and using DEMs) should be initiated.

7.1.2 Analysis of SAR Image Content

Chapters 2 and 3 deal with radargrammetric issues surrounding the individual image and characteristics of its quality, as well as with techniques of processing and information extraction. The single radar image is the type of data set to which currently most studies are directed, dealing with geometric and radiometric properties, corrections and evaluations.

Considerable clarifications are desired surrounding the concept of *geometric resolution* of SAR. As expectations from considerations of photogrammetric resolution most likely do not translate into SAR resolution, adequate formulations are presented focusing on the problems of image interpretability and pointing accuracies. It has been shown that geometric processing also relates intimately to radiometry. This implies that one can relate a specific image resolution cell to the object area that caused the specific grey value. The following clarifications are desired to obtain a proper definition of SAR geometric resolution:

- How does azimuth and range resolution relate to classical concepts of photographic line-pair resolution?
- How does range resolution relate to the standard error of slant range?
- How can one quantify the effect of specular reflections on image interpretability?
- How can one quantify the effect of monocromaticity on image interpretability?
- How do various typical terrain objects appear in SAR images as a function of resolution?
- How does pointing accuracy depend on resolution parameters?
- What is a meaningful presentation scale for SAR images?

Further issues are techniques of automated interpretation and extraction of geometric properties of objects. Techniques using image texture and tone as well as methods for edge detection, line and contour following have been reviewed. Such techniques should become a thoroughly integral and important tool of radargrammetry. However, it is evident that SAR images present a more difficult data source than common photographic imagery for automating the analysis process. This relates to speckle and the many other effects contributing to the image grey value. Speckle and specular returns hamper automated feature extraction for object recognition and are therefore of great significance to radargrammetry. Slope reconstruction from image brightness values is not feasible, either due to speckle, and radar stereoscopy limits are set by speckle effect.

7.1.3 Concepts for Multiple and Multi-Parameter SAR Images

The study of SAR *stereo concepts* reveals that past investigations were lacking actual data. Therefore, a most crucial aspect of SAR stereo remained entirely unaddressed with real data: SAR stereo-viewability. Simulations were lacking the necessary realism to be authoritative. This leads to the suggestion of the following efforts:

- creation of elaborate data sets at various incidence angles and intersection geometries over different relief types;
- improvement of current simulation techniques to include realism in speckle, specular returns, also from micro-relief and man-made features;
- thorough study of achievable accuracies using sets of look angles over one area, and over various different terrain types;
- development of automated image matching algorithms for SAR data to quantify SAR stereo acuity;
- creation of techniques to complement SAR stereo matching methods by methods of "shape from shading", to employ the thematic disparities in overlapping image sets as *information* rather than to avoid them as mere *noise*;
- develop an understanding of the effects of speckle on stereo-acuity;
- explore the utility of a wide disperity of look angles as offered by opposite-side stereo geometry.

Image Block Methods are of great importance for any current aircraft radar operation. In the case of satellite radar projects emphasis is on automated ***mosaicking***. A recommended sequence of work steps to obtain a large area coverage or image mosaick is the following:

1. geocode each image using the available ephemeris data;
2. identify tie-points among overlapping images, potentially an automated procedure of image matching;
3. itentify GCPs;
4. compute improved imaging parameters to enforce a match of tie-points and of GCPs;

5. resample individual images to achieve an improved geocoded result;

6. finalize a mosaicked product by seam matching of grey values and by proper output formatting.

One may opt in step 4 for merely computing a geometric warp of the images that were already geocoded in a preliminary manner. If topography is described by a DEM, step 1 and/or step 5 will need to exploit the DEM.

7.1.4 Usefulness of Data Composites

The analysis of remote sensing imagery increasingly requires added sophistication in combining the source image with collateral data. Technologically such capabilities are widely available for optical remote sensing data. However, such capabilities are missing with SAR data. It is thus necessary to

- provide capabilities to combine digital SAR images with non-images and maps;
- study the usefulness of stereo-ortho SAR images;
- find tools to integrate SAR images and maps for ease of interpretation;
- develop concepts to combine SAR and collateral non-image data;
- create sets of secondary SAR image products and judge their acceptance and usefulness to user communities;

The current status in the creation of *multi-sensor* image data sets consists of manual matching with the help of tie-points and subsequent image warping. Several attemps explore automatic techniques to match dissimilar images, without going much further than to use edge matching methods leading to limited results of 2 to 3 pixels. This leads to the following observations:

- A thorough investigation into possible procedures for matching dissimilar images would be urgently necessary to help process expected large data quantities from satellite SAR. This needs to be complemented by experiences with actual data sets.
- It needs to be explored in how far edge invariance is a valid assumption in combinations of SAR and non-SAR images.
- Automation of the matching process promises to be efficient if object-based methods are used.
- Existing DEMs should be applied for precision correction of component images prior to matching.
- The effort to produce independent geocoded component images and their accuracy should be evaluated with respect to achievable image match accuracies. Sub-pixel accuracy may not necessarily be achievable. A close match is expected from geocoding and therefore some post-processing may lead to the required sub-pixel level.

Despite the fact that it clearly is a major promise for future environmental and geo-scientific planning, no work has been done on techniques to monitor rapidly changing phenomena with SAR *image time series*. This topic is entirely novel: although touched upon routinely as a major application opportunity for future SAR data, the complexity of an operational process has not led to serious work. Sea-ice management in arctic oil exploration may be the effort nearest to such work. The authors of this report believe strongly in object-based techniques that rely on pattern recognition, image segmentation and feature labeling. While monitoring tasks themselves require that changes be flagged, there is only an indirect need for precision image matching.

7.2 Radargrammetric Software Developments and Experiments

It has been a matter of contention of the authors for a long time that a significant radargrammetric role needs to be taken by a central clearing-house for SAR data; this will also need to be complemented by capabilities in the hands of the end user. It has therefore been proposed to define a list of capabilities that are common to typical SAR data analysis efforts. Such capabilities would then have to be created and distributed to end users of SAR data.

Suggestions have been compiled for the specification of comprehensive software libraries to be utilized in a multitude of tasks relevant for radar image evaluation. It became evident that methods and computer programs for single and stereo radar image evaluation are much more advanced than those for the use of multi-sensor data and radar time-series. A definition of major radargrammetric software modules is contained in this report, comprising programmes for image setup, 3-D reconstruction, geometric analysis and precision rectification, radiometric manipulations, secondary image generation and representation, and various capabilities for analysis of SAR image content. The existing prototype software which is an implementation of algorithms required as the kernel elements for any kind of radargrammetric processing have been tested in the geological application study—see Part II, Chapter 10—and has proven its basic capabilities. The algorithmic details and implementation criteria for a number of other modules will have to be a matter of further investigations. In particular, the stage of developing concepts for operational implementation of these modules has so far only been achieved with geocoding software for high throughput of image data.

Further developments and tests of elementary radargrammetric software are dicussed in Part II and in the Appendix of this report.

A general outline for required software capabilities to evaluate multi-sensor data, multi-parameter SAR data and time-series of radar images is given in the description of two software libraries. However, the specific functional requirements for software have not been comprehensively identified. Instead, it is recommended to perform more exploratory work leading to a better definition of tools required for the utilization of these data. This work should orientate on the suggestions given in the foregoing subsection.

In particular, a demonstration of the geometric correction and registration of a variety of images and cartographic data is proposed. The demonstration should utilize the software tools developed so far. A number of image composites comprising SAR (spaceborne and airborne), optical and map-based data should be produced and assessed in terms of registration quality and the possibly improved potential for interpretation of the composite

data in land-based applications should be assessed.

7.3 Suggested Areas for Radargrammetric Progress — Summary

A summary of issues that appear to deserve attention in radargrammetric application are supposed to add weights to their individual entries. A subjective ranking of items obviously depends on one's anticipation of future application priorities. To support sea-ice management programs, radar stereopsis is of little relevance, automated mosaicking is not. Inversely, updating of topographic maps strongly depends on geometric resolution and 3-D reconstruction by stereo radargrammetry, but mosaicking may be irrelevant.

A global view of radargrammetric work leads us to observe that the following items may rank above others:

(a) End-to-end error budgeting of SAR processing and radargrammetric calculations to identify limitations in achievable geometric accuracies of SAR image products;

(b) Automation of *geocoding* of individual images by dead-reckoning and subsequent image matching;

(c) Automation of map-to-image correspondence;

(d) Precision matching of multi-temporal SAR image series with simultaneous change detection;

(e) Topographic shape reconstruction and backscatter measurements using parallax measurements and grey-value disparities.

The above items will lead to the automation of monitoring tasks, if images are first rectified by precision dead-reckoning and/or by using ground truth data from available reference data banks, e.g. in the form of map data bases, and are then precision-matched with previous radar images.

The ambiguity of radar image brightness is caused by composite effects of dielectric surface properties, topographic slope and roughness. Incidence angle signatures can unravel the ambiguities resulting from dielectric properties and roughness. Topographic slope needs to be determined separately. The importance of this problem is reflected by the recommendation to combine geometric and radiometric disparities into the SAR multiple image analysis.

A second level of significance in required future radargrammetric research is caused by the chronic lack of data. Although large area SAR coverages exist, there is a distinct lack of parameter variation. Therefore a further high priority item is as follows:

(f) Acquisition of extensive SAR image test data base with variation in frequency, resolution, wavelength, look angles, etc.

Any further radargrammetric work will need to quantify the interrelationship between results and properties of the input data. Quantifying of results is best achieved with algorithmic rigor. This rigor and the benefits of automating SAR image analysis tasks lead to the recommendation that:

(g) A SAR image processing and pattern recognition test bed should be built and made available.

Apart from the basic radargrammetric capabilities, this test bed also needs to include extensive grey-value processing tools. This can in turn help to learn about effects of resolution, speckle, specular returns, noise, processing concepts such as pyramiding, noise suppression, look angles, etc. on the required results.

The multiplicity of anticipated remote sensing image data, and the existence of an extensive geoscience data base, lead on to the expectation that it is important to:

(h) Develop new concepts for combining remote sensing and collateral data into synergistic data sets. This may include a host of so-called secondary image products for use by human analysts.

Radar remote sensing will increasingly be subject to pressures from the side of data acquisition: more data will be available over extendend periods and at high rates. Additional pressure will develop from processing systems and computer potentials. These combined technology-oriented "pushes" are not necessarily met by commensurate demands from user communities. This presents further major challenges to remote sensing technology including SAR and radargrammetry.

Part II

Achievements in Algorithm Development and in a Geological Application Study

Chapter 8

Further Considerations on Resection-in-Space

The situations where a refinement of the parameters in the projection equations becomes necessary in radargrammetric coordinate processing, have been described in Section 1.2.3. To put it briefly, the phase reference function used in SAR processing, the imaging parameters and the flight path information are usually not communicated to those who have to determine the parameters in the radar projection model. Even if a data link exists to the SAR processor and all the required information is available, the radargrammetrist will have to be aware of residual errors in the geolocation of pixels in a given slant range image. For spaceborne SARs typical values of location errors in azimuth direction are between 100 and 150 m on the ground, and between 20 and 50 m in range direction (not considering terrain-induced distortions). If, for example, a SAR image has to be matched to a map at sub-pixel accuracy, such location errors in the input SAR image must be considered in the geometric transformation.

In the suggested *resection-in-space* the parameters in the SAR projection equations are determined by incorporation of external information (control information from map and DEM) as a supplement to the data available from the SAR processor and from the flight path determination system. The resulting transformation model will thereby include a *compensation of location errors* in the input SAR image.

There is a number of aspects which have to be considered when the resection-in-space method is assessed: It has been noted that after a resection-in-space had been performed, the quality of pixel location (computed with the refined radar projection) was at the same order of accuracy as the estimated mean location error of the input GCPs. Besides this experimental result, there were no other indications of the geometric accuracy of the resection-in-space at the beginning of the contract. Furthermore, it was interesting to ask, how the parameters adjusted by this method are interrelated, i.e. whether an adjustment of one parameter can possibly have an effect on the way another parameter is adjusted. Such questions have been investigated in the contract by using a resection-in-space software available at DIBAG. Results are given in Section 8.1

Section 8.3 describes a new method for efficient ground control point identification, which is of practical interest if resection-in-space is used.

8.1 Analysis of Resection-in-Space Procedure

8.1.1 Description of Procedure

The parameters which define the analytical SAR sensor model and which can be refined within the resection-in-space procedure available, are:

- the orbit; in the current approach it is represented by polynomials, which are functions of the radar image azimuth (time) coordinate;
- radar image scaling factors, i.e. pixel spacings in azimuth and range direction;
- the sweep delay; this is a constant distance from the sensor to the near range edge of the image;
- a shifting factor in azimuth direction; this parameter is designed to consider erroneous time calibration in terms of differences between the time information associated with the radar image and the one associated with the orbit;
- the squint, an angular parameter to define the Doppler-cone. The squint can be represented as a polynomial function of range if this is required to compensate azimuth skew.

The procedure requires external information such as ground control points (GCPs) and is done by a so-called bundle adjustment for radar images. Input to the resection-in-space consists of the image coordinate measurements x, y of GCPs as well as their given X, Y, Z-object coordinates. These coordinate measurements define a pair of equations for each measured control point (the range and Doppler equation). These are non-linear equations, which, due to the theory of adjustment techniques, have to be developed into a Taylor-series to build the so-called observation equations from the linear terms.

For each control point two observation equations are obtained, which can be given in matrix notation as follows:

$$\underline{C_i} \cdot \vec{v_i} + \underline{D_i} \cdot d\vec{u} + \vec{w_i} = 0 \tag{8.1}$$

$\underline{C_i}$ and $\underline{D_i}$ are coefficient matrices, $\vec{v_i}$ contains the corrections of radar image coordinate measurements (x_i, y_i), $d\vec{u}$ is a vector of increments for the parameters to be refined and the elements of vector $\vec{w_i}$ are the contradictions of the basic equations (range and Doppler equation). Since $\underline{C_i}$ is a regular quadratic matrix and uncorrelated to the $\underline{C_i}$-matrices of equations for any other control point, the following conversion is possible to seperate the corrections of image coordinate measurements:

$$\vec{v}^{+} = \underline{D}^{+} \cdot d\vec{u} - \vec{w}^{+} \tag{8.2}$$

$$\begin{aligned} \text{with} \quad \underline{D_i^+} &= -\underline{C_i}^{-1} \cdot \underline{D_i} \\ \vec{w_i^+} &= -\underline{C_i}^{-1} \cdot \vec{w_i} \\ \vec{v_i^+} &= \vec{v_i} \end{aligned}$$

The overall system of modified observation equations is solved for the unknowns, which consist of small increments to the preliminary given orientation parameters, i.e. parameters of the analytical sensor model. Due to the usual overdetermination of the equation system, the solution follows the rules of least squares techniques. Depending on the quality of the input data, this procedure has to be repeated iteratively. After each iteration

Table 8.1: Results obtained with resection-in-space procedure

Orbit	Squint	r_0	m_y	t_0	m_x	RMS-x (Image)	RMS-y (Image)	RMS-X (Orbit)	RMS-Y (Orbit)	RMS-Z (Orbit)
Los Angeles										
						(mm)				
–	1	*	*	*	*	0.045	0.038	–	–	–
–	3	*	*	*	*	0.037	0.041	–	–	–
3	1	*	*	*	*	0.044	0.038	0.001	0.002	0.001
3	3	*	*	*	*	0.035	0.036	0.006	0.004	0.003
Bonn										
						(Pixel)				
–	1	*	*	*	*	0.691	0.950	–	–	–
–	3	*	*	*	*	0.674	0.950	–	–	–
3	1	*	*	*	*	0.685	0.846	0.032	0.100	0.096
3	3	*	*	–	*	0.649	0.859	0.080	0.091	0.089

Explanation:

1, 3	.....	number of polynomial coefficients
*/–	.....	parameter modified/not modified
m_x/m_y	.....	pixel spacings along/across track
t_0/r_0	.....	azimuth shift/sweep-delay

the consistency of the range and Doppler equation is checked using the up-dated (refined) parameters of the sensor model, and the process is terminated as soon as the remaining discrepancies between these equations are below a pre-defined limit. For the parameters refined within the resection-in-space error estimates can be output as well for a classification of the quality of the final result.

The procedure allows selective definition of parameters to be modified. An arbitrary parameter subset can be defined depending on input data quality and perhaps on the number of available GCPs.

8.1.2 Results of Experiments

Parameter Adjustment

For two SEASAT test areas covering the cities of Los Angeles and Bonn, respectively, results achieved by using the DIBAG resection-in-space procedure are summarized in Table 8.1.

Conclusions, which can be made from the given numbers, are:

- If the given orbit data are kept unchanged, about the same results are obtained like in cases where the orbit polynomial was modified too. However, one has to ensure that the input data are of rather high precision, as they obviously were in the present data sets. The number of unknowns to be solved within the bundle adjustment might be drastically reduced in such favourable cases. Especially for the test area of Los Angeles there were not even modifications caused for the orbit polynomial.

- For the given data sets a range-variable squint does not improve the results significantly. Higher order terms of the range polynomial for the squint have almost no effect on the resulting accuracy.
- Range and time calibration usually are the weakest points within the initial analytical sensor model. The appropriate parameters have therefore generally been modified within the resection-in-space for these tests.
- Due to the flatness of the areas more specific statements cannot be made. No comprehensive experiences could be gained for rugged terrain due to the lack of test data.

These observations imply that further investigations will have to be carried out to achieve a deeper understanding of the interaction of the various parameters within the resection-in-space procedure.

Effect of Earth Curvature

Experiments have been carried out to assess the effects of using curved earth reference surfaces instead of flat map projection coordinate systems within the resection-in-space procedure. For two SEASAT scenes taken over the rather flat area of Los Angeles (orbits 351 and 660) the resection-in-space was performed using different reference systems as follows:

- flat earth assumption, where X, Y map projection coordinates together with heights H were considered to represent a cartesian 3D-coordinate system;
- spheric earth assumption, where latitude, longitude and heights were transformed into a local cartesian 3D-coordinate system, which is tangential to the sphere representing the earth;
- elliptic earth assumption, similar to the spheric case but with Clarke's 1866 ellipsoid representing the earth.

The results of the experiments are summarized in Table 8.1.2 in terms of RMS-errors between measured and resected image coordinates. As can be seen, there is no substantial difference in the performance of the various earth reference surfaces and it is impossible to say which of the three earth reference surfaces gives best results. Since a considerable difference in accuracy between flat and curved earth assumptions was anticipated at least in across track direction, these results were somewhat surprising.

The most probable reason for the fact that introducing a spheric or elliptic earth did not improve the results, is that the parameters obtained in the resection-in-space compensate for deficiencies in the flat earth model by taking values that are appropriately "erroneous" compared to the real imaging situation. Obviously, earth curvature in across track direction can mostly be compensated by a proper modification of sweep delay and range scale, at least for relatively flat terrain such as in the case under consideration.

8.2 Identification of Control Information

As initial step of the resection-in-space *ground control points* (GCPs) have to be identified in the map or, alternatively, in the DEM, and to be matched with homolog points in the

Table 8.2: RMS-error between measured and resected image coordinates for different earth reference surfaces

Earth reference surface	Orbit 351		Orbit 660	
	RMS-X	RMS-Y	RMS-X	RMS-Y
Flat earth	0.040	0.041	0.039	0.098
Spheric earth	0.043	0.039	0.037	0.102
Elliptic earth	0.042	0.039	0.037	0.101

slant range SAR image. This is commonly done by visual comparison of map and SAR image.

The wish exists to perform the tie-point identification *automatically*. One concept would be to create *image chips* which contain ground control features by using the DEM and by simulating the radar illumination using pre-assumed radar projection equations (see Guidon [37]). The simulated chip would then be matched with the corresponding region in the SAR image by automatic similarity comparison.

However, the nature of the data sources to be matched is so different (see below) that currently no satisfactory solution for automatic matching is known which is able to meet required accuracies. As a consequence, operator interaction will be inevitable as long as no satisfactory automatic means are available. To increase the efficiency of *interactive* tie-point identification a *manual matching* method has been developed, which is presented in the following sections.

Manual matching is also of importance in simulation-based techniques for SAR image geocoding (see Appendix A), where an original SAR image has to be registered to a simulated image of the *full* scene. Tie-points are used for the computation of the registration model (e.g. for determination of coefficients of polynomial). Therefore, the following treatment applies to the tie-point identification for both the refinement of radar mapping relations and the registration step in simulation-based geocoding.

8.2.1 Analysis of Control Information

Topographic Relief

Ridges and valleys are the determining features in the simulated image or image chip. They appear as strong features if the foreslopes are steep, the ridges are sharp and the valley bottoms are narrow. This causes big relative differences in image intensity, which enhance the topographic features. An ideal control feature would be a prominent, sharp ridge which shows distinct differences in height, which trends nearly perpendicular to the illumination direction and has a foreslope gradient which does not cause foreshortening.

If the SAR image covers an area with mountainous terrain and height differences that are not too big, an identification of control features can be achieved without major problems. The only difficulties are caused by smooth ridges which do not provide a sharp limit of the bright foreslopes.

In general, terrain tie-point identification is guided by intercomparison of edges (ramp profiles) and lines (ridges or "spike" lines) contained in both images. Homologue points are identified only where one or more of the following characteristics can be observed:

- strong differences exist in intensities (strong edge) due to relief variance;
- an edge runs in a certain characteristic form (e.g. sharp corners of an edge);
- crossing of two edges exists;
- meeting of a line and an edge exists;
- end of a line exists.

Sea, Lakes and Rivers:

In the real SAR image lakes or a sea generally display a very low response with rather constant values (if surface is quiet) compared to the shore or the surrounding land. In the simulated image the shorelines are easily identified if the shore is steep and does not run sub-parallel to the illumination direction.

The identification of small rivers in the real and simulated data strongly depends on the pixel size in the images. In order to appear at all in the simulated image, river beds must be contained in the DEM. Especially for mountainous terrain, sharp bends and junctions represent excellent pass features.

Man-made and Thematic Features

The identification of GCPs implies consideration of the fact that in the simulated image no distinction between thematic differences in landcover is displayed. The simulated image usually is generated from a homogenous backscatter model. On the other hand, flat areas are devoid of ridges and characteristic topography-relevant edges, since they are usually rich in man-made features such as roads, agricultural fields, etc. As a matter of fact many scenes of interest for application in geology, vegetation studies etc., contain flat as well as mountainous scenes.

Man-made features or thematic information which serve as control information in maps should be transferred to the DEM where no topographic features are visible as tie-points, i.e. the possibility exists to code selected pixels in the DEM in such a way that they are assigned particular grey values by the image simulation (e.g. dark crosses with center pixels in tie points).

To include thematic information, i.e. to define land cover categories and to code extended parts of the DEM, causes considerable efforts for coordinate measurements, DEM coding and slows down the entire simulation process.

8.3 Procedures for Identification of Control Points

The need for efficient methods of control point identification in radargrammetric processing tasks has been recognized during the contract. Starting from an analysis of the usual visual comparison method, an improved technique has been developed to efficiently identify GCPs in SAR images and simulated images. For experiments with the new *manual matching* method a set of SIR-B images has been chosen. DEMs have been generated from contour-line maps of the test sites. The simulated images have been generated using simple cosine backscatter functions. A detailed description of test data is given in Section 10.

8.3.1 Visual Identification

Usually control points are identified by displaying the simulated besides the real radar image on a screen and by marking the homolog points in both images (Figure 8.1). The fact that points have to be identified and exactly located twice makes this procedure rather time-consuming. Attempting to locate the points in images with a zoom factor greater than 2 is not a proper method, because the perception of necessary synoptic relations gets lost—the image would rather look like a digital pattern.

After identification of the tie-points on screen (Figure 8.2), the selected points are checked for quality. The tie-points are used as control points after the determination of the radar mapping transformation (in resection-in-space), or of the polynomial relative transformation (in simulation-based geocoding). Points showing residuals greater than e.g. three times the mean error are dropped. This may lead to an unfavorable distribution of tie-points (Figure 8.2) and further identification of homologue points will become necessary.

8.3.2 Manual Matching

A new method for identification of homologue points in both images has been developed and tested during the contract. In this method, the SAR image and the simulated image are superimposed and scrolled one over the other, until locally a good match is observed. The point of best match is detected and the corresponding coordinates in both images are computed from the actual vector of relative shift. The homologue points are identified by a single measurement, so that only one error of localization occurs. However, the two images on the screen need to have the same orientation and the same resolution, which has to be considered when the simulated image is generated.

These matching algorithms can be used for single points or for regions. The latter offers the advantage that extended features can be used as control information, and not only single points. These features can be

- topography-related information (mountain ridges, valleys, break lines, etc.);
- hydrographical information (lakes, rivers, shorelines, brooks, etc.);
- man-made objects (embarkments, bridges, etc.).

The superpositions of the real SAR and simulated imagery for the purpose of manual matching, however, leads to viewability problems, because there may be plenty of misleading information contained in the SAR data (see below). Therefore, a reduction of image information to its most essential features is necessary: Either filters can be applied to the data to enhance edges, or intensity thresholds can be used. Both possibilities have been studied in the contract.

Edge-Based Matching

From the great variety of edge-operators only difference-operators, such as the non-oriented Laplace and the oriented Sobel and Roberts edge-operators have been used to extract edge-information from the real SAR and the simulated image. Edges running parallel to the flightpath have been found to be distinct, according to the characteristics of radar-mapping. Edges running exactly orthogonal to the flightpath are non-existent in the edge images.

As illustrated in Figure 8.3, only a few homologue edges have been derived from the two test images. This resulted from the simple reflection model used in image simulation and from the existing speckle and texture in the real SAR data, which produced a lot of edges.

Matching based on this type of information does not yield a satisfying distribution of control points. Information reduction in real SAR data by using simple edge operators has thus been proved to be inadequate. It would be necessary to use further processing such as thresholding, segmentation and region-growing or line detection.

Intensity-Based Matching

A look at the simulated image (Figure 8.1) while keeping in mind that its intensity only depends on the terrain slope and inclination, suggested that relief dependent features of high intensity may be more suitable for image matching. On the other hand, texture as well as man-made objects produced patches of high intensities in the real data. This had to be considered in intensity-based feature matching.

The reduction of information to the relevant features can easily be done by thresholds, where a human operator chooses the percentage of information retained. It has been provend that the relevant intensity information is contained in the brightest 10 percent of the image histogram, as illustrated in Figure 8.4. Finally the retained grey values are stretched over the whole intensity scale.

The identification of control points in terrain with great height differences and sharp ridges based on intensity matching produced good results. On the contrary, in flat terrain large regions showed less intensity variance in the simulated image.

Results

For the rolling and forest covered terrain of the test site (see Figure 8.5, description ot study area 1 in Section 10) the tie-point identification by manual matching took some 20 minutes. Better results have been obtained than by visual identification of single control points. As illustrated in Figure 8.5, the distribution of points determined by manual matching has turned out to be significantly better. Table 8.3.2 gives the results of manual matching in comparison to the conventional method.

It is obvious that the use of matching only for identification of control points is not sufficient in areas of flat terrain, where the simulated image displays no relevant features. In conjunction with the conventional method of single tie-point identification, however, it can be used as a powerful and fast instrument, which also has a positive impact on the accuracy of tie-point determination.

Table 8.3: Comparison of control point determination methods (Example for study area 1).

	single point identification	manual matching
identified control points	32	35
usable non usable	24 (75.00 %) 8 (25.00 %)	34 (97.14 %) 1 (2.86 %)
effort of time	2 hours	20 minutes
distribution of control points	bad	good

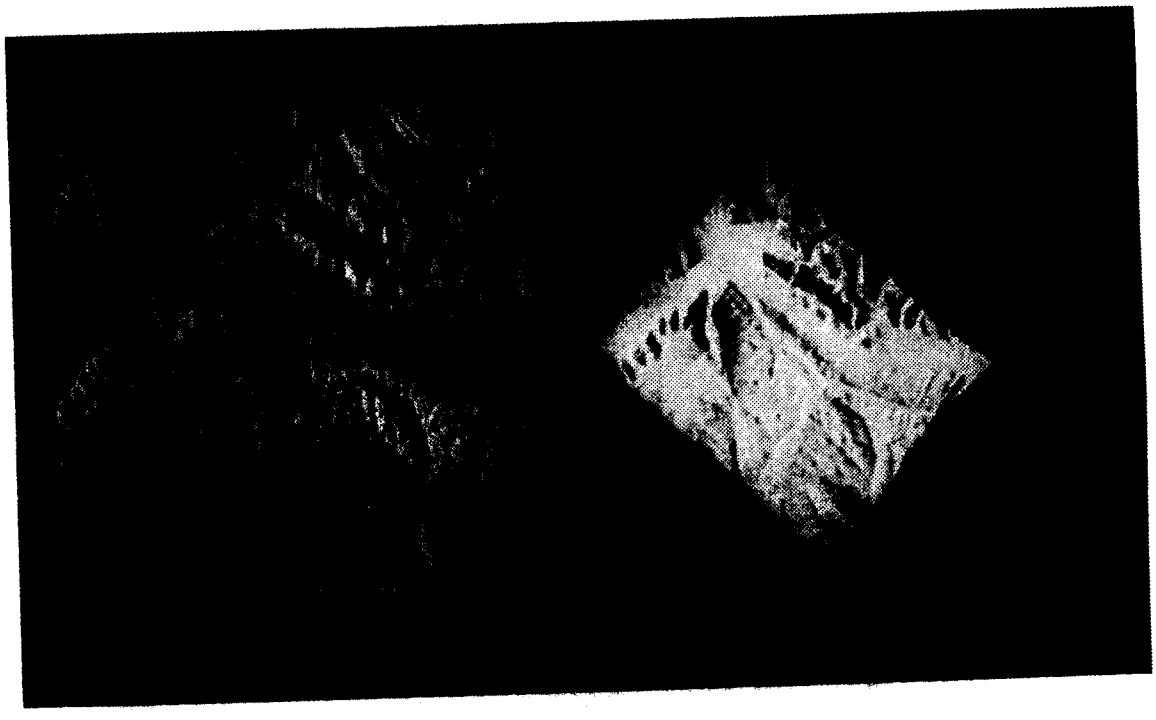

Figure 8.1: SIR-B image (left) and simulated image (right) of study area 1.

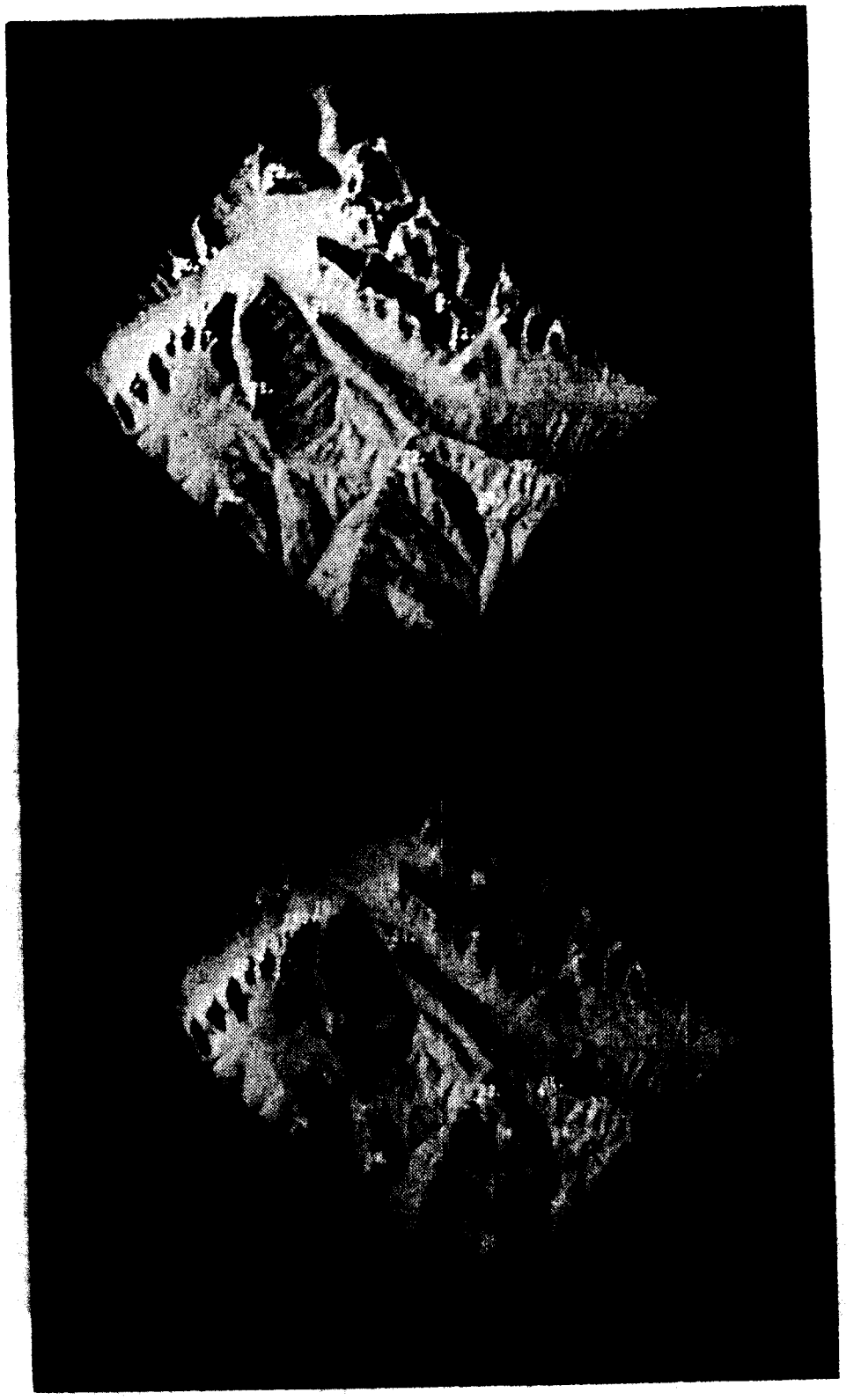

Figure 8.2: Simulated image of study area 1 superimposed by identified control points before quality control (bottom), and with remaining points after quality control (top).

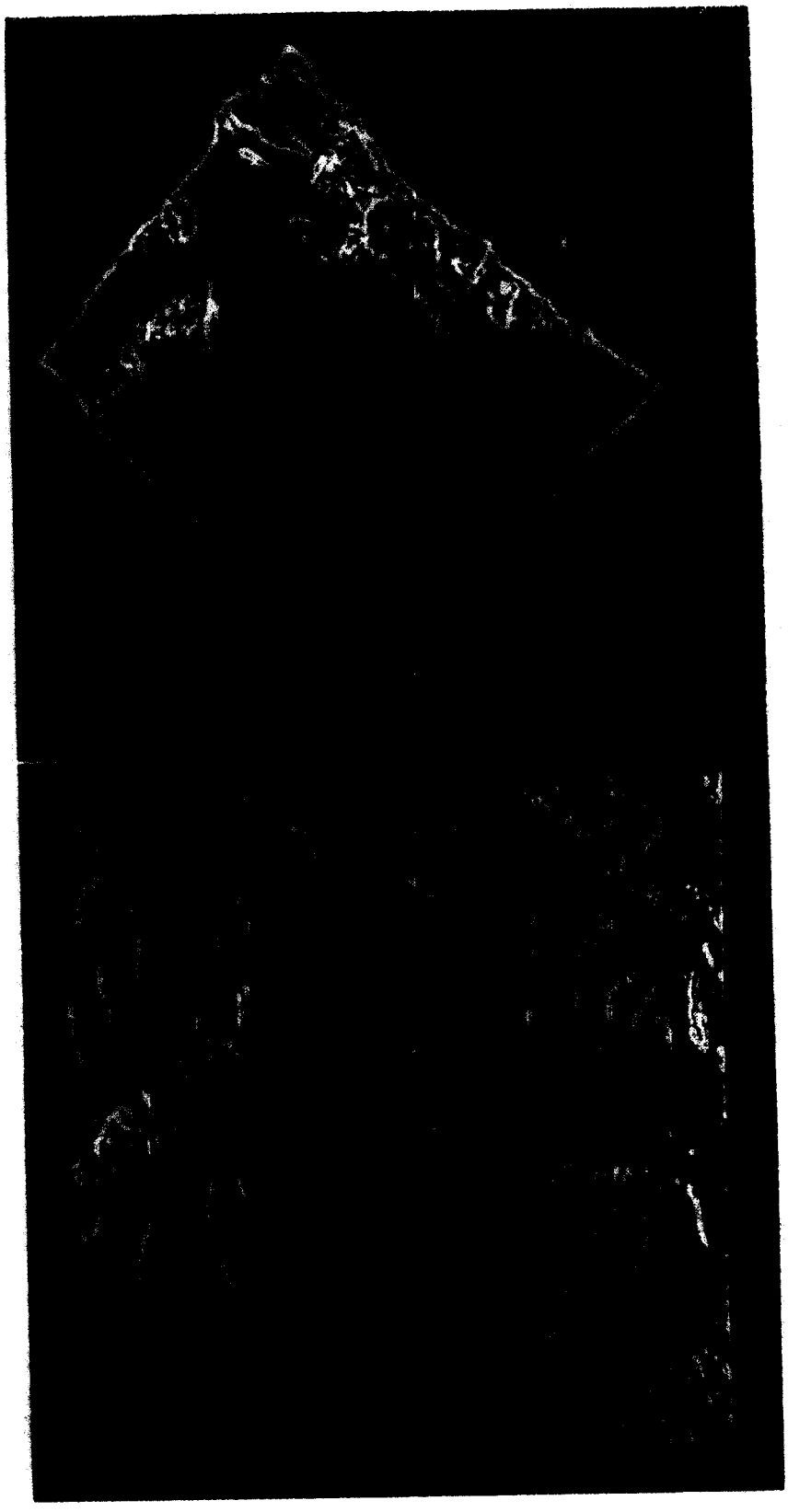

Figure 8.3: Edge images: Roberts Operator applied to the real SAR image (bottom) and to the simulated image (top) of study area 1.

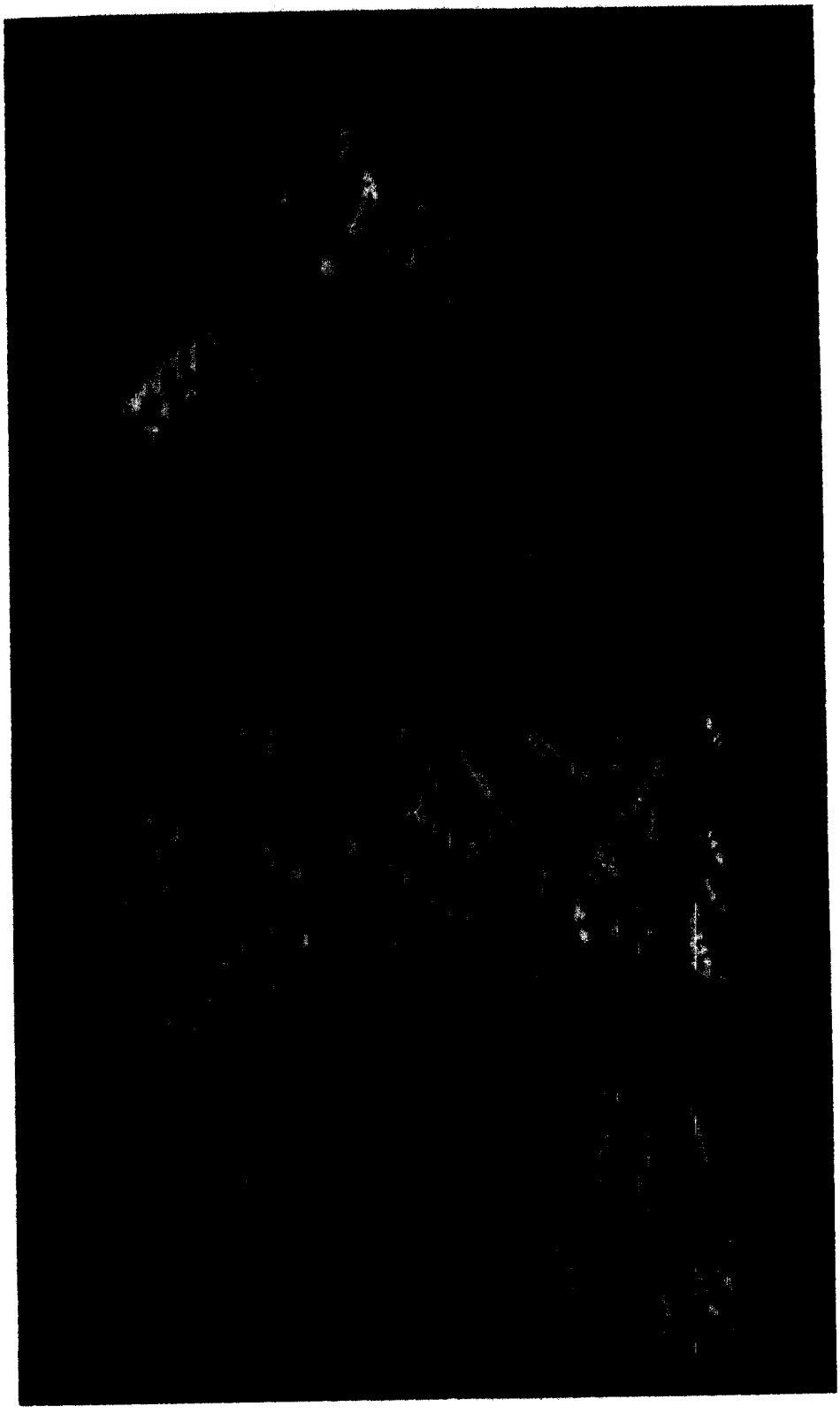

Figure 8.4: Reduction of image information to the 10 percent brightest intensities of the real SAR image (bottom) and of the simulated image (top) of study area 1.

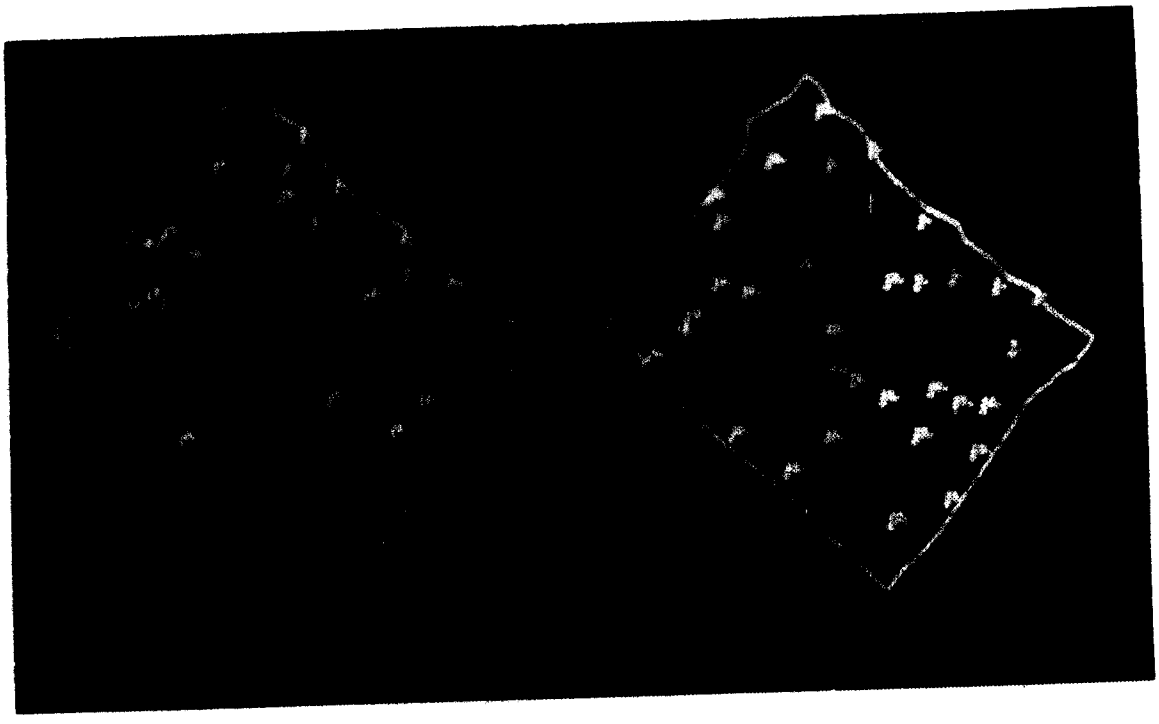

Figure 8.5: Distribution of control points resulting from single point determination (left) and from manual matching (right) after quality control.

Chapter 9

Image Compression using the Pyramid Approach

9.1 Introduction

SAR technology has become a well-developed and useful tool in many branches of scientific investigation concerning the surface of the earth. With the growing sophistication of SAR technology the need for efficient image processing techniques increases as well. As there are some characteristics of SAR images which require special algorithms for image processing it is recommendable to prepare the image for high-level processing such as feature detection with low-level processing techniques that do not only deal with SAR characteristics but make the performance of high-level algorithms easier.

First of all, radar images contain a large amount of *speckle*, which is hampering further image processing steps such as the detection of edges for pattern matching. As there exists a model for speckle in SAR images (*multiplicative noise*; Hovanessian [51]; Lee [73]; Tilley [95]), there are some special radar filters which make use of this information.

A second problem, which is not only a special feature of SAR images, is the *high data volume*. High-level algorithms are often quite time-consuming and the reduction of the data volume without loss of relevant information does not only increase computation speed but also decreases the memory space needed for it. One way to solve this problem is to make use of data structures which allow the access to different resolutions of one image. The so-called *intensity pyramid* as described below is such a data structure.

It is the aim of this section to offer possible solutions of the two problems speckle and high data volume i.e. it deals with comparing the effects of special filters for the reduction of SAR images in image pyramids.

9.2 Information Compression using Image Pyramids

Image pyramid schemes in general make essential use of relations between the different resolutions of pictorial representations of identical scenes. A pyramid is a stack of images of successively lower resolutions. The cells in the pyramid are arranged in square grids. According to Hartley [44], a cell contains a model of the region which it represents. In an *intensity pyramid*, for instance, the value of a cell represents the intensity of signal reflection of the region covered by the cell. In a *curve pyramid* (Kropatsch [61]) the value of a cell is a code, which describes how a curve traverses the cell.

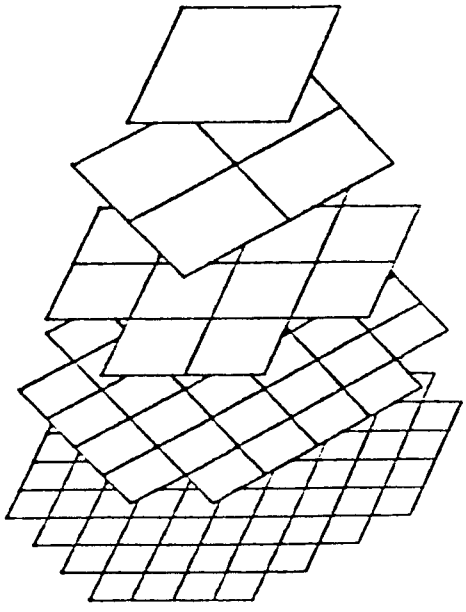

Figure 9.1: Even (2x2) pyramid

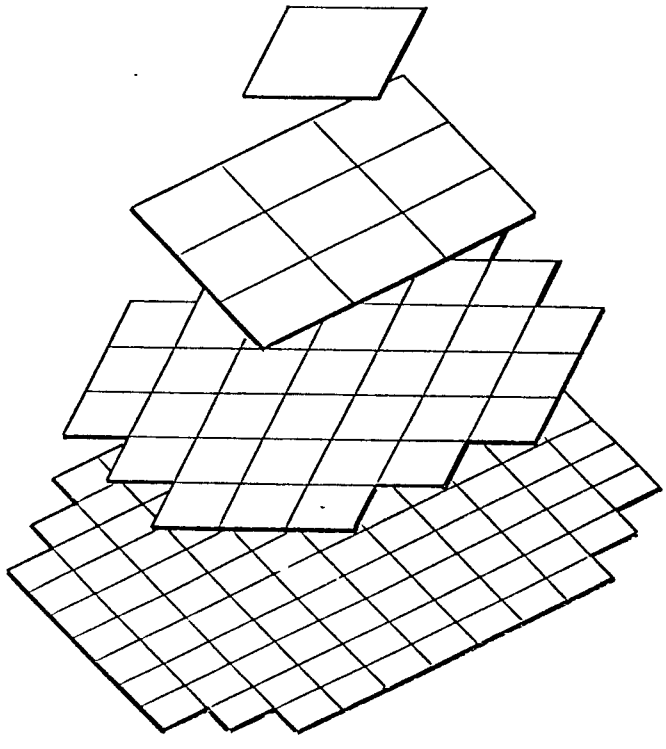

Figure 9.2: Odd (3x3) pyramid

Thus, the model establishes a relation between the information stored in a cell of the pyramid and the corresponding region in the image plane. Since one is dealing with cells at multiple resolutions, those models depend on the size of the cell. A *reduction function* summarizes the cell contents to yield a value at the next higher level. This summarization is applied repeatedly to fill the cells of the pyramid from the bottom to the top. Pyramids are called *odd* or *even* according to the type of reduction window (Figures 9.1, 9.2).

Two different types in terms of what a cell within a pyramid can contain are introduced by Ahuja [1]: one specifies the *center* of a cell, the other the *border* of a cell. Both models can further be categorized into *parametric* and *symbolic* models. The first category describes the cell by a set of parameters that are measured in the area of the cell. The other category encodes the contents by symbols or by labels. Both categories have advantages and can cooperate very closely.

Thus, different types of information can be used to build a pyramid (See the references for details):

1. For the odd pyramid (Kropatsch [59]) a parametric model is used that describes the grey-value *intensity* of the center of a cell (Hong [49]).

2. A symbolic representation of *edges* (Shneier [93]) is used to build a pyramid with even-sided windows.

3. Polynomials that represent *curve* or *line segments* that form corners (Hartley and Rosenfeld [45] and Hartley [43]).

4. Surface patches to describe *peaks* and *ridges* (Crowley [13]).

9.2.1 The Geometry of the Intensity Pyramid

During this study only pyramides derived from an odd number of cells have been considered. As a detailed description of the intensity and the curve pyramid would be beyond the scope of this treatment, the reader is kindly referred to the references by Kropatsch [61,62,58,60].

In this section pyramids with reduction functions applied to overlapped 3x3 windows (Figure 9.2) are addressed. Due to the geometrical facts, two successive levels are rotated with respect to each other by an angle of 45 degrees and the number of cells decreases by a factor 2. Some important features of three reduction functions will be discussed below. Experiments with Radar data have been used to verify the theoretical results and also to find some new statements (See also Kropatsch and Paar [63]).

9.2.2 Cell Contents

The basic operation that creates a multi-resolution hierarchy from a high-resolution image (i.e. the lowest level) is to merge the contents of cells recursively. Local operations on digital intensity images are defined within (small) odd-sided windows. Information about lower level regions is combined to form a description of a larger region at the next higher level. One basic reduction function to generate intensity pyramids, for example, averages the merged pixels. From the standpoint of visual recognition, more "general" objects are intended to be represented at higher levels, whereas "details" should be stored at lower levels of the hierarchy.

Table 9.1: Image processing aspects related to resolution

Resolution (Scale)	fine	coarse
Data amount	large	small
Computing time	(very) long	relatively short
Details amount	large	small
Survey	bad - none	well
Degree of accuracy	high	relatively low

Table 9.1 qualitatively shows the relations between level of resolution (i.e. the level of the pyramid) and some important features describing efficiency and costs of applied image processing.

9.2.3 Grey Value

The model for describing the grey value of a cell is a function that assigns every cell (k, i, j) a quantized measurement of the signal intensity reflected from the corresponding region; k is the index for the levels of the pyramid and (i, j) are the coordinates of the cell in this level.

9.3 Gauss Filter

In the odd pyramid the model of a cell is the mean grey value of the corresponding region. Since the structure of the used pyramid scheme involves overlap, the appropriate reduction function is an approximation of the Gauss filter. The weights which are used on a 3 X 3 block of pixels are given in Figure 9.3.

1	2	1
2	4	2
1	2	1

Figure 9.3: Weights for the used 3 x 3 Gauss filter.

The filtered result is normalized by a factor of 1/16. Note that all factors of this filter are powers of 2, which allows implementation by additions and shifts only and without the need of multiplication or division.

This reduction function is a linear filter (Wells [99]), that means the weights of the pixels do not depend on the grey values of the current window. They have been derived from the two-dimensional Gaussian distribution function 9.1 where $s = 0.85$ and x and y are distances from the center of the window in x- and y-direction.

$$G(x, y) = \frac{1}{s \cdot \sqrt{2}} \cdot \exp \frac{-(x^2 + y^2)}{2s^2} \tag{9.1}$$

The Gaussian kernel is not a filtering technique adapted to multiplicative noise. But, as it has already been used in pyramid algorithms (Rosenfeld [91]), many of its characteristics are well known, both theoretically and experimentally. Thus, the idea suggests itself to make comparisons between this linear filter and the Lee filter and Frost filter, so-called adaptive filters, considered below.

9.4 Frost Filter

This filter was developed by Frost [31] for the elimination of multiplicative noise. It is commonly used to reduce radar speckle as its model is exactly of that kind. Usually the Frost filter is employed only as filter but not as reduction function in pyramids. It was interesting to ask how such a filter performs when used to build a pyramid on SAR images. The local operation r on a square window is as follows:

$$\begin{aligned} r(B_n) &= W_n(B_n) * X \\ V_n(i,j) &= \exp\left[-\frac{\sigma^2(B_n)}{\mu^2(B_n)} \cdot t(i,j) \cdot f\right] \\ W_n(i,j) &= \frac{V_n(i,j)}{\sum_{k,l=1}^{n} V_n(k,l)} \end{aligned} \tag{9.2}$$

with

B_n	....	Current block with n x n elements
X	....	Matrix of grey values
$*$	....	Convolution operator
V_n	....	Matrix of weights
W_n	....	Matrix of normalized weights
$\mu(B_n)$	....	Mean of grey values in the block
$\sigma^2(B_n)$	....	Dispersion in the block
f	....	Parameter
$t(i,j)$	....	Euclid. distance from the element (i,j) to the center of the block

As one can see the weights $W(i,j)$ in the window are variable and depend upon the statistics of the window. For this reason it is called *adaptive*.

A large σ^2/μ^2 in the window causes the result $r(B_n)$ to become quite similar to the grey value of the center of the window (The weight of the center approaches 1). If σ^2/μ^2 is smaller, the result approaches the mean value of all grey values in the window. The parameter f generally controls the amount of smoothing.

In our experiments the following values for f have been found in connection with a window size of 3x3. With small $f(f < 5)$ this filter becomes approximately a mean-filter, e.g. the amount of smoothing is very high, nearly independent of the statistic parameters in the window. On the other hand, if $f > 30$, the center of the window always has approximately 1 as weight, so that there are pixels which do not have any influence on the values of the next higher pyramid level (Since only every second pixel is a center of a 3x3-window, see Figure 9.2). For airborne radar images $f = 15$ was found to be the value for the pyramid with the best optical appearance.

Figure 9.4: Unreduced radar image (= Level 0).

9.5 Lee-Filter

The Lee-filter in the existing form was developed as adaptive filter especially for the case of additive noise (Lee [73]). This is, for example, true for satellite- and aerial images of the visible domain. As this model is not adequate for speckle in radar images, it is, however, a similar one and it was interesting to see how it performs on radar images. The function r on a square window is defined as follows:

$$\begin{aligned} r(B_n) &= \mu(B_n) + K \cdot [(z(B_n) - \mu(B_n)] \\ K &= \frac{Q(B_n)}{Q(B_n) + \sigma^2_{Noise}} \\ Q &= \max\{[\sigma^2(B_n) - \sigma^2_{Noise}], 0\} \end{aligned} \tag{9.3}$$

with

B_n	....	Current block with n x n elements
$\mu(B_n)$	....	Mean of grey values in the block
$z(B_n)$	....	Grey value of the block center
$\sigma^2(B_n)$	....	Dispersion in the block
σ^s_{Noise}	....	Assumed dispersion of noise

If the dispersion of the grey values in the window is high compared with the assumed noise dispersion the weight of the center becomes large (near to 1). With small dispersion in the window the filter approaches the mean filter.

9.6 Experiments and Results

The following statements were formulated after having used some different filters as reduction function in the pyramid on airborne radar images acquired during the SAR CV-580 Campaign over the test site Freiburg, FRG, (see Figure 9.4) and in synthetic images.

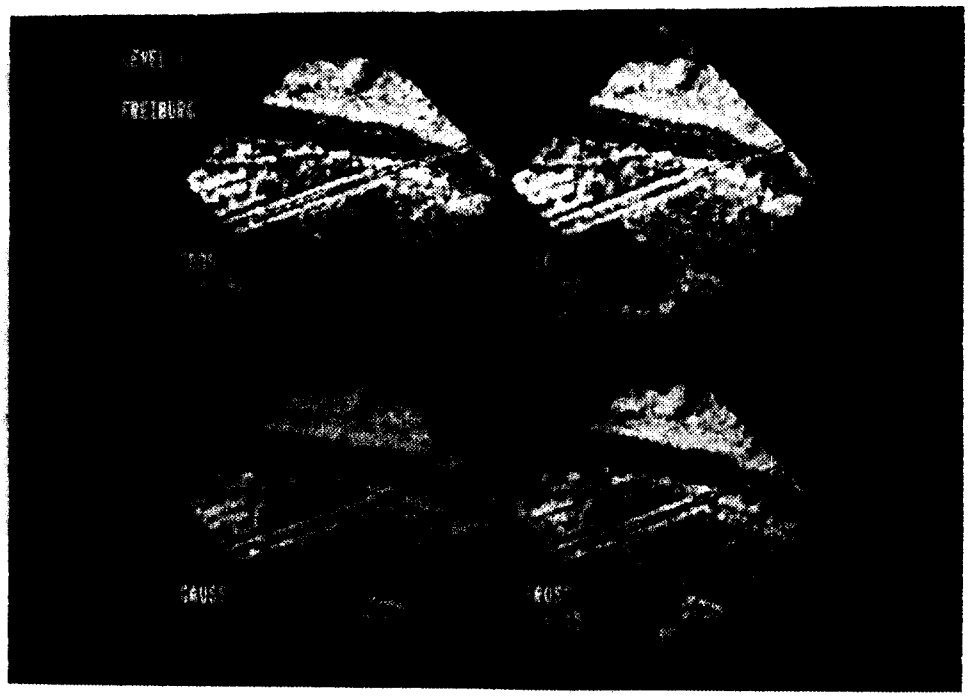

Figure 9.5: Reduced radar image (= Level 1).

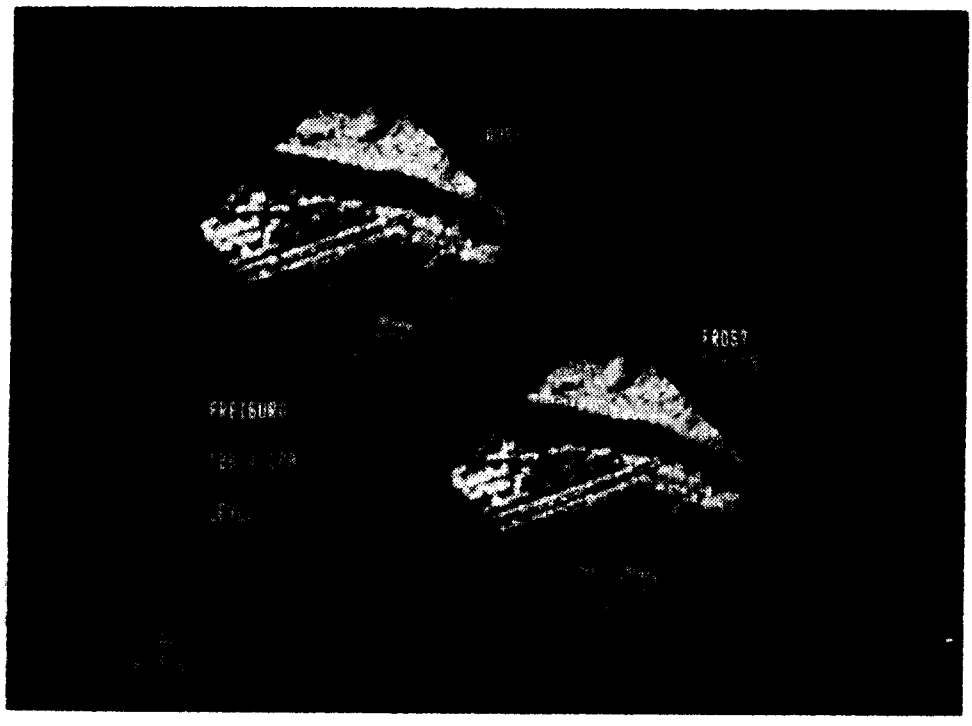

Figure 9.6: Level 1 of radar image reduced by Gauss and Frost filters (contrast stretched)

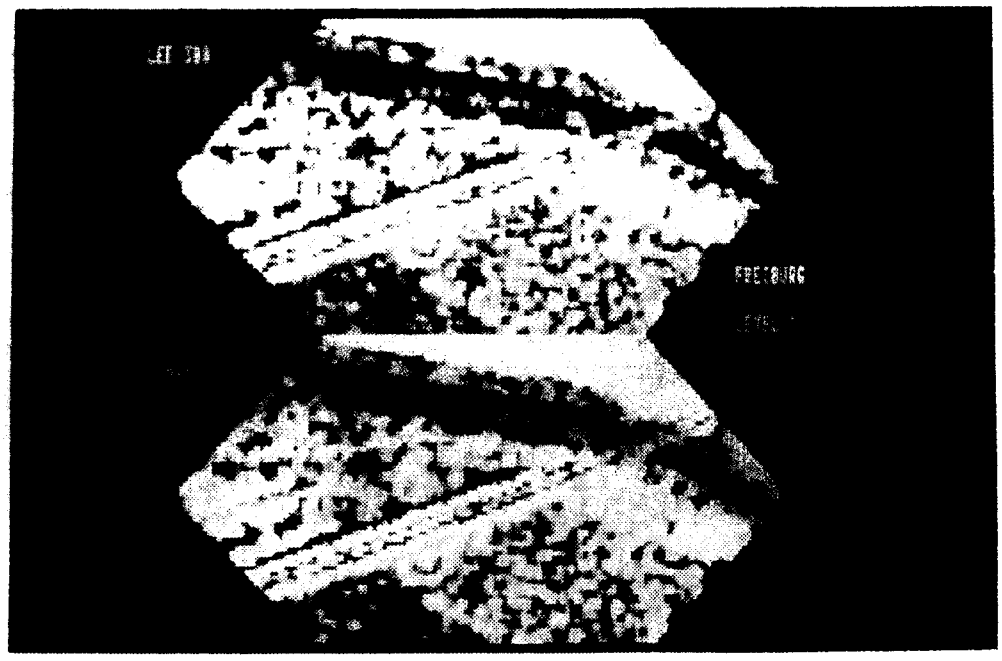

Figure 9.7: Level 1 of radar image reduced by Lee and Frost filters (contrast stretched)

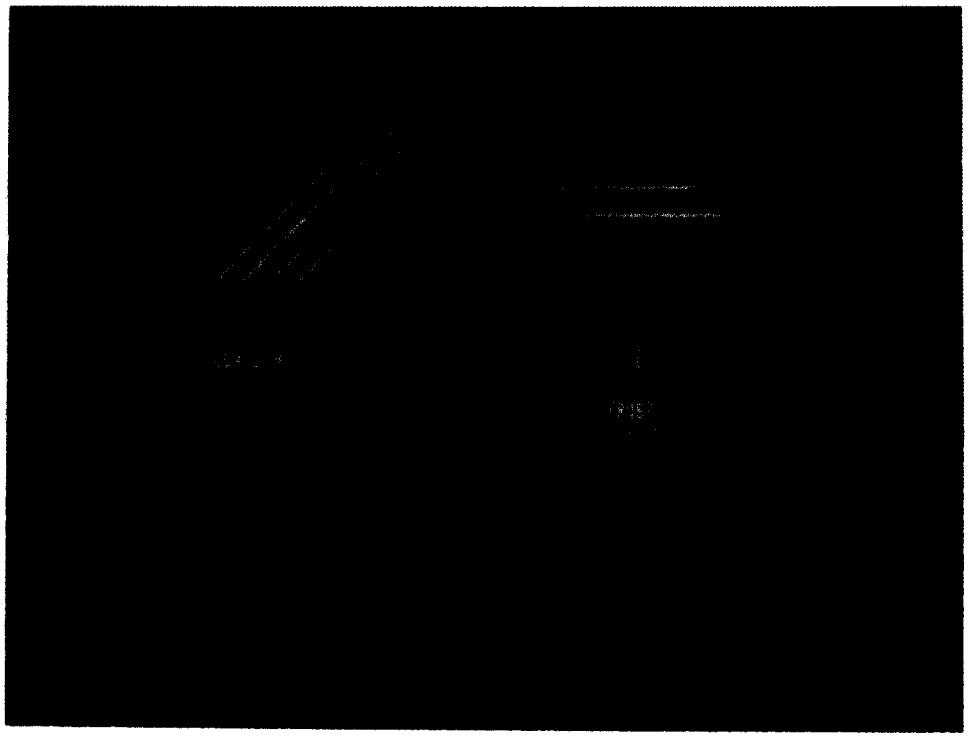

Figure 9.8: Disappearing of diagonal lines after reductive Frost-filtering

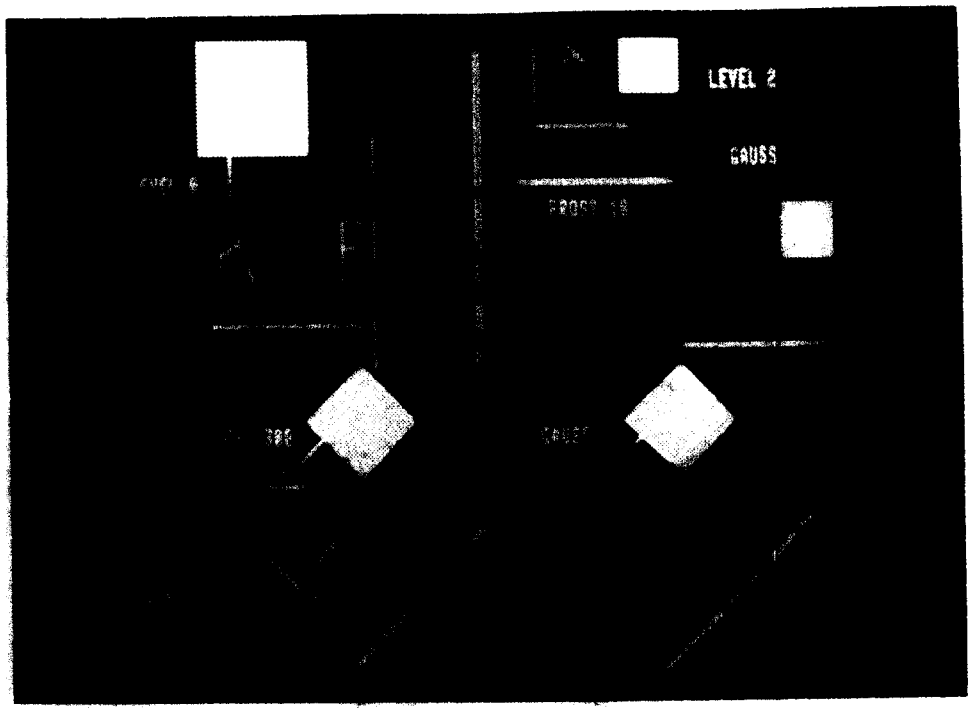

Figure 9.9: Three pyramid levels of synthetic image

1. High contrast is fairly reduced by Gauss. Frost filter ($f = 15$) and Lee filter(σ^2_{Noise}=300) tend to preserve contrasts better, especially at step edges (See Figures 9.5, 9.6 and 9.9).

2. Low-contrast regions are smoothed well by the Frost filter.

   Example: In Figures 9.5 and 9.6 there is hardly any difference between Frost and Gauss in the low-contrast regions of this image.

   Observation: As σ^2/μ^2 of equation 9.4 in windows of low contrast is low too, the Frost filter becomes approximately a mean filter.

3. The separation of straight lines is visually better after filtering by means of the Frost filter ($f = 15$) than after using the Lee filter ($\sigma^2_{Noise} = 300$), especially at low grey levels.

   Example: Figure 9.7 shows a radar image with two visual dominant features. The dark strip represents a river. It is crossed by a straight railroad. After reduction by means of the Frost filter ($f = 15$) the structure is better perceptible than after using the Lee filter ($\sigma^2_{Noise} = 300$) because of the better separation of the parallel dark straight lines.

   Observation: As the assumption of multiplicative noise is not met by Lee, the filter performs differently in dark and bright regions.

4. Thin diagonal lines disappear completely under special circumstances (Frost, Lee filter).

   Example: This is shown in Figure 9.8 where an image with 4 diagonal lines (1 pixel wide) has been reduced using the Frost filter ($f = 10$). The distance between the diagonal lines is 11 pixels in each case. Thus, the centers of the 3x3 windows are situated twice on the lines and twice beside the lines, which causes these two lines to disappear on the next level of the pyramid.

   Observation: As the centers of the 3x3 windows are arranged like the white squares of a chess-board, diagonal lines can be "black" or "white". In all cases high contrast

of lines causes a high σ^2/μ^2 in the involved windows and the centers of the windows get large weights. If the centers of the windows are not on the line, the line will therefore disappear.

The same thing happens to a vertical or a horizontal line after 2 reductions, as it becomes diagonal after having been reduced once. If the line is neither vertical nor horizontal nor diagonal, it will be taken to pieces by Frost and Lee filters. In that case connectivity gets lost (See the letters "K" and "F" on Figure 9.9 at Level 2). This problem does not appear on reduction with the Gauss filter, because the lines are smoothed, of course, but they can be identified still and connectivity is maintained.

9.7 Conclusion and Outlook

Pyramids as a tool for multi-resolution image analysis have never been employed yet especially for radar images. The images collected in the pyramid essentially contain the same information, but on higher levels there are fewer details and interpretation can be concentrated on important global features.

Digital filters have been used in connection with this concept both for the reduction of radar and synthetic images. Especially for radar images the Frost filter turned out to be a good combination of smoothing and contrast preserving because of its local statistical method. Depending on the reduction function used some features of the image can be changed or destroyed.

Further experiments on pyramids also containing symbolic information about radar images like will become necessary. This topic is currently under active investigation at DIBAG.

Chapter 10

Utilization of a Prototype System in Geological Applications

10.1 Specification of Application Field

In agreement with the European Space Agency, structural geological mapping (lineament analysis) has been chosen as application field for tests of the available radargrammetric software prototypes. One reason for this decision was that information on two-dimensional surface features such as rock units is also extracted from radar imagery within the scope of other ESA application studies in the geoscientific domain. As the analysis of linear elements plays a very important role in geology, it seemed appropriate to restrict the application for demonstration to the gaining of experience in radar lineament analysis.

10.2 Development of Utilities for Lineament Evaluation

Considering the particular software needs for the application study a number of tools for lineament analysis have been developed. The developed software contains a unit (1) for lineament acquisition from remote sensing image data, (2) for transformation of lineaments between images of different scale, orientation and geometry, (3) for statistical evaluation of lineaments and last but not least (4) for representation of the respective results. Thus, the 4th unit is split up over the 3 others.

10.2.1 Lineament Acquisition

This software module contains all functions necessary for the acquisition of linear features from the imagery, especially lineaments. It is split up into a preparatory and a digitizing step.

Preparatory Step:

Here all work for preparing the system for the digitizing of lineaments is done. This includes: selecting the type of sensor (SAR and Landsat TM are included); selecting the image and the desired geometry (for the SAR sensor: SAR = original SAR data, SIM or REG = simulated or registered image and ORT = ortho-image; for Landsat TM: UNR = unrectified image and REC = rectified image can be chosen); and selecting the image window and the reduction factor. After this set-up the desired image window will be

displayed on the screen (for SAR: one channel in black-and-white mode; for TM: up to 3 selected channels in color mode, or one channel in black-and-white mode). The operator's choice to create a new set of lineaments directly leads to the digitizing step. Continuation of work on an existing set, where the existing lineaments are displayed before, has also been forseen.

Digitizing Step:

When working on a new set of lineaments, one has to define the north direction first (stored as lineament number 0). While digitizing new lineaments, i.e. defining the beginning and the end of the lineare feature, it is possible to delete the last digitized lineament before storing it in a file.

For the verification of the mapped lineaments a number of tasks are available, which are described in detail in Section 10.3. Figure 10.10 shows a typical result.

10.2.2 Transformation of Linear Features

This working unit contains all functions to transfer lineaments from one image to another, using rigorous (radargrammetric, if necessary) transformations. Images with different orientations, scales or geometries can be treated. These functions are based on working with points which are transferred. Using the lineaments of one image as an image of its own and transforming it as an image does not yield good results (lines will become interrupted or blown up).

Geometries:

Depending on the selected sensor type the following transformations have been made available:

For the SAR sensor:

- from the original SAR image to the simulated (registered) image (SARSIM) or from the simulated image to the real SAR image (SIMSAR) by using the ancilliary information computed in the image registration step (see description of the simulation-based geocoding method given in the Appendix).
- from the simulated image to the ortho image (SIMORT) by using the data files of the geometric rectification step;
- from the ortho-image to the simulated image (ORTSIM) by using the simulation step.

For the Landsat TM sensor:

- from the unrectified image to the rectified image (UNRREC) or vice versa (RECUNR) by using ancillary information computed in the Landsat image rectification.

Scales and Orientations:

Reduction or shift of lineaments is possible, for images of different scales. It is also possible to rotate or mirror the lineaments in the case of different image orientations. For the verification of the transferred lineaments a number of possibilties are available, which are described in detail in Section 10.3.

10.2.3 Lineament Statistics

Due to the possibility of mapping the lineaments with the digitization module of the system DESBOD—a geographic information system installed at IPCG—and of including these data in the present utilities, an interface has been developed, which enables to northen the linear features and to calculate the direction and length of each lineament.

For statistical evaluation selected lineaments (selection according to lineament length) are split into direction classes (class intervals can also be selected). For each class the cumulative length and the frequency of lineaments per direction class is calculated.

Table 10.2.4 shows lineament statistics based on direction classes. Graphic representations of the statistics (rose diagrams and bar histograms are available) are described in Section 10.2.4.

10.2.4 Graphic Representation

The same way of representing the results is available for the acquisition and transformation steps. The tasks are to list and print the files with the lineaments as well as to display and plot them. In the case of graphic representation one can decide to have all lineaments or a selected number displayed, a selected direction class or a selected length range of the lineaments. It is also possible to display the lineation superimposed on an image (see Figure 10.11) by selecting one of 6 available colors.

In the third step—the representation of statistical results—one can select graphic representations that can be displayed or plotted besides the common functions of printing and listing. This can be done in the form of a bar histogram—either separately for the cumulative lenghts and for the frequencies—or combined in one bar histogram showing the cumulative lenghts above the axis and the frequencies below. The latter are more suitable for comparisons. For synoptic presentations geologists like to use circular diagrams. Here the upper half shows the length distribution of lineaments per direction class and the lower half indicates the frequency per direction class (see Figure 10.12). For graphic representation up to 3 statistics can be combined in one diagram using different colors.

10.3 Preparatory Activities

10.3.1 Identification of Suitable Radar Data Available

Presently the only space-borne radar data available are those of Seasat or of the Shuttle Imaging Radar. As for the location of the study areas a region in SW Europe was proposed, the only data available came from the orbit no. 66.4 of the Shuttle Imaging Radar Mission B. Through postal and telephone contact with the respective processing units at the Jet Propulsion Labarotory in Pasadena, California, it has been found out that scene no. 18 from this orbit had been processed digitally and turned out to be of reasonable quality. Hence, this image data covering an area of 85 x 20 km2 has been selected for the demonstration study. For location see index map in Figure 10.1.

Investigations at the ESRIN facilities of ESA in Frascati, Italy , resulted in the information that there also exist recent high-quality Landsat Thematic Mapper data of the area covered by the above mentioned radar imagery, which is located in NW Spain. The provision of a computer compatible tape with this data through ESA shall be thankfully mentioned here.

Table 10.1: Output of statistical lineament analysis showing different direction classes.

STATISTICS OF LINEAMENTS
****

SPAIN, STUDY AREA 1, SAR

CLASS INTERVAL: 15 DEGREES
TOTAL NUMBER OF CLASSES: 12

USED FILE(S):
SITE1_SAR.LINES

	DEGREES (Azimuth North)		KILOMETERS	FREQUENCY
CLASS NUMBER	CLASS MIDMARK	CLASS BOUNDARIES LOWER-, UPPER LIMIT		
1	270.	262.5 - 277.5	51.3	14
2	285.	277.5 - 292.5	13.3	3
3	300.	292.5 - 307.5	5.0	2
4	315.	307.5 - 322.5	35.0	9
5	330.	322.5 - 337.5	8.8	2
6	345.	337.5 - 352.5	0.0	0
7	0.	352.5 - 7.5	2.8	1
8	15.	7.5 - 22.5	32.0	6
9	30.	22.5 - 37.5	0.0	0
10	45.	37.5 - 52.5	0.0	0
11	60.	52.5 - 67.5	0.0	0
12	75.	67.5 - 82.5	22.7	6
TOTAL:			170.8	43

MAXIMUM VALUES: KILOMETERS 51.3
FREQUENCY 14

10.3.2 Identification of Study Region

It has been attempted to use study areas which provide non-vegetated, slightly and densely vegetated regions and which comprehend low- and high-relief terrain. This led to the decision to outline three study areas, one of them being mostly situated in rolling and two of them in mountaineous terrain. The mountain ranges S of the main divide of the western Cantabrian Mountains and the Duero Basin S of the Cantabrian Chain fullfill all the above mentioned requirements. Their geoscientific characteristics, complemented by a few illustrative photographs, are given in the Photo Documentation below.

The strange shape of the three study areas selected (Figure 10.2) is due to the following facts:

- SIR-B data take strip;
- geological characteristics;
- type of relief;
- digital terrain model available (Figure 10.3).

10.3.3 Identification and Procurement of Collateral Data

Apart from 1 : 200000 hardcopies of Landsat MSS images of this area, the above mentioned Landsat Thematic Mapper data in digital form were also available. These data of the fourth quarter scene of scene no. 203-30, acquired on September 4, 1985, have been used for comparative structural geological evaluation, and they have also been geometrically rectified.

For the generation of digital terrain models film sheets with contour and drainage lines of the respective 1 : 50000 topographic maps have been provided by the Instituto Geologico y Miñero de Espana in Madrid. The courtesy of the Spanish authorities in this respect is thankfully acknowledged. Moreover, the topographic map sheets 1 : 50000 and 1 : 200000 of the area were available as well.

As far as geological collateral information is concerned, 4 sheets of geological maps at a scale of 1 : 50000 and 1 : 250000 (partly also unpublished manuscript maps) where used as background information. Several papers on the geological structure of the region served the same purpose.

10.4 Geoscientific Outline of the Study Region

10.4.1 Geographical Setting

The studied region is situated on the Iberian Peninsula, in the NW of Spain. The Cantabrian Chain, which follows part of the northern coast of the peninsula, acts with its southern slopes, N of the city of Leon as the scenario for the study areas.

The flight path of the studied SIR-B data covers two different types of terrain, geologically known as Cantabrian Zone and Duero Basin.

The Cantabrian Zone is a mountain belt with humid climate and a comparatively dense canopy of vegetation demanding high humidity (Picture 10.4). On the other hand, the isolated flat surface and relatively high altitude of the Duero Basin in addition to the

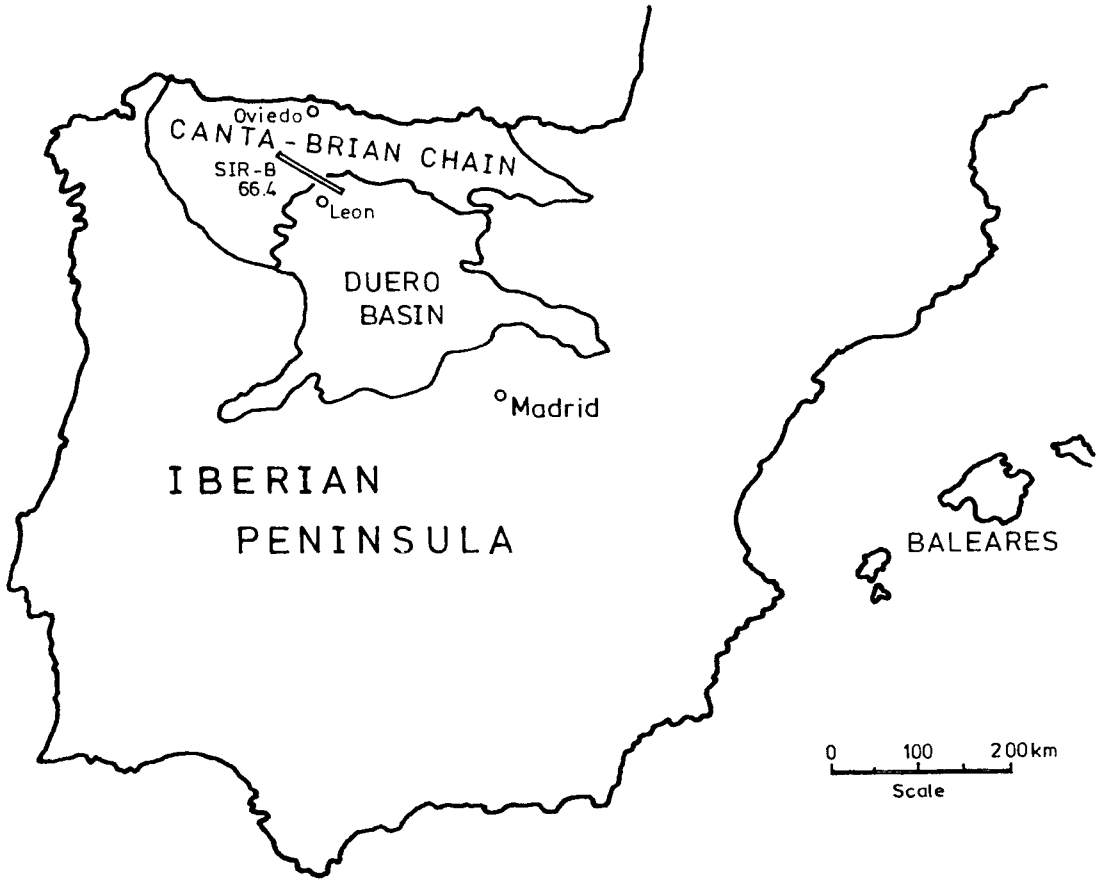

Figure 10.1: Location map of scene no. 18 of SIR-B orbit no. 66.4. The two major geomorphological/geological units covered by this scene are also indicated.

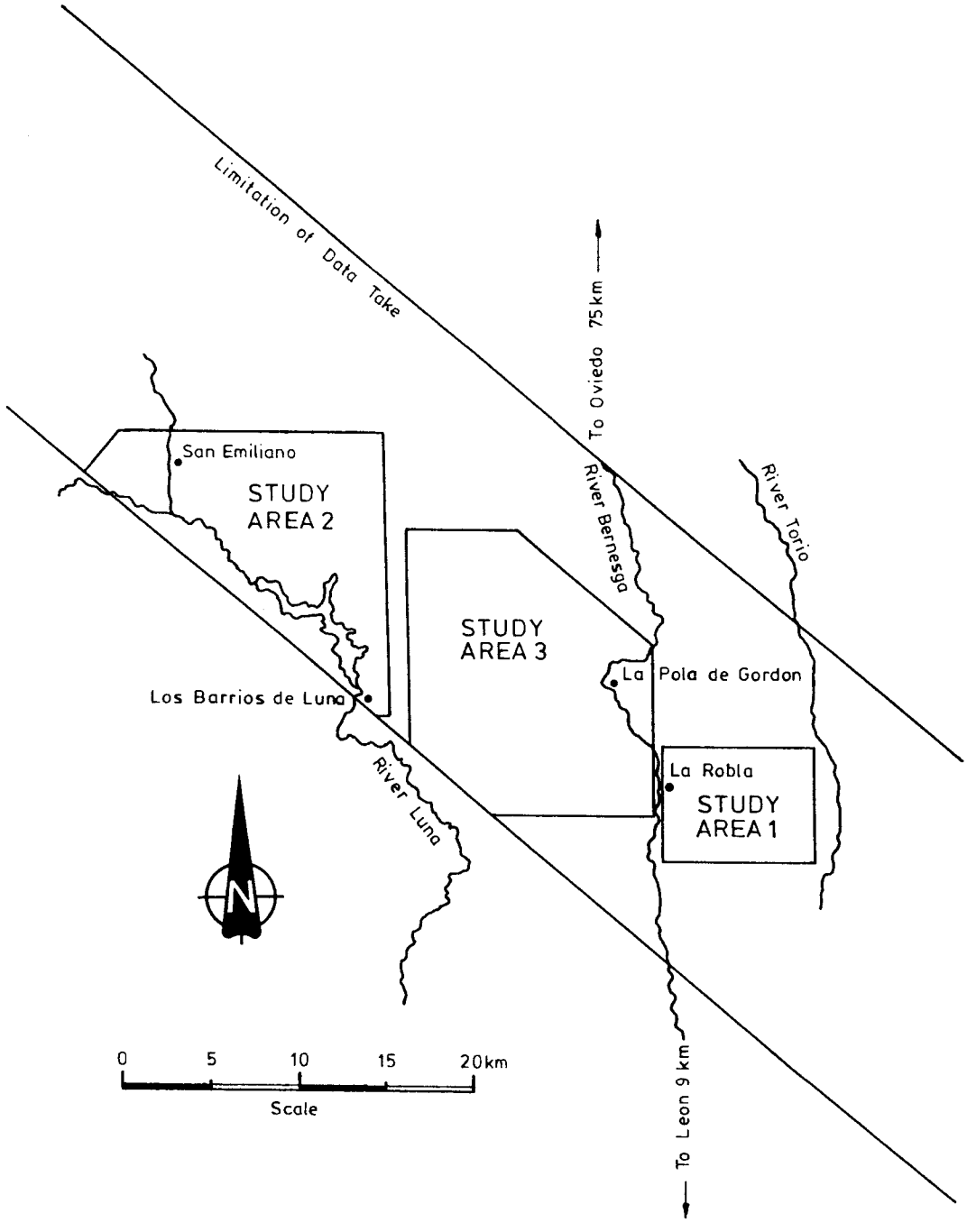

Figure 10.2: Location of the three study areas within the provided SIR-B scene no. 18 of data take no. 66.4 in the Cantabrian Mountains.

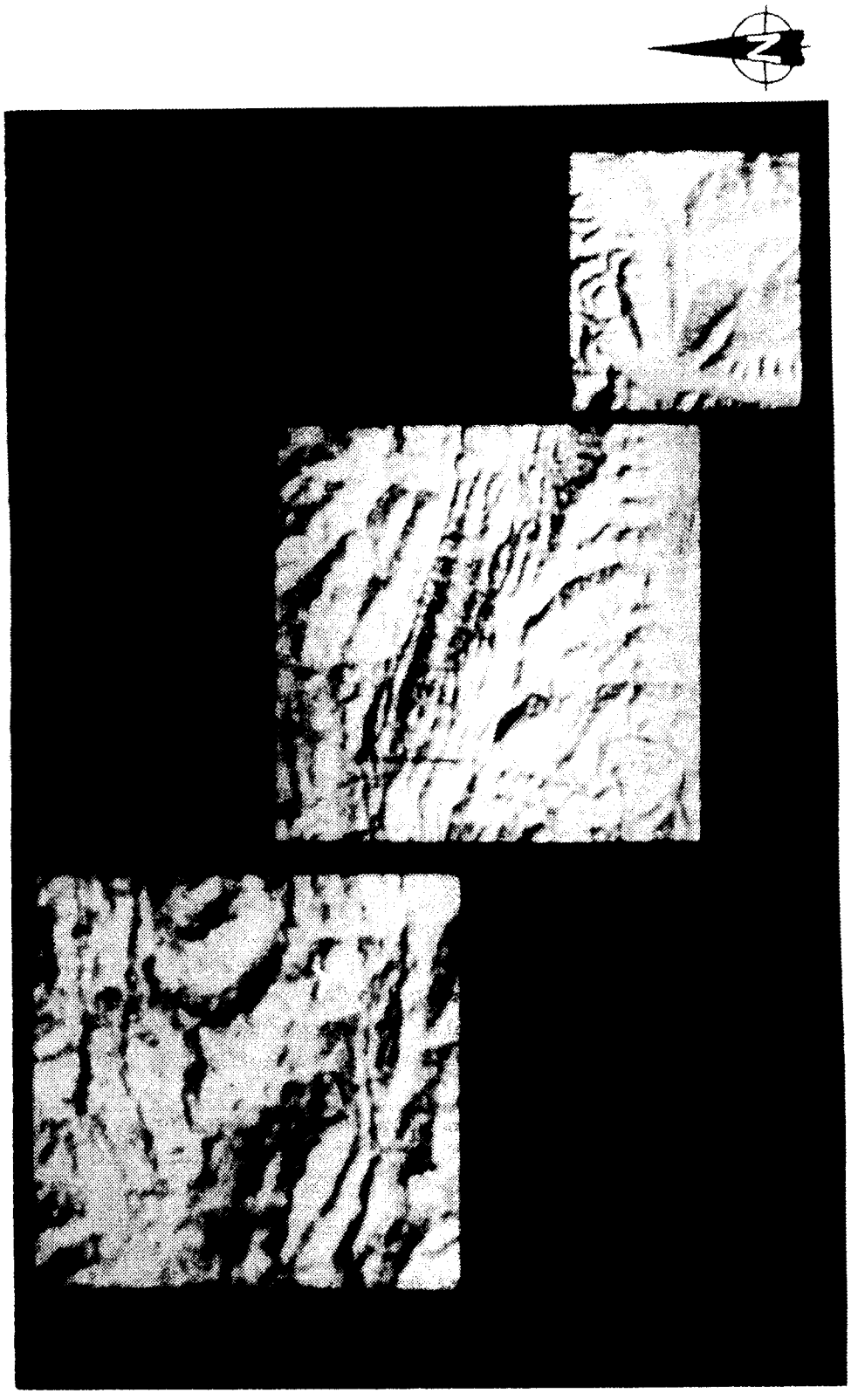

Figure 10.3: Illuminated DEMs of the study areas displaying terrain relief.

mediterranean summer drought there determine a climate with long and cold winters, very warm summers and low precipitation throughout the whole year.

The population is small and spread over villages and small towns situated along the valleys. The most important towns are situated along the road from Madrid to Oviedo, which crosses the scene in the N–S direction, following the valley of the river Bernesga.

10.4.2 Vegetation

The whole area has a more or less dense coverage of vegetation which conceals lithological features. However, there exist specific plant coverages associated with different geological environments, which help to draw conclusions about lithology.

Most of the smooth hills of the Duero Basin have been actively reforested with conifers (Picture 10.5). Where conifers do not grow, heather and brooms of different sizes occur (Picture 10.6). They form a nearly continuous canopy. In the flat valley bottoms along the rivers one finds cultivated fields. During the past thirty years, due to a decrease in population, the intensity of cultivation has receded considerably.

In the Cantabrian Zone, the mountains set limits to a more varied distribution of vegetation. Rock outcrops along ridges frequently show poor vegetation. Some shrubs take advantage of the joints in limestones, while the surface of quartzites is uniformly covered by lichens. Hazelnut and oak trees (Picture 10.7) are associated with the contacts of limestones. On the other hand, shales and sandstones provide a typical associations of heather and brooms (Erica, Sarothamnus). Therefore, belts of different lithological units striking parallel to the ridges of resistant materials coincide with corresponding belts of different botanical associations.

10.4.3 Geology

Introduction

In its western half the Iberian Peninsula is covered by a big remnant of the ancient Hesperian Chain, the so called Hersperic Massif, which represents part of the Iberian segment of the European Hercynian orogenic belt. To the E it is bordered by two Tertiary basins, drained by the rivers Duero and Tajo.

In its extremities the Hercynian structures are distinctly delimited by two very different elements: to the North the Cantabrian Coast, and to the South the Guadalquivir Basin and the Betic Front. They cross the Iberian Massif in a SE-NW direction curving in the form of an arc near the northern boundary of the massif. The southern part of the arc is well represented, the northern one is well-developed in a very small sector only, the Cantabrian Zone, in which two of the test areas are located.

The southern portion of the provided SIR-B data covers the northern part of the Duero Basin, which is mainly filled with Tertiary sediments. It is a very well defined geological and geomorphological unit consisting of a wide plateau (200 km long and 250 km wide) at an average altitude of 850 m. The geological border with the Cantabrian Zone is a clear ENE-WSW trending fracture line.

The above metioned two domains have a very different geology and show striking differences in relief, climate and vegetation.

Cantabrian Zone

Structure

The Cantabrian Zone shows a sequence of Palaeozoic rocks with varying lithology mainly of the Upper Carboniferous age. Traces of magmatic activity are rare, plutonism is almost non-existent. Limestones, sandstones and shales are abundant.

Deformation during the Hercynian period took place under epidermic conditions in which contrasts in ductility largely controlled the deformation. No metamorphism has accompanied the deformation. Cleavage is absent or weakly developed.

An early tangential phase gave way to decollement nappes through slipping along bedding planes of the Lower and Middle Cambrian formation. Later, a flexure mechanism produced two systems of longitudinal folds with almost vertical axial planes: an arched system that follows the Asturian arc and a radial one that intersects the former one.

Study areas 2 and 3 and the northern part of study area 1 are a good example of the decollement structures and longitudinal folds of the arched system.

Relief and Drainage

The Cantabrian Chain represents the main divide between the large river systems draining into the Atlantic and the Mediterranean Sea. At the same time, this divide is a barrier that, by intercepting the north-westerly winds, creates two different climatic areas on the Iberian Peninsula: the humid northern Atlantic fringe, and the dry southern Mediterranean lands.

Differential erosion has taken advantage of the varying resistance of the underlying rocks in the area, where Devonian and Carboniferous limestones and Ordovician quartzites are the resistant elements that form the pronounced headlands, while the valleys are carved into softer Silurian, Devonian or Carboniferous slates. This landscape can be described as an Appalachian ridge-and-valley type of relief (Picture 10.8).

The rivers of the study area represent the heads of the streams which run from the drainage divide of the Cantabrian Chain in the N southwards across the Duero basin to join the river Duero, which drains into the Atlantic.

Karst Processes

Devonian and Carboniferous limestones in the area show karstic features, such as dolines and sink holes, through which water drains into the massif and reappears at the contact with the shales (Picture 10.9).

Some of those dolines act as nivation hollows, which allow dolomitization processes to take place.

It could be demonstrated in the field that in many cases there exists a clear interrelation between the intersection of lineaments (major ones with minor ones) and the occurrence of karstic features.

Frequently, canyons can be observed within the limestone formations.

Duero Basin (with Emphasis on Study Area 1)

Study area 1 covers the southern fringe of the Cantabrian Zone in the N and the rather flat Duero Basin in the S. Its border is formed by a sharp tectonic feature trending parallel to the contact with the Palaeozoic series of the Cantabrian Zone, displaying its surface expression in the form of a gentle depression.

Some Cretaceous sandstones and limestones with steep dips to the South along the edge of the Cantabrian Zone form an isolated ENE-WSW trending ridge which separates the two domains.

Right to the S of this ridge, the flat-lying Tertiary conglomerate series produce a gentle relief with flat valleys and smooth slopes along rather equally flat-topped ridges. Steep escarpments along the valleys are rare.

The composition of the conglomerates representing different alluvial fan facies is responsible for a massive appearance and the formation of gentle hills. The contact between the slope and the bottom of the valley is concave, suggesting the inheritance of a former periglacial fluvial net.

The emplacement of the drainage net is active. Streams are eroding the deposits of the slopes and building their own cones of dejection at their mouths. The main rivers run N–S, with tributary streams in NW–SE direction.

In study area 1 only in two places indications of fault could be identified in the field through slight vertical (and horizontal) displacements of conglomerate layers in steep river escarpments.

10.4.4 Photo Documentation

The following pages are supposed to give a sort of background information on what the study region selected looks like.

Figure 10.4: Typical settlement and countryside in the Cantabrian Zone. The mountainous relief and the humid climate in this area allow some humidity-demanding trees such as chestnut, oak and hazelnut to grow. Village of Geras in study area 3

Figure 10.5: Reforested conifers in the Duero Basin (study area 1). Reddish-brown areas inserted into smooth hills and flat forested valleys are covered with dense shrubs of heather and brooms.

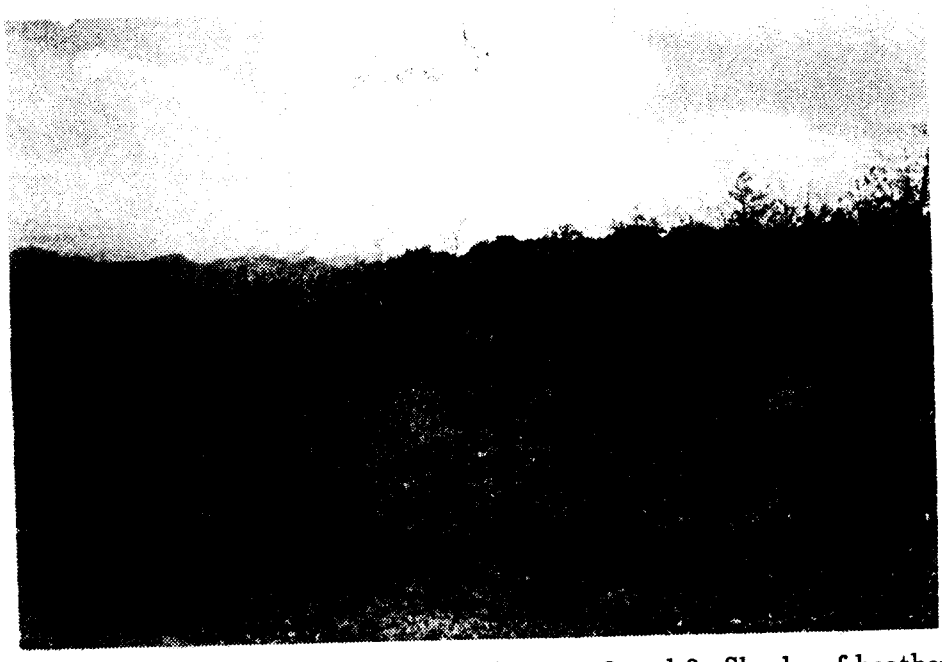

Figure 10.6: Typical vegetation cover in study areas 2 and 3. Shrubs of heather (purple flowers) and brooms (yellow flowers) intercalated with young oak trees.

Figure 10.7: Differential distribution of vegetation depending on the underlying rocks. Hazelnut trees are associated with limestones and limestone intercalations. Heather and brooms grow on shales and sandstones more down the slope as well as on pasture land and cultivated fields in the lower part.

Figure 10.8: Appalachian ridge-and-valley type of relief in the Catabrian Zone. Ridges built by competent rocks (mainly limestones) and valleys carved out in less competent shales and sandstones. Study area 3 west of Barayos de Gordon.

Figure 10.9: Gentle relief terrain with dolines and sink holes in Carboniferous limestones. This type of landscape is locally intercalated into the ridge-and-valley terrain. Near Porto de la Cubrilla east of San Emiliano, study area 2.

10.5 Geological Lineament Analysis

10.5.1 Processing Tools for Lineament Analysis

The utilities for lineament evaluation which have been developed and implemented during the study are discussed in this chapter. These software tools were able to provide a test-bed for a number of initial steps in geology-related processing of SAR data. Consequently, the use of the developed software prototypes has been a valuable aid for the identification of

- further processing requirements for semi-automated lineament analysis and
- interface requirements to support the lineament mapping and analysis tasks performed by the geological operator.

As effective simple filters for the preparation of radar data for structural geological evaluation, an interactive Gauss and a Frost filter have been programmed. The same is valid for an image pyramid program (cf. Chapter 9), which has been tested for its usefulness in supporting efficient lineament mapping.

Statistical programs for the evaluation and display of frequency distribution as well as cumulative lengths per direction interval have been developed and brought to an operational level. These programs enable the direct analysis of the lineament pattern on the screen of the image processing system. They turned out to be necessary tools to obtain valid statements on the various types of lineament analysis carried out within this project.

10.5.2 Field Verification of SAR Image Information

Like in thematic airphoto interpretation, field checking is—at least in the form of spot checks—inevitable in radar mapping. For the selection of test areas and to familiarize themselves with the structural geological characteristics of these sites a 5-days field campaign was undertaken by the geologists participating in this study. It turned out that in mountainous terrain even geologists with a reasonably ample experience in radar mapping can have serious orientation problems when using geometrically unrectified radar imagery only during the field campaign. Apart from the strong geometric distortions, in the first instance extreme foreshortening, within the present demonstration study, also the fact that there were no changes in the grey values which might have indicated specific surface types, made orientation even more difficult.

Decent work in the field can only be accomplished within a reasonable period of time if geometrically rectified radar images are used. This is at least valid for high-relief terrain.

10.5.3 Radar Data Analysis

The lineaments of all three study areas have been drawn both on the screen of the image processing system using a cursor and on transparencies fixed on hardcopies. The latter have been enlarged to a scale of 1 : 100000 which has been considered most suitable in relation to the original spatial resolution and the synoptic view necessary for lineament analysis. With 1 : 200000 the imagery turned out to be too small for the recognition of supporting details.

10.5.4 Study Area 1

The two geological domains existing in study area 1 show different patterns of lineaments.

The analysis of the geometrically corrected image, which has been generated by using the simulation-based rectification technique, yielded a denser net of lineaments than the uncorrected one. When comparing the two results, the most striking feature is the enhancement of N-S trending lineaments in the Palaeozoic domain, which do not appear in the uncorrected image. Those lineaments have an angle of 45 degrees or less to the SAR illumination direction.

10.5.5 Study Area 2

The number of mapped lineaments might be too low for statements about their directional distribution.

10.5.6 Study Area 3

As far as lineament density is concerned, for study area 3 the same is valid as for study area 1. In the ortho-image of study area 3 slightly more lineaments show up than in the uncorrected image. Nevertheless, some lineaments which trend more or less parallel to the illumination direction, cross the main geological strike and are hence not so obvious in the ortho-image, can be seen in the uncorrected image. V-shapes formed by incisions in the ridges, which are aligned in a "cateniform" way, let these lineaments occur with a fairly high density in the uncorrected image.

10.5.7 Analysis Using Compressed Image Data

The geologists who had to perform the lineament mapping expressed the need for an image of about 10 km x 10 km to be displayed on the screen at once to obtain a satisfying synoptic impression. Therefore, the images had to be reduced to lower resolution. This image reduction can easily be done by incrementing. Using a factor greater than 2 causes too much information loss so that the geologist sometimes is not able to extract the desired linear features. Another way of reducing the data is the use of intensity pyramides. The image pyramid technique is explained in chapter 9. Here, a few results from applying this technique are reported.

Image compression was done for study area 1 by using an intensity pyramid of 5 levels based on a Gauss filter. The different hierarchical levels of image compression in the pyramid are named from level 4 for the original data (as base of the pyramid, in the actual case a 1024 x 1024 SAR image) to level 0 for the top, where the data are reduced in area by a factor of 256. This means that 256 pixels of the original image are represented by 1 pixel in the image of compression level 0. Table 10.2 shows the relation between the different levels.

Due to the application in lineament analysis the compression of level 0 does not seem to be useful, so only the levels up to 1 were used. As shown in Figures 10.13 and 10.14 the number of extracted lineaments is decreasing between 15% and 50% when going up one level in the pyramid.

Curve pyramides (cf. Chapter 9) can also be possibly used for lineament detection, but this has not been investigated in this study.

Table 10.2: Different levels of the intensity pyramid.

level	reduction in area	number of pixels represented
4	1 x 1	1
3	2 x 2	4
2	4 x 4	16
1	8 x 8	64
0	16 x 16	256

10.5.8 Complementary Analysis of Landsat TM Data

Following the recent and logical trend of multi-data geoscientific analysis, Landsat Thematic Mapper data were analysed for lineaments in addition to the SIR-B data. As could be anticipated from the experience of the geologists contributing to the study, it turned out that a combination of Landsat data with the radar data does not significantly improve the information content, at least with respect to lineament analysis. On the contrary, morphological as well as vegetational features indicating faults or fractures were hidden by the merging which was partly due to the difference in illumination. This is valid for simple RGB combinations as well as for IHS transformations. Therefore, three-band composites of Thematic Mapper data of the three study areas were analyzed inividually. Comparisons between the lineament analyses of geometrically unrectified and geometrically corrected TM imagery resulted in more or less identical lineament patterns. The proof of the highly significant similarity of the interpretation results was accomplished by geometric transformation of the lineament pattern obtained from the unrectified Landsat images.

10.5.9 Conclusions

Both corrected and uncorrected images can be used for geological lineament analysis. To acquire full information on linear features of geological significance out of radar imagery, complementary evaluation of both types is needed.

The angular relationship between the directions of structures and the illumination direction is responsible for the preferent occurence of lineaments in certain directions in the uncorrected image and in the ortho-image. Nevertheless, minor directional preferences of the lineaments could be observed in the geometrically rectified images.

On average (mean over the 3 study areas) some 5 % more lineaments can be obtained from the ortho- than from the unrectified images.

The directional preferences and also the aspect of an easier and less time-consuming, effective work in the field very much favor the radar ortho-images. There is no doubt that an additional lineament analysis of Landsat (Thematic Mapper) data makes a lot of sense. It seems appropriate to make a separate Landsat lineament analysis of the identical area and only combine the results of this evaluation with the radar lineament interpretation. In most cases the density of the radar and the Landsat TM lineament pattern might be more or less the same. The point is that both evaluations have to be used complementary.

Morphologically determined lineaments are, at least in mountainous terrain, better identifiable in the radar ortho-image than in the geometrically rectified Landsat TM image. This is valid for SIR-B data.

10.5.10 Recommendations for Demonstration Studies

Based on the experiences of the present project it seems advisable to gain a lot more experience in the operational utilization of spaceborne radar imagery for (structural) geological applications. Spaceborne radar data with varying elevation angles should be used for the mapping of mountainous regions. High-relief terrain seems to be the best test area for spaceborne radar imagery. Moreover, different types and densities of vegetation cover are another desirable requirement for test sites.

10.6 Structural Geological Aspects of Lineament Analysis

In the following some results with relevance for the geoscientist shall be given.

10.6.1 Study Area 1

In the Palaeozoic mountainous domain a preferent direction striking in an angle of about 60 degrees to the SAR illumination direction is obvious. This direction follows the E–W-trending bedding planes. In the Duero Basin, on the contrary, two main directions related to fracture sets appear. A NW–SE striking one, which is prevailing, and an E–W direction, which occurs in the SW corner of the image.

10.6.2 Study Area 2

Study Area 2 is rather difficult to evaluate in terms of geological structures. Although the geological features of the area could be used as excellent text book examples for air photogeology, it is difficult to find relevant indications in the radar images.

Beside some NNW–SSE striking major lineaments, there exist some long, significant E–W trending lineaments in the northern part of the image. One of them might be the manifestation of a decollement front which comes out along the northern limb of the San Emiliano Anticline.

10.6.3 Study Area 3

Although study area 3 is located in a mountainous area of uniformly high relief, two different patterns separated by a NW-SE line can be distinguished. The south-western portion shows lighter radar grey values, and lineaments of varying length in the N–S direction. In this part E–W striking lineaments occur.

In the northeastern portion of the SIR-B image dark-toned NW–SE trending stripes of backslopes seem to be associated with long lineaments and traces of short ones distributed around the N–S direction. This pattern occurs in an area which is occupied by the Alba Syncline. The two patterns correspond to different dispositions of geological structures with respect to the illumination direction. The lithology of both units, however, is quite similar.

The intersection angle of the main structures with the illumination direction is also responsible for the manifestation of the linear feature which limits the Alba Syncline to the S. This feature coincides with the above mentioned border between the two regions described. It is more obvious in the original (unrectified) image than in the rectified one.

10.6.4 Lithological Units and Lineament Distribution

Apart from the anticipated and verified differentiation of the Palaeozoic terrain of the Cantabrian Chain and the Tertiary Duero Basin, no significant changes due to alterations in rock types could be observed.

In the Cantabrian Mountains a pattern of rather bright foreslopes and rather dark backslopes dominates the SAR intensity distribution. This rather "binary, black-and-white" type of image veils any other surface information in the high relief terrain.

Only in the comparatively gentle terrain of the Duero Basin surface information could be obtained. Reforested areas with pine trees, patches of heather as well as alluvial deposits could be distinguished due to their grey values. No information on lithology or soil types could be obtained.

10.6.5 Comparison of Lineaments with Field-Mapped Features

Within a one-week field campaign the lineament evaluation carried out on the radar and on the Landsat TM imagery has been checked. In most cases the interpreted features checked in the field displayed clear morphological indications in the field , sometimes only on a small scale. In several places there was also clear evidence of tectonic movements. Figure 10.15 gives an example of NNE trending lineaments evaluated in the radar image of study area 2 which can be seen very nicely in the field.

10.6.6 Lineaments Mapped in Compressed Image Data

For a detailed description of how the compressed image data were obtained by the pyramid approach see Chapter 9.

Based on the experiences of the demonstration study no definite statements on the interrelation between lineaments extracted on the various levels of the image pyramids and the tectonic nature of the respective faults/fractures can be made. Nevertheless, the lineaments extracted on the 3rd and 4th level (almost exclusively) represented features of high structural geological significance (i.e. major faults). Due to this fact, weighting classes of two or more weighted categories of lineaments can be achieved.

Statistical quantification of lineament analysis with respect to structural geological statements will not be given, as this does not seem appropriate for the scope of this study.

10.7 Evaluation of Demonstration System Used and Recommendations

In its basics the developed demonstration software system used seems to be sufficient for geological lineament analysis. In principle it fullfilled all the tasks needed for a decent and sound evaluation of data. Major improvements desired refer to a more user-friendly handling in the widest sense. This, in the first instance, implies a time-saving high-accuracy geometric rectification. In order to achieve this, tools for automatic rectification have to be developed.

The support of a visual lineament analysis by semi-automatic preparatory steps using filtering and image pyramid approaches will be highly appreciated by geologists. Especially the latter data transformations should be of great help for a weighting of lineaments, which is a rather difficult and until present also rather subjective task.

User-friendly and fast programs for statistical evaluation of the lineament distribution seem to be inevitable.

One of the most important requirements from the user side is the availability of fast and easy-to-handle programs for rectification. With the present software system the time factor is still a drawback in application.

Color Pictures on opposite folded page:

Figure 10.10 Lineaments superimposed on an ortho-image.

Figure 10.11 Lineaments superimposed on rectified Landsat TM data.

Figure 10.12 Rose diagram of lineament statistics.

Figure 10.13 The major lineaments of study area 1 mapped in a compressed image based on intensity pyramids of level 3.

Figure 10.14 The major lineaments of study area 1 mapped in a compressed images based on intensity pyramids of levels 2 and 1.

Figure 10.15 Lineaments superimposed on the rectified Landsat TM image of study area 2.

Figure 10.16 Lineaments of study area 3 mapped in unrectified Landsat TM data.

Figure 10.17 Rose diagram for study area 3 comparing mapping results in rectified Landsat TM data and rectified SIR-B data.

Appendix A

Review of Geocoding Algorithms

A.1 Geocoding Algorithms Reported in Literature

Kratky [57] describes an algorithm for the computation of geometric distortions in spaceborne SAR images from considering the elements

- shape of the orbital envelope surface;
- shape of the earth reference ellipsoid;
- orbiting motion and earth rotation.

Since the algorithm was proposed for SEASAT's ocean surveillance, terrain relief displacement was of no concern. images. The rectification process was based on the assumption that the orbit of the satellite (described by a circle), the earth's rotation and the shape of the earth (described by an ellipsoid) can be described in one orbit model ("composite orbit"). With time t as the only independent variable, any position of the satellite on the orbit and its relation to the earth ellipsoid can be defined. Doppler plane, Doppler nadir and Doppler track are essential to correct the slant ranges into ground ranges and to correct geographic annotation of images. The model was designed to support the creation of "primary" SAR images and was intended to resample the signal histories. No results from practical tests using this algorithm were reported by Kratky.

Curlander [15] strives for an automated algorithm to avoid the need for operator interaction because of the large quantity of data expected from a satellite SAR. The method was demonstrated with SEASAT images by correcting them from slant to ground range, by tests employing small features on the ocean surface, and by mosaicking of adjoining scenes. Input data consist of spacecraft position (in the case of SEASAT timing information accurate to 1 ms is available, which corresponds to 7 m in azimuth), velocity and characteristics of the data collection and image formation system. No ground control is used. The precise pixel location to generate a mosaic is determined by intersecting

- a model describing the earth's surface (ellipsoid);
- the SAR Doppler equation;
- the SAR range equation defining the distance from the sensor to the target.

The distortions caused by the ground range nonlinearities are removed by correcting from slant to ground range. A linear correction is used to remove the along-track (azimuth)

skew of the image. Ground range nonlinearities and azimuth skew are denoted as first order image distortions by Curlander. No correction was applied for topographical effects. Curlander reports an object coordinate accuracy with SEASAT expressed by an RMS error of less than 60 m, which corresponds to 2 to 3 pixels in a SEASAT image and results from uncertainty in the spacecraft and deviation of the target from the assumed geoid.

Processing four images by the described method showed that an average discrepancy between map and image of 150 to 200 m existed across a 100 km frame.

The PARES Group (Preprocessing of Airborne Remote Sensing data) in the Netherlands developed an operational rectification system for an airborne real aparture radar system [50]. In this case the SLAR system is mounted on an airplane operating at low heights of 300 m to 3000 m; this causes severe disturbance by irregular platform motions. These motions can be corrected by using information on angles of pitch and roll, true heading, velocity, latitude and longitude of the airplane. These parameters are provided by an inertial navigation system. They are reported to be sufficiently accurate to geometrically correct the flight path within the resolution of the SLAR system. Further geometric corrections concern slant to ground range, squint angle and antenna position within the aircraft coordinate system.

Guindon, Goodenough and Teillet [39] investigated the geometry of a high-resolution airborne SAR and found large geometric discrepancies in the location of objects. By integrating a height model into the rectification residual errors were reduced to less than a fifth of the error in the original SAR image. In search of an algorithm to be implemented and used for large amounts of data, the authors decided to model the flight path by a resection-in-space where recorded flight parameters and ground control points (GCPs) are entered.

The ground distances between the nadir line related to the preliminary flight path and GCPs are calculated in two ways: First, as the distance in the object system and, second, from the image range coordinate. The differences between these two ground range estimates are used for a least-squares-fitting of the flight path nadir line. For each ground coordinate (i, j), which is represented by a DEM grid coordinate, a grey value is resampled in the corresponding image neighborhood (x, y) and stored together with the (i, j) coordinate of the ortho-image.

Advantages of this algorithm listed by the authors are the requirement of only a few control points and the improvements obtained by the integration of a digital height model.

Additionally to the improvement in accuracy, the DEM helped to identify image areas of layover and shadow and therefore can be used to support image analysis. For example, the accurate estimation of timber volume and biomass computations, has been performed by using the SAR imagery.

Naraghi, Stromberg and Daily [82] experimented with an algorithm to integrate a DEM into the rectification of a SEASAT image, but wanted to avoid the usually tedious effort of finding a large number of well distributed GCPs. The authors identified a few GCPs to define the location and orientation of the image coordinate system of the DEM. To obtain locations of a set of points in the SEASAT image and also in the map, a simulated image (essentially, an illuminated height model) was generated from the digital terrain data. Thus the requisite number of tiepoints can be found by visual (manual) matching of the image and the illuminated height model. In a preprocessing step the image is rotated, scaled and deskewed so that its pixel rows fit the rows of DEM pixels. GCPs also serve for the calculation of a range offset and a factor for range pixel spacing.

With the help of ephemeris data, the DEM coordinates and a few GCPs, the range can be calculated for each DEM cell (i, j) and converted into (x, y) image coordinates. The grey values for the ortho-image can be resampled at this location (x, y) and stored into the proper ortho-location (i, j). The result was a radar image geometrically rectified to the map projection in which the topographic data were provided in that case.

Meier and Nuesch [79] follow the principles of Curlanders approach, but utilize a DEM for the representation of the terrain surface in order to consider the displacements caused by topographic relief. GCPs are used to determine the squint angle as a second order function of the slant range to compensate for the effects of azimuth skew. Besides, GCPs are used for a least-squares-fitting of a range offset and a scaling factor in range direction. Analogous to the approach of Curlander the procedure requires ephemeris data to be available.

A.2 Georeferencing Algorithms Implemented at DIBAG

A.2.1 Map-to-Image Registration

Besides algorithms for rectification of radar images to the geometry of a map projection, a method to project object space information into the image space of a SAR image (map-to-image correspondence) was developed at DIBAG by Lukes and Raggam [77].

The registration of three-dimensional map features to a radar image can be useful, if users want to work with grey values of the original SAR image which are not changed by rectification processes. Map-to-image correspondence can be realized through simple polynomial transformations as well as by rigorous radargrammetric projection.

The implemented algorithm consists of processing steps as follows:

- generation of a three-dimensional digital map data base by augmentation of digitized two-dimensional planimetric data with height values interpolated from a DEM;
- recovery of geometric image acquisition parameters by means of a single radar image resection-in-space. This is done by a radar bundle adjustment as described in Section 1.2.3;
- map-to-image correspondence by transforming the three-dimensional coordinate streams of the map features into radar image coordinates.

A.2.2 Image-to-Map Registration (Geocoding)

Various methods for the rectification of radar images are currently implemented at DIBAG:

- rectification based on polynomial transformation (realized in software system RECTIF).
- rectification based on simulation and use of a DEM (realized in software system GEOREC)
- rectification based on the recovery of image acquisition parameters and use of a DEM (realized in software module GEOCOSA).

The first approach makes no use of any projection equations and thus represents a simplified method for the rectification of images with arbitrary imaging geometry. The other two methods are much more specific due to the employment of digital terrain models as well as radar projection equations.

Rectification Based on Polynomial Transformation

A rectification algorithm utilizing simple polynomial interpolations is available at DIBAG in the form of the modular software system RECTIF (Diarra, [21]). Input is a set of homologue ground control points, with coordinates known in the SAR image and in the map projection. Control points will usually be defined by hand or by digital correlation. These are used to compute the coefficients of the correction polynomials to describe the trend of image deformations. Residuals at control points serve to compute refined corrections with a number of higher order interpolative methods. Rectification is thus done via "warping" or "rubber-sheeting". The polynomials are limited to degree 3 or less, so that they remain both stable and overdetermined, for a reasonable number of points.

These correction polynomials are used for resampling based on a grid of anchor points; each set of object coordinates of the grid points is assigned one image-position. Residuals are extracted at each anchor point, and serve to modify the original polynomials. Various methods may then be applied to determine grey values at those positions: interpolation followed by nearest neighbour assignment, bilinear interpolation, and bicubic interpolation are the current options.

Rectification Based on Simulation

For the rectification of SAR images a preliminary multi-step algorithm, implemented under the name of GEOREC, was described by Domik et al. [25,23]. It employs image simulation using a DEM and is thus also suitable for geocoding of mountainous scenes. Available flight recordings (flight positions, altitude, sweep delay)are used to reestablish the imaging environment (flight path, illumination direction). An illumination value (grey value) is assigned to each DEM grid cell according to the calculated incidence angle and a theoretical backscatter curve. In the first implementation GCPs were only used if the recorded flight and imaging parameters were incomplete or had to be improved.

The output of this computation is a grey value file (simulated radar image) displaying the geometric properties of the real radar image (layover, shadow). The originating address of each grey value in the DEM is stored on an auxiliary file for later processing.

An operator now has to identify "auxiliary match points" in the real and simulated images to obtain coordinate pairs which indicate geometric discrepancies between real and simulated image. These deviations can originate from

- errors in the simulation input or
- errors in recording and/or processing of the real image.

The geometric discrepancies or coordinate shifts are used to calculate a warping function (polynomial of first, second or third order), so that in a next step the real image can be registered to the simulation via this function. This is done by means of the software system RECTIF.

The grey values of the warped or "registered" image can now be entered into the auxiliary address file stored during simulation; they are resampled at these addresses in a final step resulting in the geocoded image.

Rectification Based on Recovery of Image Acquisition /- Parameters

The availability of reliable accurate parameters of the analytical sensor model allows to directly relate real radar image pixels and object coordinates. Radar image geocoding

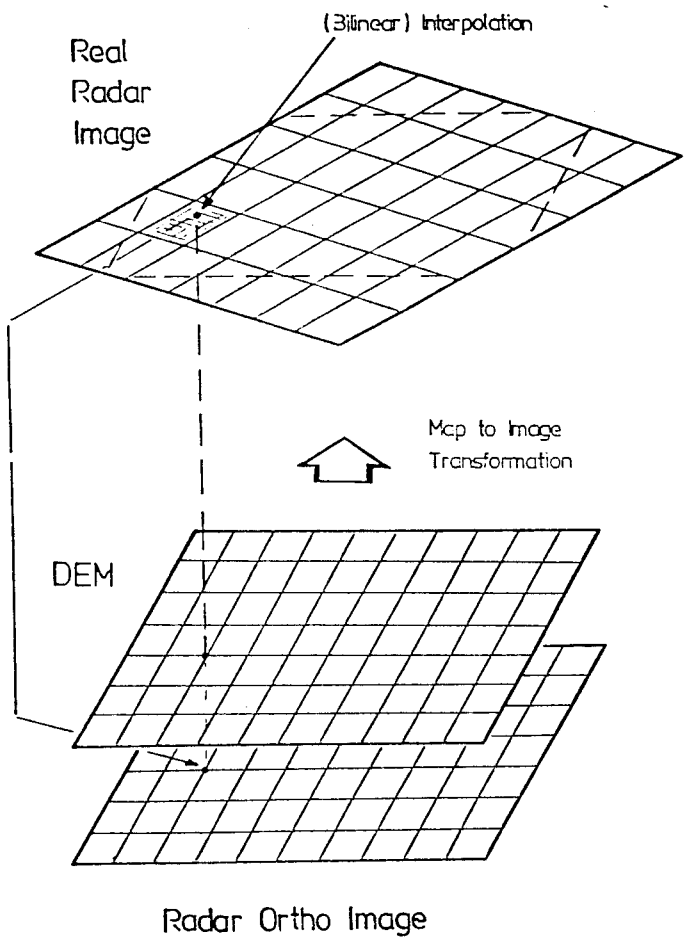

Figure A.1: Principle of radar image rectification with the GEOCOSA-algorithm.

could then be employed without need the for intermediate products such as simulated or registered images.

For such a direct geocoding of radar images a method based on the recovery of the geometric image acquisition parameters by a resection-in-space has been developed—see Section 1.2.3. It also utilizes a DEM.

This algorithm, which has been implemented at DIBAG under the name of GEOCOSA (GEOCoding using an Object Space Algorithm), is illustrated in Figure A.1. The geocoding is a resampling process relating ortho-image pixels to the input image through projection equations with recovered imaging parameters.

A.2.3 Comparative Assessment of Implemented Geocoding Algorithms

In the following the most important advantages and disadvantages of the described rectification methods are outlined:

RECTIF: This rectification method is based on polynomial transformations and is therefore only a simplified approach to radar image rectification without consideration of projection equations and effects of mountainous topography in the range projection. However, if the terrain of the imaged area is sufficiently flat, this algorithm might

lead to quite reasonable results. No radar imaging parameters, but a set of well distributed GCPs is needed for this procedure.

GEOREC: This rectification procedure employs radargrammetric projection equations, but no requirement for precise image acquisition parameters, since an intermediate registration step removes discrepancies between real and simulated radar images. Rectification is done in several steps comprising time-intensive processing tasks such as simulation, registration and resampling.

Advantages of this method might be the creation of a simulated image, if this intermediate product is desired, and the fact, that it works without GCPs in object space but with homologue points between real and simulated images. However, identification of such points might be difficult for flat terrain, because the information content of a simulated image strongly depends on the roughness of the terrain. In this context the employment of ground truth and backscatter data bases might be useful in cases of flat terrain for close-to-reality simulation, but it would also lead to an increase of processing time.

GEOCOSA: One advantage of the GEOCOSA-algorithm is that it is based on the modification of the geometric image acquisition parameters instead of a modification of the real SAR image, as it is done in GEOREC. Rectification itself is performed in one single step and is thus much less time-consuming. If accurate estimates for the imaging parameters are given, only a few GCPs need to be available within the bundle adjustment procedure. A comparatively larger set of homologue points is needed in the GEOREC rectification procedure, so that usually less interactive work is required. If one considers the processing of multitemporal data, and if GCPs were stored in a GCP data base, the identification of the control points would be necessary only in the radar images.

Bibliography

[1] N. Ahuja. On approaches to polygonal decomposition for hierarchical representation. *Computer Vision, Graphics, and Image Processing*, 24(2):200–214, November 1983.

[2] P. Anuta. *SAR - Landsat Image Registration Study. Final Report.* LARS Contract Report 082478, LARS-Perdue Univ., 1978.

[3] P. Anuta, M. Hixson, and D. Swain. *Multisensor Multidata Spatial Feature Matching, Correlation, Registering, Resampling and Information Extraction.* Processing Techniques Development Vol. 3, pp. C-1 to C-56, LARS-Purdue Univ., 1978.

[4] B. C. Barber. Theory of digital imaging from orbital synthetic-aperture radar. *Int. J. Remote Sensing*, 6(7):1009–1057, 1985.

[5] P. Binnenkade, H. Van Kasteren, and G. Heuk. Semi-operational identification of agricultural crops from airborne SLAR data. In *Proc. Machine Proc. of Rem. Sensed Data*, pages 241–247, 1985.

[6] A. Bloom. Tectonic geomorphology of the Andes with SIR-B. Oral Presentation at the 2nd Satellite Radar Symposion at the Jet Propulsion Laboratory, April 1986.

[7] W. M. Brown and L. J. Porcello. An introduction into synthetic aperture radar. *IEEE Spectrum*, 6(52), 1969.

[8] P. Churchill, G. Hane, and J. Trebett. An evaluation of SAR-580 multi frequency radar data over the norfolk test site(GBG4). In *Proc. SAR-580 Investigator's Workshop*, page 6, ISPRS, 1984. Vol 2.

[9] J. Cimino, A. Brandani, D. Casey, J. Rabassa, and S. Wall. Multiple incidence angle SIR-B experiment over Argentina: mapping of vegetation. *IEEE Trans. Geoscience, Rem. Sensing*, 24(24), 1986.

[10] A. Colvocoresses. An automated mapping satellite system. *Photogrammetric Engineering and Remote Sensing*, 48:1585–1591, 1982.

[11] A. Colvocoresses. Image mapping with the thematic mapper. *Photogrammetric Engineering and Remote Sensing*, LII(9):1499–1505, 1986.

[12] C. E. Cook and M. Bernfeld. *Radar Signals.* Academic Press, New York, 1967.

[13] J. Crowley and A. Parker. A representation of shape based on peaks and ridges in the difference of low-pass transform. *IEEE Trans. Pattern Analysis and Machine Intelligence*, PAMI-6:156–170, 1984.

[14] J. Curlander. Location of spaceborne SAR imagery. *I.E.E.E. Trans. Geoscience and Remote Sensing*, GE-20(3):359–364, July 1982.

[15] J. C. Curlander. Utilization of spaceborne SAR data for mapping. *IEEE Transactions on Geoscience and Remote Sensing*, GE-22(2):106–112, March 1984.

[16] J. C. Curlander, R. Kwok, and S. S. Pang. A post-processing system for automated rectification and registration of spaceborne SAR imagery. *Int. Journal of Remote Sensing*, 8(4):621–638, 1987.

[17] *Research Studies and Investigations for Radar Control Extensions.* Defense Documentation Center Report 530784L, DBA-Systems, Inc., P.O. Drawer 550, Melbourne, Florida, 1974.

[18] E. E. Derenyi. Metric evaluation of radar and infrared imageries. In *Proc. 2nd Canadian Symp. on Remote Sensing*, Univ. of Guelph, Guelph, Ontario, 1974.

[19] E. E. Derenyi. SLAR geometric test. *Photogrammetric Engineering*, 1974. XL.

[20] H. Derin, H. Elliot, and R. Soucy. Segmentation of SAR imagery using GIBBS distribution models. In *Proc., Machine Proc. of Rem. Sensed Data*, pages 282–291, 1985.

[21] G. Diarra. *A Digital Image Rectification System, Description and Examples.* Technical Report DIBAG Report 10, Graz Research Center, May 1982.

[22] G. Domik. Evaluation of radar stereo viewability by means of a simulation technique. In *Proc. Conf. IGARSS 84, ESA-SP 215*, pages 643–646, 1984.

[23] G. Domik, M. Kobrick, and F. Leberl. Analyse von Radarbildern mittels Digitaler Höhenmodelle. *Bildmessung und Luftbildwesen*, 52(5):249–263, 1984.

[24] G. Domik, F. Leberl, and J. Cimino. Multiple incidence angle SIR-B experiment over argentina: generation of secondary image products. *IEEE Trans. Geoscience Remote Sensing*, 24(4), 1986.

[25] G. Domik, J. Raggam, and F. Leberl. Rectification of radar images using stereo-derived height models and simulation. *International Arch. of Photogramm. and Remote Sensing*, 25(3a):109–116, 1984.

[26] G. Dowideit. *Eine Blockausgleichung für Aufzeichnungen des Seitwärtsschauenden Radar (SLAR).* Wissenschaftliche Arbeiten der Lehrstühle für Geodäsie etc. 75, Technische Universität Hannover, FRG, 1977.

[27] I. J. Dowman and A. H. Morris. The use of synthetic aperture radar for mapping. *Photogrammetric Record*, 10(60):687–696, 1982.

[28] C. Elachi. Spaceborne radar research in the 80's and 90's. 2nd Spaceborne Imaging Radar Symposion, Pasadena, California, 1986.

[29] D. Evans. Analysis of a multisensor image data set of South Rafael Swell, Utah. In *Proc. of ISPRS Comm. VII Vol. 1*, pages 255–259, Toulouse, 1982.

[30] J. Eyton, R. Li, and F. Ulaby. *Combined Radar and Landsat Multi-Imaged Crop Classification.* PÖSL Tech. Rep. 360-10, Kansas Univ., 1979.

[31] V. S. Frost, J. Stiles, K. S. Shanmugan, and J. C. Holtzmann. A model for radar images and its application to adaptive digital filtering of multiplicative noise. *IEEE Trans. Pattern Analysis and Machine Intelligence*, PAMI-4(2):157–165, 1982.

[32] K. Fullerton, F. Leberl, and R. Marque. Opposite side SAR image processing for stereo viewing. *Photogrammetric Eng. and Remote Sensing*, LII(9):1487–1498, 1986.

[33] *Preliminary Imagery Data Analysis Goodyear Electronic Mapping System (GEMS).* Report GIB-9342, Goodyear Aerospace Corp., 1974. Code 99696.

[34] G. Gracie. *Stereo Radar Analysis.* Report FTR-1339-1, U.S. Engineer Topographic Laboratory, Ft. Belvoir, Virginia, 1970.

[35] L. Graham. An improved orthographic radar restitutor. Pres. Paper, 12th Congress, Int. Soc. Photogramm., Ottowa, Canada, 1999972.

[36] J. P. Guignard. Advances in trends in the SAR image-quality assessment area. In *Proc. ESA Seasat Workshop, ESA SP-172*, pages 1–3, Frascati, Italy, December 11–12 1980.

[37] B. Guindon. Automated control point acquisition in radar optical image registration. *Con. J. of Remote Sensing*, 11(1):103–112, 1985.

[38] B. Guindon. Relief effects and the use of terrain models in SAR image processing. In *Proc. of the 3rd Seasat-SAR Workshop on SAR Image Quality*, pages 89–92, Italy, 1980.

[39] B. Guindon, D. G. Goodenough, and P. M. Teillet. The role of digital terrain models in the remote sensing of forests. In *Proc. 7th Int. Symp. Machine Processing of Remotely Sensed Data*, page 24, Perdue Univ., 1981.

[40] B. Guindon, J. Harris, P. Teillet, D. Goodenough, and J. Meunier. Integration of MSS and SAR data for forested regions in mountainous terrain. In *Proc. 14th Intl. Symp. on Rem. Sensing of Eng.*, pages 1673–1690, San Jose, 1980.

[41] R. T. Hall and D. A. Rothrock. Sea ice displacement from Seasat synthetic aperture radar. *J. Geophys. Res.*, 86(C11):11078–11082, 1981.

[42] R. O. Harger. *Synthetic Aperture Radar Systems.* Academic Press, London, 1970.

[43] R. L. Hartley. A Gaussian-weighted multiresolution edge detector. *Computer Vision, Graphics, and Image Processing*, 30:70–83, May 1985.

[44] R. L. Hartley. *Multi-Scale Models in Image Analysis.* PhD thesis, University of Maryland, Computer Science Center, 1984.

[45] R. L. Hartley and A. Rosenfeld. *Hierarchical Curve Linking for Corner Detection.* Technical Report 1288, University of Maryland, Computer Science Center, September 1983.

[46] E. A. Herland. Platform motion compensation in SAR processing. In *Proc. ISPRS Comm. II Symp.*, Baltimore, May 26–30 1986.

[47] R. A. Hevenor. *Third-order Co-occurence Texture Analysis Applied to Samples of High Resolution Synthetic Aperture Radar Imagery.* Technical Report ETL-0396, US Army Engineer Topographical Laboratories, August 1985. Fort Belvoir, Virginia 2.

[48] I. C. Holtzman. *Radar Image Simulation: Validation of the Point Scattering Method.* Report ETL-0017, USA Engineer Topographic Laboraty, Ft. Belvoir, USA, 1977.

[49] T. H. Hong. *Pyramid Methods in Image Analysis.* PhD thesis, University of Maryland, Computer Science Center, 1982.

[50] P. Hoogeboom, P. Binnenkade, and L. Veugen. An algorithm for radiometric and geometric correction of digital SLAR data. *IEEE Trans. Geoscience and Remote Sensing*, GE-22(6), 1984.

[51] S. A. Hovanessian. *Introduction to Synthetic Array and Imaging Radars.* Artech, Deadham, Massachusetts, 1980.

[52] M. Y. Jin. Optimal doppler centroid estimation for SAR data from a quasi-homogeneous source. *IEEE Trans. Geoscience and Remote Sensing*, GE-24(6):1022–1027, November 1986.

[53] V. H. Kaupp, H. C. MacDonald, W. P. Waite, J. A. Siles, and F. S. Frost. *Analysis of Geological Terrain Models for Determination of Optimum SAR Sensor Configuration and Optimum Information Extraction for Exploration of Global Non Renewable Ressources.* Technical Report, Arkansas Remote Sensing Laboratory, Part 1–3, 1982. In Cooperation with Kansas Univ., Center of Research.

[54] V. H. Kaupp, W. P. Waite, and H. C. MacDonald. Incidence angle considerations for spacecraft imaging radar. *IEEE Trans. Geoscience Remote Sensing*, GE-20(3):384–390, 1982.

[55] M. Kobrick, F. Leberl, and J. Raggam. Radar stereo mapping with crossing flight lines. *Canadian Journal of Remote Sensing*, 12(2):132–148, 1986.

[56] G. Konecny, W. Schuhr, and J. Wu. Untersuchungen über die Interpretierbarkeit von Bildern unterschiedlicher Sensoren und Plattformen für die kleinmaßstäbige Kartierung. *Bildmessung und Luftbildwesen*, 6(50):187–200, 1982.

[57] I. N. Kratky. Analytic method for photogrammetric processing of a single radar photograph. *Geodezia i Aerofotosjomka*, 2:115–124, 1979.

[58] W. G. Kropatsch. Curve representations in multiple resolutions. In *Proc. Eighth International Conference on Pattern Recognition*, Paris, France, 1986.

[59] W. G. Kropatsch. Ein Konzept mit zwei sich ergänzenden Pyramiden. *Mustererkennung 1986. ÖCG-Schriftenreihe der steirischen Arbeitsgruppe für Mustererkennung*, 36:158–171, 1986. R. Oldenburg, (Publ.).

[60] W. G. Kropatsch. Grauwert und Kurvenpyramide, das ideale Paar. *Mustererkennung 1986. Informatik Fachberichte 125*, 79–83, 1986. G. Hartmann (Ed.), Springer Verlag.

[61] W. G. Kropatsch. *Hierarchical Curve Representation in a New Pyramid Scheme.* Technical Report 1522, University of Maryland, Computer Science Center, June 1985.

[62] W. G. Kropatsch. A pyramid that grows by powers of 2. *Pattern Recognition Letters 3*, 315–322, 1985.

[63] W. G. Kropatsch and G. Paar. Aufbau einer Pyramide auf Radarbildern. *Berichte aus Informatikinstitutionen, ÖCG-Schriftenreihe*, 37:221–232, 1987. Wien. G.Pernul, A Min Toja (Eds.). R. Oldenburg (Publ.),Wien-München.

[64] G. L. La Prade. An analytical and experimental study of stereo for radar. *Photogrammetric Engineering XXIX.*, 1963.

[65] F. Leberl. Evaluation of single strips of side looking radar imagery. In *Arch. Int. Soc. Photogrammetry, 12th Congress*, Ottowa, Canada, 1972. invited paper.

[66] F. Leberl. *The Geometry of, and Plotting from, Single Strips of Side Looking Airborne Radar Imagery.* Technical Report 1, Int. Inst. for Aerial Survey and Earth Sciences (ITC), 1975. Enschede, The Netherlands.

[67] F. Leberl. Imaging radar applications to mapping and charting. *Photogrammetria*, 32, 1976.

[68] F. Leberl. *Metric Properties of Imagery Produced by Side-Looking Airborne Radar and Infrared Line Scan Systems.* Series A 50, International Institute for Aerial Survey and Earth Sciences (ITC), 1970.

[69] F. Leberl. Photogrammetric aspects of remote sensing with imaging radar. *Remote Sensing Reviews*, 1(1):71–158, 1983.

[70] F. Leberl, G. Domik, J. Raggam, J. B. Cimino, and M. Kobrick. Multiple incidence angle SIR-B experiment over Argentina: stereo-radargrammetric analysis. *IEEE Trans. Geoscience and Remote Sensing*, GE-24(4):482–491, July 1986.

[71] F. Leberl, H. Fuchs, and J. Ford. A radar image time series. *International Journal of Remote Sensing*, 2(2), 1981.

[72] F. Leberl and W. Kropatsch. Concept for the automatic registration of satellite images with a digital map data base. In *Proceedings, Symposium of Comm. IV of the Intl. Soc. of Photogrammetry*, pages 411–424, Ottowa, Canada, 6–8 October 1978.

[73] J. S. Lee. Refined filtering of image noise using local statistics. *Computer Graphics and Image Processing 15*, 380–389, 1981.

[74] J. S. Lee. A simple speckle smoothing algorithm for synthetic aperture radar images. *I.E.E.E. Trans. on Systems, Man and Cybernetic*, SMC-13(1):85–89, January 1983.

[75] R. Li, F. Ulaby, and J. Eyton. Crop classification with Landsat/radar sensor combination. In *Proc. Machine Processing of Rem. Sensed Data*, pages 78–87, 1980.

[76] F. K. Lin, D. N. Held, J. C. Curlander, and C. Wu. Doppler parameter estimation for spaceborne synthetic-aperture radars. *IEEE Trans. Geoscience and Remote Sensing*, GE-23(1):47–56, January 1986.

[77] G. Lukes and J. Raggam. Implementation of map-to-image correspondence for SAR image analysis. In *Proc. ASP-ACSM Convention*, pages 202–210, Washington D. C., 1986.

[78] G. Mader and W. McCandless. *Space Based Topographic Mapping Experiment Using Seasat- SAR and Landsat-3-RBV Imagery.* Technical Report VA22102, Phoenix Corp., McLean, 1981.

[79] E. Meier and D. Nüesch. Geometrische Entzerrung von Bildern orbitgestützter SAR-Systeme. *Bildmessung und Luftbildwesen*, 54(5):205–216, 1986.

[80] S. Murai and H. Maedra. Image registration of Landsat MSS data and Seasat SAR data. In *Proc. Asian Conf. on Remote Sensing*, pages F.1.1.–F.1.13, 1981.

[81] S. Murphrey. *SAR- Landsat Image Registration Study. Final Report.* Technical Report, IBM Corp., Gaithersburg, MD, 1978. 164 pages.

[82] M. Naraghi, W. Stromberg, and M. Daily. Geometric rectification of radar imagery using digital elevation models. *Photogrammetric Eng. and Remote Sensing*, 49:195–199, 1983.

[83] D. R. Nüesch. *Augmentation of Landsat MSS Data by Seasat SAR Imagery for Agriculureal Inventories.* Remote Sensing Series, Vol.7/ NASA IT-E2-04233, Univ. Zürich, 1982.

[84] S. Quegan. Measurement of geometric distortion in airborne SAR images. In *Proc. of IGARSS 84, ESA-SP 215*, pages 595–599, 1984.

[85] S. Quegan and A. Wright. Automatic segmentation techniques for satellite-borne synthetic aperture radar (SAR) images. In *Proc. 10th Anniv. Int. Conf. National Remote Sensing Society*, pages 161–167, Reading, UK, September 1984.

[86] J. Raggam. *Untersuchungen und Entwicklungen zur Stereo-Radargrammetrie.* PhD thesis, Technical Univ. Graz, Austria, may 1985.

[87] J. Raggam, D. Strobl, and G. Triebnig. *The Rectification of SAR Image Data using a Digital Elevation Model and Image Simulation Techniques. Phase-B Study for ERS-1 Processing and Archiving Facility.* ESA Contract Report 6292/85/HGE-I, Technical Note 17, Graz Research Center, Austria, August 1986.

[88] R. K. Raney. Processing synthetic aperture radar. *Int. J. Remote Sensing*, 3, 1982.

[89] Y. Rauste. Effects of height errors in a digital elevation model on the accuracy of a geocoded SAR image. In *Proc. Int. Workshop on SAR Image Rectification Techniques*, Graz Research Center, Loipersdorf, Austria, January 14–16 1987.

[90] P. Rebillard, C. Elachi, M. Naraghi, J. Soha, and W. Stromberg. Seasat/SIR-A digital registration over Algeria. In *Intl. Soc. Photogrammetry and Remote Sensing Comm. Int. Symp.*, pages 271–276, Toulouse, 1982.

[91] A. Rosenfeld, editor. *Multiresolution Image Processing and Analysis.* Springer, Berlin, 1984.

[92] J. B. Rosenfield. Stereo radar techniques. *Photogramm. Eng.*, XXXIV:586–594, 1968.

[93] M. Shneier. Two hierarchical linear feature representations: edges pyramids and edge quadtrees. *Computer Graphics and Image Processing*, 17:221–224, 1981.

[94] D. Smith, N. Veck, J. Macklin, and A. Luscombe. *SAR Simulation Concept and Tools.* Technical Report, M.S.D.S. Research Laboratory, Marcony Research Centre, Chelmsford, Essex, 1984. Final Report, ESA Contract 5430/83/GP-I.

[95] D. G. Tilley. The use of speckle for determing the response characteristics of doppler imaging radars. In *Proc. Intl. Conf. of S.P.I.E., Vol.556*, pages 202–209, 1985.

[96] K. Tomiyasu. Tutorial review of synthetic aperture radar (SAR) with applications to imaging of the ocean surface. *Proc. IEEE*, AES-18:563–575, May 1980.

[97] F. T. Ulaby, C. Dobson, J. Stiles, R. K. Moore, and J. Holtzman. A simulation study of soil moisture estimation by a spaceSAR. *Photogrammetric Engineering and Remote Sensing*, 48(4):645–660, April 1982.

[98] F. T. Ulaby, R. K. Moore, and A. K. Fung. *Microwave Remote Sensing, Active and Passive, Vol. I–III. Remote Sensing*, Addison-Wesley, Reading, Massachusets, 1981.

[99] W. Wells. Efficient synthesis of Gaussian filters by cascaded uniform filters. *IEEE Trans. Pattern Analysis and Machine Intelligence*, PAMI-8(2):234–239, January 1986.

[100] R. L. Wildey. Radarclinometry for the Venus radar mapper. *Photographic Engineering and Remote Sensing*, LII(1):41–50, 1986.

[101] S. S. Yao and J. R. Gilbert. Registration of a synthetic aperture radar image to thematic mapper imagery for remote sensing applications. *IEEE Trans. Geoscience and Remote Sensing*, GE-22(6):557–563, November 1984.

[102] K. Yorimoto. Methods and instruments for the restitution of radar pictures. *Arch. Int. Soc. Photogrammetry, Proc. 12th Congress*, 1972. Ottawa, Canada.

Selective Bibliography on Geology

[103] J. Alvarez-Marron. *La estructura de la unidad de Correcilla en el sector situado al este del rio Luna (Leon, zona Cantabrica.* Internal Report, Instituto Geologico y Minero, Madrid, 1984.

[104] C. F. Embleton. *Geomorphology of Europe.* McMillan Reference Books, 1984. 465 pages.

[105] Julivert. A Cross-Section through the Northern Part of the Iberian Massif. *Geologie en Mijnbouw*, 0016–7746/81/0300–0107:107–128, 1981.

[106] Julivert. *L'Evolution Structurales de l'Arc Asturian en Histoire Structurale du Golfe de Gascogne.* Technical Report, Inst. Francaise du Petrole, 1971. 4. Vol., 1. Pupl., Ed. Technip, pp. T-2-1–T-2-28.

[107] F. Layva, J. Matas, and L. R. Rodriguez Fernandez. *Mapa geologico y Memoria de la Hoja no. 129(13–8), La Robla.* Publicaciones del IMGE(Project), Insituto Geologico y Minero, Madrid, 1984.

[108] F. Lopez-Diaz. *La Estructura de la unidad de Abelgas (Manto de-Correcilla, Zona Cantabrica, Leon.* Internal Report, Instituto Geologico y Minero, Madrid, 1984.

[109] L. R. Rodriguez Fernandez, J. L. Garcia Alcalde, and J. R. Menendez Alvarez. La Succesion del Devonico Superior y Carbonifero Inferior en el Sinclinal de Alba (Leon, Nordeste de España). In *Proceedings 10th Congr. Internat. Estrat. Geol. Carbonifero., España*, pages 133–144, 1983. Vol.1.

List of Figures

List of Tables